Stony Brook University

OFFICIAL COPY

The official electronic file of this thesis or dissertation is maintained by the University Libraries on behalf of The Graduate School at Stony Brook University.

© All Rights Reserved by Author.

SPECTROSCOPIC STUDIES ON NOVEL POLYSACCHARIDE MATERIALS USED FOR ENVIRONMENTAL APPLICATIONS

A Dissertation Presented

by

Dong Han

to

The Graduate School

in Partial Fulfillment of the

Requirements

for the Degree of

Doctor of Philosophy

in

Materials Science and Engineering

Stony Brook University

August 2009

Stony Brook University

The Graduate School

Dong Han

We, the dissertation committee for the above candidate for the

Doctor of Philosophy degree,

hereby recommend acceptance of this dissertation.

Dr. Gary Halada, Advisor
Associate Professor, Department of Materials Science and Engineering

Dr. Dilip Gersappe
Associate Professor, Department of Materials Science and Engineering

Dr. Jonathan Sokolov
Professor, Department of Materials Science and Engineering

Dr. Brian Phillips
Associate Professor, Department of Geosciences

This dissertation is accepted by the Graduate School

Lawrence Martin
Dean of the Graduate School

Abstract of the Dissertation

Spectroscopic studies on novel polysaccharide materials used for environmental applications

by

Dong Han

Doctor of Philosophy

in

Materials Science and Engineering

Stony Brook University

2009

The research and development of novel cost-effective and efficient matrices used as water filtration system fillers, such as ones employed in permeable reactive barrier (PRB), has drawn great attention. This study focused on assessing the ability with which selected polysaccharides, both modified (electrospun and non-electrospun oxidized cellulose) and natural (low and high molecular weight chitosan), removed heavy metals from acidic metal ion solutions (U, Ce and Eu) of pH ranging from 1 to 6 under different reaction time, and comprehending the mechanism of the reaction occurring between targeted functional groups of polymers, carboxylic group in oxidized cellulose and amino group in chitosan, and metal ions in the solution. Direct-coupled plasma (DCP) spectroscopy was used to determine the amount of metal that polymeric matrices

adsorbed, and FT-IR and Raman spectroscopy facilitated the investigation on the mechanism of the reaction. Scanning electron microscopy (SEM) and Energy Dispersive Spectroscopy (EDAX) were used to study the morphology and compositions of polymeric matrices and polymer-metal complexes. Field tests were also carried out at Department of Energy's Oak Ridge Field Research Center (ORFRC) and the preliminary result showed the consistency with laboratory-scale experiment data. Molecular modeling using Gaussian software was also used to provide theoretical standards. The result suggests that both oxidized cellulose and chitosan possess the capability of immobilizing heavy metals to a certain degree and have the potential of being used as inexpensive PRB filler alternatives.

我多想你一直都在我身旁，未曾離去。
I wish you had been with me all the time.

Table of Contents

List of Figures

List of Tables

Acknowledgements

I would like to express my sincere gratitude to my advisor, Dr. Gary Halada, for his continuous support, inspiration, motivation, encouragement, and guidance throughout the course of my PhD studies and research. Not only have I learned immense knowledge and mastered technical skills, but also I have been able to polish other aspects during my stay in his laboratory. I am grateful for the rest of dissertation committee members, Dr. Dilip Gersappe, Dr. Jonathan Sokolov, and Dr. Brian Phillips.

Appreciations also go to Dr. James Kubicki (Penn State University) for his help in the molecular modeling work in this research, Dr. James Quinn for his kind assistance in microscopic experiments, Dr. Dilip Gersappe for his inspiring discussion in the preliminary research work, Dr. Scott McLennan for his help and invaluable discussions and suggestions in the DCP experiments, and Dr. Scott Brooks and Dr. Brian Spalding (Oak Ridge National Laboratory) for their help with the field tests. Without these helps, this dissertation would not have been possible.

I would also like to thank my fellow laboratory colleagues, Mr. Prashant Jha, Mr. Christopher Young, Dr. Jose Mawyin, Dr. Donald Roeper, and Mr. Michael Cuiffo, for their support and help.

Special thanks go to Dr. Yuhong Wu, Ms. Yuan Liu, and Mr. Zhenrui Cao for their unfaltering support and genuine help when I was in difficulty. I could not imagine how I would be without them. And I also wish to thank my friends, Dr. Yi Chen, Ms. Yan Lu, Dr. Hui Chen, Dr. Xiaohu Guo, Ms. Li Wang, Mr. Jia Zhu, Mr. Hao Zhang, Mr

Yi Gu, Mr. Hao Huang, Mr. Feng Zuo, and many others, who have made my stay at Stony Brook pleasant and memorable.

This work has been supported by U.S. Department of Energy's Office of Science Environmental Management Science Program (EMSP), contract number DEFG0204ER63729 and the Center for Environmental Molecular Science, (CEMS) funded by the National Science Foundation, contract number CHE0221934.

This research has also been funded in part by the U.S. Department of Energy's Office of Science, Biological and Environmental Research, Environmental Remediation Sciences Program (ERSP). Oak Ridge National Laboratory is managed by UT-Battelle, LLC, for the U.S. Department of Energy under contract DE-AC05-00OR22725.

Last, but not least, I wish to dedicate this dissertation to my family members who have loved and supported me ceaselessly and unconditionally.

And to you.

CHAPTER 1 INTRODUCTION

1.1 The history of radiation

1.1.1 Discovery of uranium

The discovery of uranium was in actuality a byproduct of silver mining in the town of Sankt Joachimsthal (now Jáchymov, a spa town in the Czech Republic), which began in early sixteenth century [1]. At the time when silver was detected and explored, a seemingly strange mineral which was black and shiny was also found but yet to be understood. Pechblende (pech means pitch or bad luck and blende means mineral in German) was the name given to this newly found mineral. Martin Klaproth, a German chemist and mineralogist, performed the first analysis of pitchblende in 1789, and he was able to successfully isolate the oxide form of the element, which was later named Uranium (U, atomic number 92) after the newly discovered planet, Uranus [1, 2].

Before the in-depth understanding of U, the early applications of U, mostly in oxide forms, resided in glass, ceramics and porcelain industry, in which U was used as a coloring agent in order to add a yellow color to ceramic glazes. And later the application

of U was expanded to the photography industry, in which uranyl nitrate was applied onto prints and films to add sepia effect [1].

In 1841 Eugène Péligot, a French chemist, isolated the very first sample of U through reducing uranous chloride (UCl_4) with potassium metal by using a thermal reaction. Dmitri Mendeleev, a Russian chemist, later in 1870 demonstrated that U was the last natural element in his famous periodic table of elements [1, 2]. The radiation generated by the decay of uranium was first perceived by Friherre Berzelius, a Swedish chemist in 1815 and Waldemar Brøgger, a Norwegian mineralogist in 1893, respectively [3]; however the recognized phenomena remained not understood until the discovery of radiation, which took place in the early twentieth century.

In 1895, Wilhelm Röntgen, a German physicist, discovered a new kind of ray, which was later termed X-ray, when he was testing his idea that a Hittorf-Crookes tube impregnated with barium platinocyanide might cause a fluorescent effect. This discovery earned Mr. Röntgen the first Nobel Prize in physics [1]. The major step in the scientific direction of radioactivity was made by Marie and Pierre Curie in Paris in 1898. Pierre Curie, along with his brother Jacques, had previously developed a device which could be used to measure the electric current generated by ionized air with precision. This discovery worked to Marie's advantage when she observed that the unprocessed uranium ore, the pitchblende, emanated radiation of far greater intensity than the purified uranium and came to the conclusion that there must be another unknown element which contributed to greater activity. Two other radioactive elements, polonium (Po, atomic number 84) which was 400 times more radioactive than U and radium (Ra, atomic number 88) which was 900 times more radioactive than U, were found after two years'

exhausting chemical separation process [4]. Radium was later employed in medical applications for cancer treatment along with surgery, and was found to be the only effective method before the emergence of chemotherapy [1]. In 1903, the Curies shared the Nobel Prize for physics with Becquerel for their contribution in radiation discovery and research. Later in 1911, Marie Curie was awarded a second Nobel Prize in Chemistry purely for her extraordinary work in the discovery of Po and Ra.

At the time when scientists were performing experiments related to radioactive materials, no protective precautions were used by the researchers, such as Mrs. Curie, who were handling the strong radioactive sources. A long-term belief was a small dosage of radiation was helpful to health; however this belief had never been approved or disapproved.

Figure 1-1 shows the image of uranium ore and Table 1-1 summarizes the major events related to the discovery of U.

Figure 1-1 Uranium ore (Image source: http://resourcescommittee.house.gov/subcommittees/emr/usgsweb/photogallery/images/Uranium_jpg.jpg)

Year	Events
1789	• U (in its oxide form) was found by German chemist Martin Klaproth.
1841	• U was first isolated by the French chemist Eugène Peligot.
1870	• U was found as the last and heaviest element present on earth, demonstrated by the Russian chemist Dimitri Mendeleev.
1895	• Radiation was first found by German professor Wilhelm Röntgen.
1896	• X-rays were discovered by Henri Becquerel.
1898	• New more radioactive materials were found albeit not yet identified by Marie Curie.
1901	• Wilhelm Röntgen won the Nobel prize in physics. • The theory of radioactive transformation of elements was detailed by Ernest Rutherford and Frederick Soddy.
1903	• Marie Curie became the first woman to obtain a PhD in science in France. • Marie Curie and Pierre Curie (Marie's husband) were awarded Nobel prize in physics for their studies into radiation phenomena, along with Henri Becquerel for his discovery of spontaneous radioactivity. • The road to the discovery of fission began. • The first version of a radioactive decay was published. • The recognition that radioactivity released both heat and He was made.
1904	• The first gram of Ra was separated by Curies.
1911	• Marie Curie was awarded a second Nobel Prize in chemistry for her part in the discovery of Ra and Po.
1913	• Soddy coined the word "isotope" to depict the various types of the same element. • A ^{238}U decay series was published.
1919	• Lord Rutherford became the first person to produce an artificial transmutation.
1921	• Soddy received the Nobel Prize for chemistry for his work in isotopes.
1932	• James Chadwick discovered the neutron.
1934	• Frederic Joliot and Irène Curie discovered artificial radioactivity.
1945	• Atomic bomb “Little Boy” was dropped on Hiroshima, Japan.

Table 1-1 Timeline of major events related to the discovery of radioactivity [1, 5]

1.1.2 The properties and characteristics of U

U belongs to the actinide series of elements, and is a soft metal with silver-white color. It is by far the heaviest metal element discovered. It is assumed that the electronic configuration of U is owing to the valence electrons $5f^3 6d 7s^2$, the excitation of which generates the characteristic spectra of the element. There are three isotopes of U discovered in nature, of which natural U usually consists [6]. Table 1-2 shows the three isotopes according to abundance in earth and half-life. Amongst all three isotopes of U, ^{235}U is used for the applications in nuclear energy power generation due to its thermal neutrons, while two others may have the potentials for the use in fast reactors [6].

Isotope	Abundance	Half-life/year
^{234}U	0.0056%	245,500
^{235}U	0.72%	7.038×10^8
^{238}U	99.28%	4.468×10^9

Table 1-2 Isotopes of U [6]

Comparing with other elements in nature, U is much more easily discovered, located, and quantified due to its radioactive properties. The detection of U is made through measuring the amount of Ra in the igneous rocks, because it is widely supported by independent researchers that the ratio of U/Ra is constant, which is 2.84×10^6 to 1. Therefore, the amount of U can be easily calculated upon obtaining the data for Ra [7]. Table 1-3 lists the amount of U and Th in different types of rocks in nature. It is believed that the estimated amount of U is around 4×10^{-6} g/g of rock. U is also observed to be a

constituent in living matter, such as plants and animals. The ratio of U/Ra in ocean is not the same value as it is in the earth. The estimated amount of U in oceans through direct fluorescence analysis is from 0.36 x 10^{-6} to 2.3 x 10^{-6} g/L in sea water. Therefore, considering the total volume of ocean water is around 2 x 10^{9} km^3, the amount of U in ocean can be calculated to be 4 x 10^{9} tons. It has also been discovered that many springs are radioactive, chiefly due to the presence of Ra [7].

Type of rock	U/g	Th*/g
Granite	9.0	20.0
Granodiorite	7.7	18.0
Diorite	4.0	6.0
Central basalts (continental)	3.5	9.1
Central basalts (oceanic)	3.6	7.1
Plateau basalt	2.2	5.0
Gabbro	2.4	5.1
Eclogite	1.0	1.8
Peridotite	1.5	3.3
Dunite	1.4	3.4

*Th is a decay product of U [97]

Table 1-3 Contents of U and Th in different types of rocks (amount per metric ton) [7]

The preparation of U usually involves the reduction of uranium tetrafluoride, UF_4, through using the reducing agent, either magnesium (Mg, atomic number 12) or calcium (Ca, atomic number 20). Mg is of more attraction in practice due to its relative inexpensiveness and easy handling. The reaction between UF_4 and Mg needs to be

initiated by electrically heating up the system to around 600-700 °C [6]. The reaction route is shown below.

$$UF_4 + 2Mg \rightarrow U + 2\ MgF_2 + 82kcal\ [6]$$

U is easily oxidized at room temperature with the water in the air.

$$U + 2\ H_2O\ (g) \rightarrow UO_2 + 2\ H_2\ [6]$$

U is a poor electrical conductor, and is difficult to machine. [6]

Uranium dioxide (UO_2) is one of many U oxides and it has a dark-brown color [8]. The preparation is usually achieved through calcining either uranyl nitrate ($UO_2(NO_3)_2$) or ammonium diuranate (ADU), $(NH_4)_2U_2O_7$, at around 450 °C to form UO_3, and then at a higher temperature (650-800 °C) to reduce UO_3 to UO_2 [6]. UO_2 readily dissolve in HNO_3, and can dissolve in sulfuric acid (H_2SO_4), but does not dissolve in hydrogen chloride (HCl) [8]. U_3O_8 has a black/dark-green color and can be obtained through igniting U oxide, such as UO_2 or UO_3, in the air. It is readily soluble in HCl, and the rate of dissolving can be faster if the heat is applied to the system and the concentration of HCl is high [8].

The most common and stable oxidation state of U is +6, in which U loses all six valence electrons in the configuration of $5f^36d7s^2$. However, lower oxidation states of U are also observable in the forms of +3, +4, and +5. The 5f electrons determine the magnetic moments on the U ions. U^{6+}, which is contained in compounds such as UN_2

and US_2, is diamagnetic due to its absence of unpaired electrons. It has been reported that the U^{5+}, contained in compounds such as U_3O_8 and UCl_5, possesses the $5f^1$ configuration, in which ligand field power and coordination number has a large impact. The theory for +5 oxidation state is also applicable to +4 oxidation state. It has been discovered that for U^{3+} ion the configuration is $5f^3$ [6]. U^{3+} is quite not stable in solution, and it is readily oxidized to the +4 oxidation state even without oxygen's presence [8].

Table 1-4 lists the colors of different oxidation states of U in solution. Each solution has a characteristic spectrum which can be used to categorize the oxidation state of the U in the solution. Formal potentials are used to elucidate the oxidation/reduction relationships of the oxidation states of U in solution. Figure 1-2 demonstrates the potentials (in volts) for U in different oxidation states.

Oxidation state	Color
U^{3+}	Rose-purple
U^{4+}	Deep-green
UO_2^{2+}	Bright-yellow

Table 1-4 Color of different oxidation states of U in solution [6]

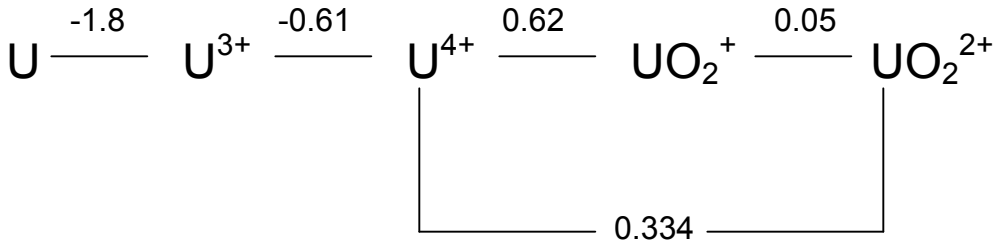

Figure 1-2 Potentials of U (in volts) in different oxidation states [9]

One of the most important U salts is $UO_2(NO_3)_2$ because it is the starting form of U when it is processed from the ores, and also because of its use in the reprocessing of fuel elements [6]. The color of $UO_2(NO_3)_2$ is bright yellow. The crystal form of $UO_2(NO_3)_2$, uranyl nitrate hexahydrate, $UO_2(NO_3)_2 \cdot 6H_2O$, has an orthorhombic crystal structure and can be obtained through evaporating the solution, in which U or U oxide is dissolved in nitric acid (HNO_3), and then cooling the system down to room temperature. The melting point of $UO_2(NO_3)_2 \cdot 6H_2O$ is 60.3 °C [6].

The transport of actinides, such as U and Th, largely depends on the aqueous chemistry of these elements, which can be obtained through analyzing the data from thermodynamic and kinetic reactions which control the solubility of solids, uptake of dissolved elements by organic materials, species separation between different phases, etc [10]. Due to the coexistence of dissolved species in different oxidation states, radiolysis effect, and colloid stability, the aqueous chemistry of actinides is rather complicated. Some characteristics of aqueous actinides are summarized as follows [10]:

(1) Th and U are commonly existent in both surface and sub-surface waters.

(2) In low temperature solutions, the aqueous speciation of actinides is mainly affected by the oxidation-reduction potential, the pH of the environment, and the concentration of dissolved carbonate.

(3) Hydroxide and carbonate are two major actinide complex forming ligands.

(4) Th and U occur mainly in the tetravalent state under reducing conditions. But, under oxidizing conditions, Th occurs mainly in the tetravalent state, while U occurs mainly in the hexavalent state.

Actinide elements can coexist in different oxidation states individually in solution. Some oxidation states are easily oxidized or reduced, and radiolysis causes these states to disproportionate. Redox reactions can control or largely affect the solubility and transport of actinides. Many actinides exist in colloidal form in solutions, either in the form of polymeric compounds or natural colloids. Temperature is also believed to have a strong influence on the aqueous speciation of actinides [10].

Concentrations of actinides are generally low in natural environment. U occurs at 1.26×10^{-11} mM and Th occurs at 2.59×10^{-9} mM in the ocean [10].

1.1.3 The applications of U

As discussed earlier, before the discovery of nuclear energy, the use of U was very limited, largely in the industries of glass, ceramics and porcelain as a color reagent. With the advent of the atomic era, U has been so far exploited in a number of different fields, which have great impacts on both civil and military levels.

Electric power generation is one of the many applications of U. Worldwide, 17% of the electric power was produced through nuclear power plants in 1995 in 31 countries [11]. Though the United States owns the largest number of nuclear power plants, 109, in the world, which accounts for 20% of the total electricity production annually, the proportion of the electricity generated through nuclear power is less than some of the European countries, including France (75%) and Belgium (55%) [10]. The trend of the usage of nuclear power plants to produce electricity has been increasing steadily ever since. In the year of 2000, the electricity generated through nuclear power plants

provided 2448 TWh totally. Nuclear power electricity generation method is third after fossil and hydropower in terms of power generated [12]. The use of nuclear power plants to generate electricity has inevitably produced toxic by-products, which are very harmful to the environment, but which on the other hand have reduced the emission of carbon dioxide (CO_2), which is a byproduct of fossil fuel combustion [10]. CO_2 is one of the five main trace gases that contribute to the greenhouse effect, the other four being methane (CH_4), nitrous oxide (NO_2), chlorofluorocarbons ($CFCl_3$ and CF_2Cl_2) [12]. The reduction of CO_2 may have an impact on lessening global warming, and therefore, the use of nuclear energy has unquestionably drawn particular interest of some [10]. In some countries, utilizing nuclear power to generate electricity is a very competitive alternative to its opponents, such as oil, gas, coal, which are believed to start being depleted by 2050. Another advantage nuclear power plants possess is that the waste volumes are very limited compared with other energy sources [12]. Table 1-5 lists the current distribution of energy sources used to supply human beings' activities with future predictions.

Year / Source	2000/%	2020/%	2050/%
Oil	40	36	20
Gas	22	29	25
Coal	24	21	25
Total fossil	86	86	70
Renewables	7.5	7	8
Nuclear	6.5	7	22
Total	100	100	100

Table 1-5 Distribution of energy sources [12]

Besides the provision of energy, radioactive materials have also been used in the area of medicine, especially in disease diagnosis and treatment. Not long after the discovery of Ra, it had been used widely in cancer treatment. It has been reported that naturally existing radiation sources, such as ^{60}Co, betatrons, and cyclotrons, have been employed in the external beam radiation therapy; and artificial radionuclides, such as ^{99}Tc, have been exploited in medical applications too, including imaging, diagnosis and also treatment [10].

Radiation has also been utilized to produce powerful nuclear weapons, such as armor-penetrating weaponry [13]. Hiroshima and Nagasaki were the witnesses of these powerful weapons [10].

Having a half-life of 4.468 x 10^9 years, ^{238}U has been utilized to determine the age of some igneous rocks. ^{238}U can also be used to produce more new fissionable radioactive materials by following this chain: ^{238}U(n, gamma)->^{239}U-(beta)->^{239}Np(beta)->^{239}Pu.

Many other applications have been observed in the fields of inertial guidance devices, gyro compasses, counterweights for aircraft control surfaces, ballast for missile reentry vehicles and shielding materials [14].

Natural U enriched by ^{235}U has applications in nuclear power plants to produce electricity. ^{233}U, an important isotope, can be produced through irradiating natural Th with neutrons as follows: $^{232}Th(n, gamma) ->^{233}Th$--(beta)$\rightarrow^{233}Pa$—(beta)$\rightarrow^{233}U$.

1.1.4 Analogs for Transuranic elements

Transuranic elements are the chemical elements with atomic numbers greater than 92, the atomic number of uranium. Those elements were first discovered artificially. Only plutonium (Pu) and neptunium (Np) exist naturally on earth.

Transuranic elements, which also require remediation in radioactively polluted areas, are dangerous and hence difficult to work with. Therefore, it is necessary to use approximate chemical analogs for transuranic materials, such as Np, Pu, Am and Cm. Analogs need to compare as closely as possible in several regards: (1) periodic table similarity; (2) ability to exist in multiple oxidation states; (3) similarities in terms of core electronic structure; (4) formation of similar compounds with oxygen and hydroxyl; (5) similar potential-pH behavior; (6) reactivity with organic ligands. However, no analogs will be perfect in this regard, matching as many as possible of these criteria is desirable.

In the present work, U (VI) was used as an analog for 6+ states transuranic elements, such as Np^{6+}; Ce(III) and Eu(III) were used as an analog for 3+ states of

transuranic elements, such as Pu^{3+}. U and Np share chemical similarity, while all elements mentioned here can exist in multiple oxidation states.

1.2 Environmental concern

In reviewing literature from the earliest days of experimentation with radioactive materials, it is interesting to notice that the storage of radioactive waste was described as simple as "canvas bags filled with brownish residues" [1]. Circumstances and technologies have changed dramatically ever since. And consequently, the radioactive waste has become an important issue requiring a complex decision-making process, socially and politically [1]. There are 70 sites in the US to store the used nuclear fuel from nuclear power plants. The generation rate of this waste is as high as 2000-3000 metric tons per year. Yucca Mountain is one of those sites and several billion dollars has been invested on this site. Another major source of high-level nuclear waste comes from the production of nuclear weapons. About 400,000 cubic meters of nuclear waste has been created by this, most of which were stored underground in the states of Washington and South Carolina [10]. Amongst the nuclides generated, U and the fission product technetium (Tc) are two key radionuclides contributing to waste. U mining for both civil and military purposes has also contributed to the waste to be remediated. A large amount of radioactive residues such as U, Th, Ra and Rn and some other heavy metals which are hazardous to public health were generated as the byproducts of milling and chemical treating U ore. Those residues are easily leachable by rain and as a consequence, they contaminate the groundwater [10]. Some sites lack the proper or perfect storage methods

resulting in contamination of trillions of gallons of groundwater and enormous amount of contaminated soil and debris. This consequence was also contributed to by accidental release (e.g. from Chernobyl in 1986) [15].

As well as groundwater, adjacent lakes and rivers can also be contaminated by the leaching and erosion of mine and mill tailings. If irrigated by the contaminated water, fish and plants can also be in danger. As far as scientists know, U is a kidney chemotoxin and a suspected human carcinogen [10].

With continuously growing attention paid to environmental protection and pollution prevention issues, many government organizations have started to fund the projects on cleanup of radioactively contaminated areas, most of which were the result of radioactive materials processing facilities. For example, in October, 2005, U.S. Department of Energy merged Natural and Accelerated Bioremediation Research (NABIR) program and Environmental Management Science Program (EMSP) to form the Environmental Remediation Sciences Program (ERSP). This program will be continuingly supporting the research carried out on resolving environmental cleanup problems related to wastes from former nuclear material processing sites and current nuclear power generation (http://www.lbl.gov/ERSP/generalinfo/intro.html).

1.3 Remediation technologies

Mill tailings, containing both radioactive elements such as U, Ra, radon (Rn, atomic number 86) and Th and non-radioactive heavy metals in solid and aqueous forms, are unavoidable residues from mining and milling of U ores. These metals can pose a

major potential threat to human health by means of contaminating air, soil, surface water and groundwater in the vicinity of the processing site for a very long time if appropriate treatment is not administered in a timely fashion. Separation and confinement of solid and aqueous forms of tailings are expected in proper waste management, in which both portions should be distanced from groundwater access. However, weathering and breakdown during storage can release the contaminants, which has unfortunately occurred at various milling and tailings sites [10]. In general, U mill tailings impact the environment through contaminating either surface soil or water or the subsurface including groundwater [10]. Additionally, many other industries, such as tanneries, also generate heavy metal wastes which pollute the groundwater in the nearby area.

U can be generally immobilized or dissoluted through one or more of the following processing methods under different conditions, either aerobic or anaerobic [16, 17].

- Alteration of the pH and E_H can affect the oxidation state and/or the speciation of U;
- Formation of chelating complexes with other species, such as iron-chelating compound siderophore, and phosphate or carbonate;
- The process of remineralization can also assist in U bioaccumulation, movement and release.

The major dissolution of U from ores is caused by a common oxidant Fe (III) [17], which is generated through oxidizing Fe(II) by *Thiobacillus ferrooxidans* [18, 19]. The mechanism involves oxidation of UO_2 to UO_2^{2+} [17].

1.3.1 Conventional technologies (Pump-and-Treat)

The conventional method to treat U-contaminated groundwater is Pump-and-Treat, which generally includes two steps: extraction of U-contaminated groundwater and a subsequent separation processes carried out above ground [10].

The main separation processes are as follows: ion exchange, reverse osmosis, bioremediation and reductive precipitation of U. Ion exchange is efficient in removing U from solution, the theory of which was used in extracting U from U ore. Although ion exchange, a process usually utilizing cation-exchange resins of macroporosity or in gel form, easily removes U, it is difficult to lower the concentration of U to drinking water standard, which is on the order of 30 μg/L [10].

Compared with the ion exchange process, reverse osmosis, a process using a semi-permeable membrane together with pressure to remove contaminants, is used in household systems to provide drinking water of high quality. Apart from being a common water treatment process on small scale, reverse osmosis has also been used on a larger scale to produce drinking water directly from seawater in some cities worldwide, a process known as hyperfiltration and ultrafiltration [10, 20].

Bioremediation comprises of three major processes: bio-sorption, bio-accumulation and bio-reduction. Microorganisms are used in bio-sorption to react with U

and other contaminants, including Cd, Cu, Fe, Ag, etc., through either adsorption or ion exchange, the theory of which is physico-chemical mechanisms. During the reaction, cell wall surfaces and cell envelopes of microorganisms serve as adsorption matrices to take up the metals from contaminated streams or treatment on the surface. Although this method is advantageous in remediating U and other metals because it does not need living cells, which circumvents the concern of contaminant toxicity, it is not feasible for in situ applications because clogging of pores can happen with the biomass [10].

1.3.2 Innovative technologies

The target of research and development of novel remediation technologies has shifted from Pump-and-Treat process to cheaper, more effective and efficient, and environmentally more compatible in situ processes. The conventional Pump-and-Treat process has been criticized by many researchers for its insufficiency in lowering the concentration of contaminants from contaminated aquifers [21]. Although initially the Pump-and-Treat process is effective in lowering the concentration of the contaminants by a factor of 2 to 10, continuous treatment has little or no effect in reducing the concentration. The termination of the Pump-and-Treat process leads to a rise in concentration of the contaminants [10].

A chemical and biological treatment process has been suggested, which includes the extraction of U from soil by using metal citrate complexes and a subsequent treatment by bacteria. The separation of the metals is carried out through photochemical treatment.

This process has been proven to be successful in treating contaminated soil and sludge [22].

Phytoremediation has also been suggested, in which conventional plants are replaced by some selected plants, such as red clover and tansy mustard, that possess the capability of hyperaccumulating heavy metals more efficiently in lightly contaminated lands or water than conventional plants [23].

The application of permeable reactive barriers is another rising technology that has been tested for U removal from contaminated groundwater. A permeable barrier can be applied in the flow path of a contaminant plume. Zero-valent iron (Fe^0) is the most common permeable barrier filler in use for U. Fe^0 has been found to be effective in removing U (VI) [24]. The pH of the reaction environment has been tested to have little effect on the reduction rate of U [25]. In addition to U, Fe^0 has also been reported to be effective in degrading MoO_4^-, TcO_4^- and CrO_4^{2-} [24]. Other materials have also been tested for permeable barrier fillers. For example, Ba chloride ($BaCl_2$) and Ca phosphate ($Ca_3(PO_4)_2$)have been found to be effective in reducing U, as well [26].

Due to the fact that a great many contaminants are mobile only under oxidizing conditions, it is feasible to reduce the redox potential of an aquifer in order to immobilize or precipitate those redox-sensitive contaminants [10].

Bioremediation is currently favored for testing and development by many researchers and scientists worldwide. Microbes in this process are not a reaction product, but a catalyst which increases reaction rates by several orders of magnitude. However, if a chemical reaction can not happen spontaneously (which means the $\Delta_R G$ is positive), it can not be catalyzed by any kind of microbes. C, N and P are the essential elements that

must exist during the process for cell synthesis. The following equations take $UO_2(CO_3)_2^{2-}$ as an example for the redox process [10].

¼ $O_2(g) + H^+ + e^- = 1/2H_2O$

$1/5NO_3^- + 6/5H^+ + e^- = 1/10N_2(g) + 3/5H_2O$

½ $MnO_2(s) + 1/2HCO_3 + 3/2H^+ + e^- = 1/2MnCO_3(s) + H_2O$

$1/2UO_2(CO_3)_2^{2-} + H^+ + e^- = 1/2UO_2(s) + HCO_3$

$FeOOH(s) + HCO_3 + 2H^+ + e^- = FeCO_3(s) + 2H_2O$

$1/8SO_4^{2-} + 9/8H^+ + e^- = 1/8HS^- + 1/2H_2O$

In this research, uranyl nitrite was used over uranyl carbonate, because uranyl nitrate represents one of the most common mobile contaminants, especially at lower than neutral pH and in plumes in groundwater at former nuclear material processing sites.

There are two ways for microorganisms to reduce U: indirect abiotic reduction (by producing H_2S or H_2) and direct enzymatic reduction (using their enzymes) [10]. As early as 1986, Kauffman et al. [27] showed a result that U concentration was reduced from 1 mg/L to less than 0.1 mg/L from the water and soil samples with the treatment of sulfate-reducing bacteria of the genus *Desulfovibrio*. Later in 1991, Lovley et al. [28] identified two Fe-reducing bacteria, *Geobacter metallireducens* and *Shewanella putrefaciens*, for the very first time during the enzymatic reduction of U(VI). The research work concluded that the reaction rate of U(VI) reduction could be accelerated to a large extent with the presence of the selected bacteria, and the authors suggeted that this would be a new method for remediation of U. The study of the reduction of U(VI) by

using different types of sulfate-reducing bacteria was conducted by Lovley et al. in 1993 [29]. The study showed that only *Desulfovibrio* species could reduce U(VI) to U(IV) and result in forming uraninite. Fe(III) was also reduced from a 10mM solution. *Clostridium sp.* was shown to reduce the oxidation state of U from VI to IV by Francis et al. in 1994 [30]. It was found that U(III) existed during the process but was not stable and soon converted to U(IV) in an aqueous medium. The researchers also concluded that the higher concentration of U(VI) (240 μM) hindered the growth of *Clostridium sp*. Barton et al. [31] in 1996 studied the effect of anaerobic bacteria in transforming U(VI) to U(IV). In this research, both sulfate-reducing bacteria such as *D. baculatus*, *D. gigas* and *D. vulgaris* and nitrate-reducing bacteria such as *Pseudomonas sp*. and *P. putida* were used as the reagents. It was shown in the result that all these bacteria reduced U(VI) to U(IV) and therefore, it was suggested that anaerobic bacteria could be used as a potential microorganisms for in situ removal of U from groundwater.

A study of the dependency of the reaction rate for U reduction on the organic composition of the waste system was carried out by Ganesh et al. in 1997 [32]. A sulfate-reducing bacterium, *D. desulfuricans* and an Fe-reducing bacterium, *Shewanella alga.* were tested. The results confirmed that the reduction rate was dependent upon both the nature of organic complex and the type of bacteria. The reaction rate of the reduction of U(VI) complexed with malonate, oxalate, and citrate by *D. desulfuricans* was slower than that of U(VI) complexed with acetate or 4,5-dehydroxy-1,3-benzene disulfonic acid. Differently, U(VI) complexed with malonate, oxalate, and citrate was reduced by *Shewanella alga*. more quickly than those with acetate and the aromatic complexes. Suzuki et al [33] reported that stimulated microbial constituents removed the uranium

nearly entirely within a month from the U-contaminated solution obtained from an inactive uranium mine. Two different types of prokaryotic cells were observed to precipitate only a UO_2 or both UO_2 and sulfate-reducing bacteria. The results suggested that *Desulfosporoinus spp*. would be a major contributor to U(VI) and sulfate reduction and *Clostridium spp*. to U(VI) reduction.

1.4 Permeable Reactive barriers (PRBs)

Figure 1-3 shows a schematic structure of a typical PRB process.

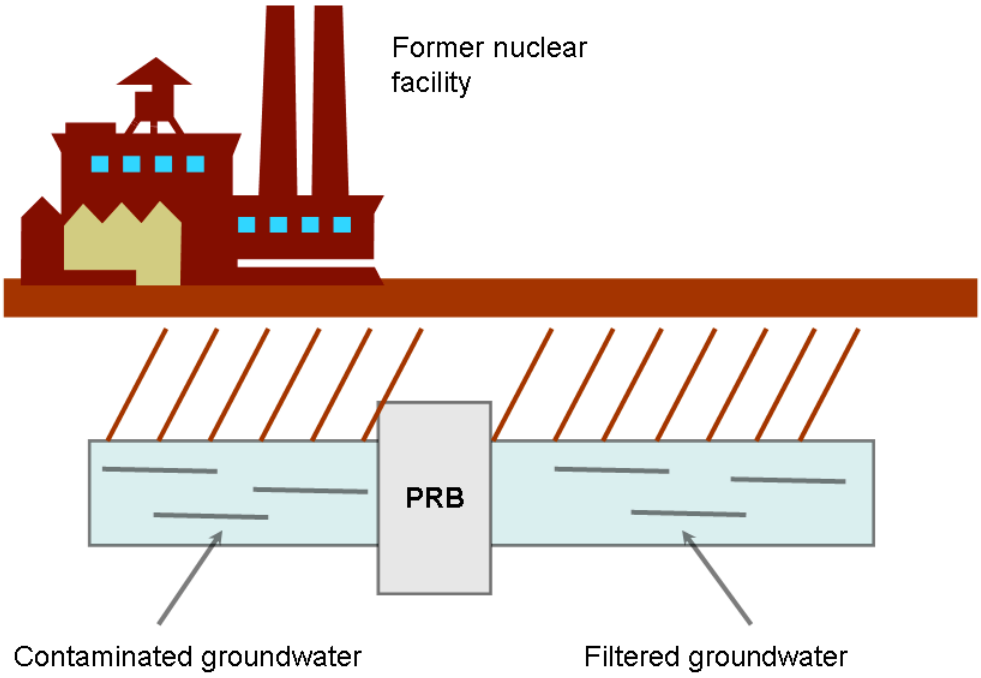

Figure 1-3 Scheme of PRB

As discussed before, use of PRBs has been a much more favorable remediation process because it is an easily operated and maintained (the main advantage of PRB compared to other conventional remediation technologies), inexpensive, and is an in situ passive technique. However, the shortcoming of PRB is that over time the PRB fillers may lose their capacity for adsorbing or precipitating contaminants existing in the flow plume, and pore clogging can also occur [34]. Hence, in order to overcome this drawback, the design of PRB needs to allow barriers to be renovated after a few years [35] or PRB fillers to be easily replaced [36].

The selection of PRB filler materials should also be based on choosing materials that would not generate counterproductive reactions and poisonous/damaging by-products. The time to service , cost and the ability to not interrupt the flow path of ground water through the PRB filler materials (permeability) should also be taken into consideration [34].

The mechanism of the PRB technique is based on the capability of fillers for adsorbing and precipitating certain types of metals, and associating metals with solid materials through chemical reaction as well [34]. Fe^0 has been reported to be an effective PRB filler material in reducing Hg, U, and Cu under reductive conditions [34]. It is important to note that if the environment changes to oxidizing condition, the immobilized metals will become mobile again [37]. Inorganic cations, such as Ag, Co, Cu, Fe, Ni, and Zn, can be reduced by reactions catalyzed by biological processes, the mechanism of which is that these metals can form sulfide complexes [38].

PRB filler materials are generally highly selective, which means certain types of materials are only effective in immobilizing certain types of metals, and also pH of the reaction is another key factor in determining the reducing or precipitating ability of the materials. For example, under conditions of low pH (5-6), hydroxyapatite is a successful matrix for immobilizing the element lead (Pb) [39].

Tree bark can be obtained as a byproduct of the timber industry. It has been reported that bark is an effective material in reducing metals due to its tannin content, containing polyhydroxy polyphenol groups, which are believed to be active sites to form chelating complexes with metals [40, 41]. Peanut skins, walnut expeller meal and coconut husks, all of which contain tannin content, have also been investigated for their capability of reducing metals [40, 42].

Lignin, containing polyhydric phenols and other functional groups, is an extracted material from waste black liquor in the paper industry. It has been found to be capable of adsorbing metals, particularly Pb and Zn (1587 mg/g for Pb and 73 mg/g for Zn at 30 ^{o}C; 1865 mg/g for Pb and 95 mg/g for Zn at 40 ^{o}C) [43].

Waste dead biomass can be obtained in large quantity from biosynthesis and penicillin production industries. Due to the ionized groups existing in the cell wall, dead cells are able to attract metals, to a degree equal to or larger than living cells. One advantage of the use of dead cells instead of living cells is that the use of dead cells avoids the issues of waste toxicity and nutrient needs [44]. Dead *Penicillium chrysogenum* biomass has been found to be able to uptake Pb to the extent of 116mg/g [45].

The presence of polysaccharide content causes seaweed to be an effective matrix for removing metals. Brown algae, such as *Ascophyllum nodosum*, has been investigated and found to be able to adsorb Cd in the amount of approximately 67mg/g [46].

Sulfur-bearing compounds have been found to have higher tendency to associate with heavy metals than lighter metals. One sulfur-bearing compound, xanthate, is highly insoluble and inexpensive to produce. The adsorption capability of xanthate sawdust on Cd has been found to be 15.7-21.4 mg/g. Some factors can affect the adsorption capacity, such as the pore size, adsorbing time and air condition [47].

1.5 Real-world contaminated site: Oak Ridge National Laboratory SS5 well

The U.S. Department of Energy's (DOE's) Environmental Remediation Sciences Program (ERSP) has funded three multi-year Integrated Filed-Research Challenge (IFRC) projects, which are located in Oak Ridge Field Research Center (ORFRC) in Tennessee, Old Rifle UMTRA site in Colorado, and the Hanford 300 area in Washington, respectively. The focus of ORFRC has been defined as "Multiscale Investigations on the Rates and Mechanisms of Targeted Immobilization and Natural Attenuation of Metal, Radionuclide and Co-Contaminants in the Subsurface" [48].

Research is currently being conducted at two portions of ORFRC, contaminated and uncontaminated areas. The contaminated site of ORFRC includes a contaminated groundwater plume containing U, technetium (Tc, atomic number 43), Th, nitrate (NO_3^-), organic compounds, dichloromethane (CH_2Cl_2), toluene (also known as methylbenzene,

$C_6H_5CH_3$), and tetrachloroethylene ($Cl_2C=CCl_2$). Originally, this site was the former S-3 Waste Disposal Ponds and it was neutralized and capped in 1998, before which time the ponds had received 3.2×10^8 liters of acidic, nitrate and uranium-bearing waste for 32 years. Currently, they are transformed to an asphalt-covered parking lot, which prevents the release of the contaminants into surface and groundwater triggered by rainwater. However, a majority of the contaminants have migrated away from the original site to geologic matrices through adsorption or diffusion, which has generated extensive sources of secondary contaminated wastes [48]. Figure 1-4 shows the images of the site before (a) and after (b) the transformation.

(a) Waste Disposal Ponds (b) transformed parking lot

Figure 1-4 S-3 ponds (a) Waste Disposal Ponds; (b) transformed parking lot (Image sources: http://public.ornl.gov/orifc/orfrc2_information.cfm) [48]

ORFRC is a unique facility that allows researchers to carry out studies on transport and fate of subsurface contaminants on a large-scale at a real-world contaminated site. Shale saprolite and gravel are two main pathways, which are different in their geologic, hydrologic, and microbial aspects, for contaminated wastes to travel

through. Nitrate and Tc travel through shale saprolite; while U travels through gravel [48]. The pH of the groundwater varies from 3.2 at the sites closer to the Ponds to more than 7.0 at the sites that are further down-gradient. The impact of pH is believed to be massive on the processes of subsurface and the transport of the contaminated wastes. Gases have also been detected in groundwater, including CO_2, carbon monoxide (CO), nitrous oxide (N_2O), N_2 and methane (CH_4). Figure 1-5 shows the major zones and flow paths in the Bear Creek Valley watershed.

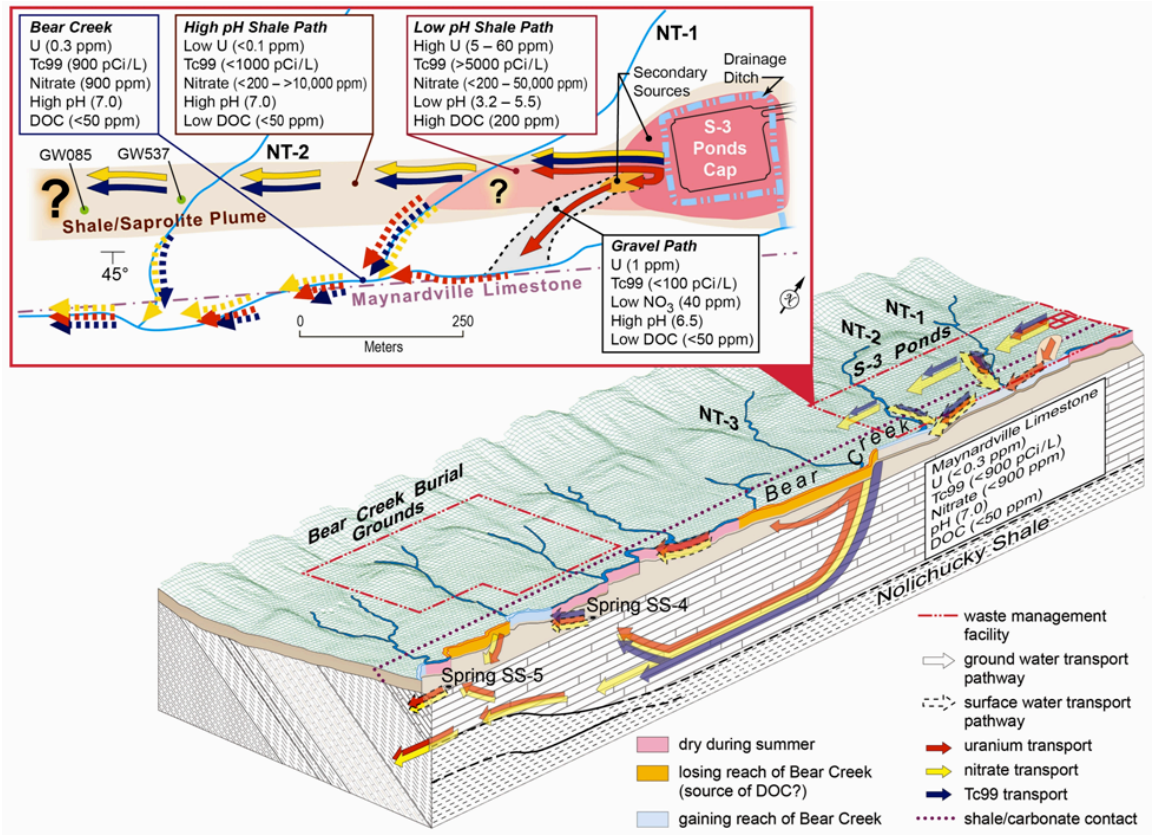

Figure 1-5 Major zones and flow paths in the Bear Creek Valley watershed (Image source: http://public.ornl.gov/orifc/orfrc3_site.cfm) [48]

1.6 Engineered and natural materials used for adsorption of heavy metal ions

In this research, several engineered or natural, small molecular and high molecular weight, materials have been investigated on their adsorption capacity of selected metal ions.

1.6.1 Oxidized cellulose

The history of the use of cellulose from numerous sources for various applications including as an energy source, and for clothing and building materials, can be traced back thousands of years. However, it was not until 1838 that its molecular formula was first analyzed by the French chemist A. Payen, and shortly afterwards the term "cellulose" was coined to describe this essential constituent in plants [49]. It is the unique molecular structure of cellulose, a 1,4-β- D-linked polyanhydro glucopyranose, illustrated in Figure 1-6, as well as its status as the most abundant organic material on our planet, that have drawn great attention from scientists and engineers involved in the investigation of the properties of cellulose and research on reformulating manufacturing processes to respond to a growing number of applications [50].

Generally, chemical and enzymatic methods are the two major methods to degrade cellulose to glucose. According to different crystalline structures and biochemical modeling, cellulose could be typically divided into two major categories: amorphous structure and highly crystalline structure. Endogluconase plays an important

role in degrading amorphous cellulose and exogluconase plays a primary role in degrading highly crystalline cellulose. It is worthwhile to note that the hydrolysis rate of amorphous cellulose is faster than that of highly crystalline structure cellulose. Cellulase may actually comprise several enzymes [51].

The molecular length of cellulose can vary from 1,000–15,000 monomers depending upon different origins and degree of degradation. Cellulose can be obtained copiously from a vast array of sources such as wood, cotton, and grasses. Several methods can be used to oxidize or degrade cellulose, including hydrolysis with acids, thermolysis, and alkaline degradation. Cellulose viscose, cellulose acetate, cellulose nitrate, and cellulose propionate are some examples of cellulose degradation products generated through industrial manufacturing [50]. Another important class of cellulose degradation products is oxidized cellulose (OC). OC has a functional carboxyl group, as illustrated in Figure 1-7, which is often a key factor for its usefulness in medical and related areas [52]. It is widely used in surgery to stop bleeding and also to avoid formation and reformation of post-surgical adhesions [53]. OC has also been found to possess beneficial medical properties such as antibacterial (due to the presence of ionogenic group H^+ or OH^-) [54], antitumor [55], etc.

Commercially, OC with a carboxyl content of 16-24% can be purchased either in a form of powder or knitted fabric [56]. And it is produced through reaction of cellulose with oxidants, such as nitrogen dioxide (NO_2) or dinitrogen tetraoxide (N_2O_4) [56]. Table 1-6 summarizes the commonly used oxidants for producing OC.

Oxidants	Researchers
Dichromate($Cr_2O_7^{2-}$)/N_2O_4	Walimbe et al. [57]
HNO_3	Gert et al. [58]
HNO_3-$NaNO_2$	Gert et al. [58]
HNO_3/H_2SO_4-$NaNO_2$	Wanleg [59]
H_3PO_4-$NaNO_2$	Painter [60]
H_3PO_4- $NaNO_2$- $NaNO_3$	Besemer et al. [61]
H_3PO_4/NO_2	Bertocchi et al. [62]

Table 1-6 A summary of commonly used oxidants for producing OC

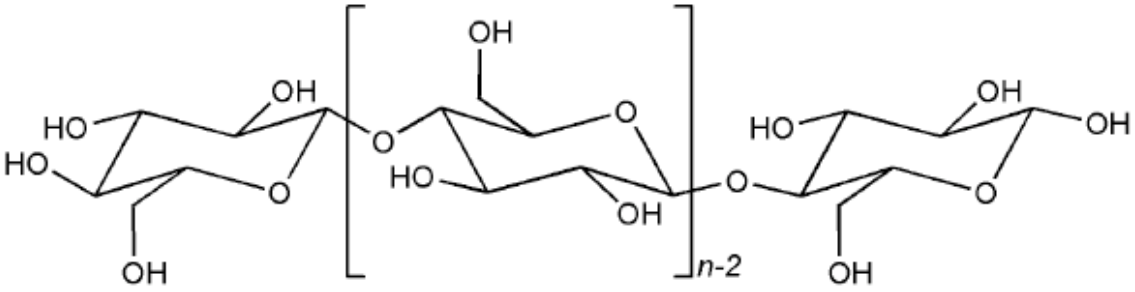

Figure 1-6 Molecular structure of cellulose (n=degree of polymerization)

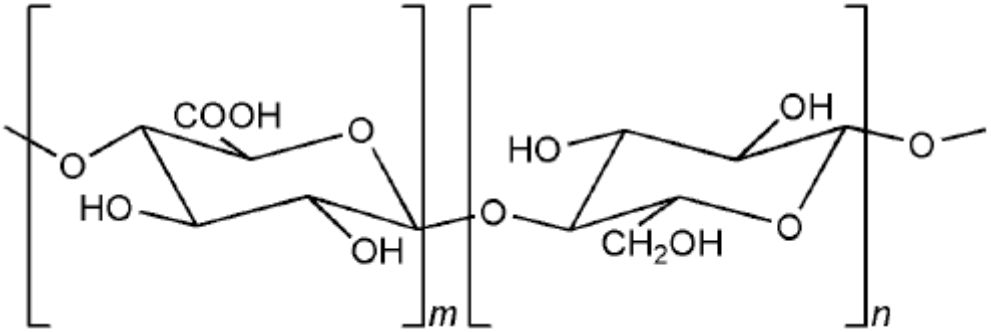

Figure 1-7 Molecular structure of oxidized cellulose (n, m=degree of polymerization)

1.6.2 Chitosan

Another major polysaccharide with an abundance second only to cellulose in nature is chitin, composed of long-chains of β-D-glucosamine, which is a key component of cell walls of fungi, arthropods, such as crustaceans and insects, and helminthes [63, 64]. Chitin can also be obtained from the crab meat canning industry, where it is a waste product [63]. It is estimated that the annual amount of chitin from crustacean fisheries is greater than 40,000 tons [65]. Chitin is believed to be an effective chelating material due to the presence of one linear amino group, in which the amine nitrogen is postulated to be the binding site for metals, per glucose unit [66]. In addition to the amino group that chitin possesses, the hydroxyl group contained in the structure has also been suggested as the participating site for metal binding [67]. Chitosan, a derivative of chitin and also known as glucosamine (the average degree of deacetylation is about or lower than 0.5 [68]), comprises a polymeric structural chain of N-acetyl-glucosamine and can be obtained either naturally from some types of fungal cell walls or from chitin through chemical modification (deacetylation) [63, 64]. Figure 1-8 shows the molecular structure of chitosan. The free amino groups that chitosan possesses enable it to chelate certain types of heavy metals at several times the chelating capacity of chitin [69]. However, chitosan is not a successful biosorbent for alkaline and alkaline-earth metals [70]. Table 1-7 summarizes the reported metal-adsorption (selected metals) capacities of chitosan. Chitosan has also been reported to have potential uses in medical applications, due to its capacity for carrying drugs [71], accelerating wound healing [72], anti-microbial properties [REF: R. Shepherd, S Reader and A Falshaw, "Chitosan Functional

Properties", Glycoconjugate Journal, v. 14, no. 4, pp. 535-542 (1997).], etc. Several factors, including crystallinity, reactions with water, deacetylation degree, pH of the reaction environment, temperature, ionic strength and percent of amino groups, can affect the adsorptive capacity of chitosan [70, 73].

Material type	Cd	Cr(III)	Cr(VI)	Hg	Pb
Chitin [74]				100	
Chitosan [74-77]	6.4, 558	92	27.3	1123, 815	796
Chitosan (from lobster shell) [78]				430	
Chitosan powder [79]	420				
Chitosan beads [79]	518				

Table 1-7 A summary of the reported metal-adsorption capacities of chitosan (mg/g)

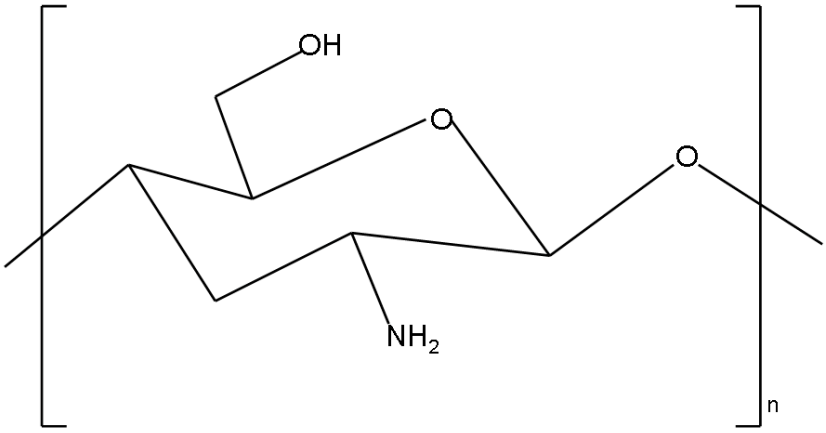

Figure 1-8 Molecular structure of chitosan (n=degree of polymerization)

CHAPTER 2 STATEMENT OF THE PROBLEM AND OBJECTIVES OF RESEARCH

2.1 Statement of the Problem

Research on developing a processing method and seeking effective and efficient matrices, either metallic or organic, for immobilizing U and other hazardous elements existing in various sites worldwide, has been the focus of great effort in the past few decades. However, the problem still remains to fully understand the mechanism of the reactions between the matrices and metal ions, and more importantly, to synthesize environmentally compatible materials which have the capability for adsorbing heavy metal ions. Other factors which are of interest to take into consideration in the studies include economic feasibility and ease of production on a large scale. Experimental data obtained from vibrational and electron spectroscopies, combined with theoretical data obtained from molecular modeling can lead to a better understanding of both the mechanisms of matrix-metal complexations as well as efficiency and effectiveness of examined organic binding materials.

2.2 Objectives of Research

The research goal of this study is to develop and examine cost-effective organic materials that are used for forming complexes with U and other environmentally hazardous heavy metals. The materials are to be used in environmental remediation technologies, particularly as PRB filler substitutes, to immobilize metal ions generated from both civil and military nuclear processing facilities. The objectives are as follows:

(1) Synthesize two polymeric materials, which are postulated to be used as binding materials for metal ion adsorption. Electrospinning will be used to modify the surface structure of one of the two polymeric materials, to increase its surface area and porosity.

(2) Polymer-metal ion complexes will be synthesized in water solution, the pH of which will be adjusted to mimic the pH of the groundwater in the field test site at Oak Ridge National Laboratory. Aforementioned polymeric materials are tested in the real-world polluted groundwater stream to determine their effectiveness and efficiency of adsorbing certain types of metal ions existing in the water.

(3) FT-IR, Raman, and XPS spectroscopy will be used to analyze and examine the structural changes of the polymeric materials after being exposed to metal ion solutions.

(4) DCP-AES will be used to determine the amount of metal ions polymeric materials adsorbed under different reaction time and pH of the solution. After gathering

this information, it will be feasible to conclude under what conditions the optimum efficiency and effectiveness of the polymeric materials can be achieved.

(5) *Gaussian* molecular modeling will be performed to provide calculated theoretical spectroscopic data of polymer-metal complexes, which then will be compared with experimental data to demonstrate the feasibility of the use of molecular modeling for identifying binding sites and predicting structural changes.

CHAPTER 3 MATRICES PREPARATION AND CHARACTERIZATION

3.1 OC

3.1.1 Preparation

3.1.1.1 Materials

Cellulose (fibrous, medium) and cellulose acetate (CA) (39.8 wt % acetyl, average Mn ≈ 30,000 g/mol by GPC) were purchased from Sigma-Aldrich Co. and used without further purification. Figure 3-1 shows the molecular structure of CA. Acetone (A.C.S. reagent, 99.7% by GC, corrected for water) and nitric acid (HNO_3) (A.C.S. reagent, 69.0–70%) were purchased from J. T. Baker. Sodium nitrite ($NaNO_2$) (99.999%), potassium hydroxide (KOH) (KOH content ≥ 85%, K_2CO_3 content ≤ 2.0%) and phosphoric acid (H_3PO_4) (85 wt % in H_2O) were also purchased from Sigma-Aldrich Co. Deionized (DI) water (> 1 MΩ) was used in all cases.

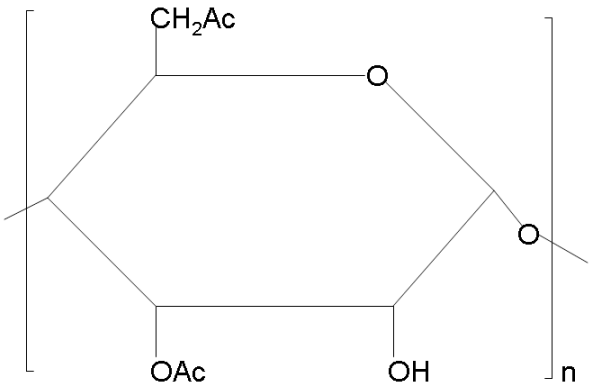

Figure 3-1 Molecular structure of cellulose acetate

3.1.1.2 Preparation of OC and electrospun OC (E-OC)

Preparation of OC

Cellulose (5 g) was added to 70 mL of a solution of a mixture of nitric acid and phosphoric acid (2/1 v/v), followed by adding 1.0 g of sodium nitrite. The reaction was allowed to proceed for 48 hours at 25 °C/room temperature. Then, the reaction was terminated by adding water, and the diluted solution was filtered to obtain the white solid which was continually washed until a pH of 4 was reached. The solid was then washed by acetone and dried in air.

Preparation of electrospun CA fibers and E-OC

A 17 wt % CA solution was prepared at room temperature in an acetone/water solvent (85/15 v/v). The CA solution was then used as a feed stock for electrospinning to fabricate a polymeric CA mat. Table 3-1 shows the electrospinning parameters. Figure 3-2 shows the undergoing electrospinning process, in which ejected polymer fibers from the tip of the syringe and the deposition of the fibers can be observed. Figure 3-3 shows the appearance of electrospun CA fibers on aluminum foil. The CA mat was swollen in a solution of acetone and water (1/1 v/v) and was then soaked for 1 hour in a KOH/ethanol solution (0.5 N KOH/12.5 mL ethanol) to deacetylate the swollen mat at room temperature. The mat was then treated with HNO_3/H_3PO_4–$NaNO_2$ and the reaction was allowed to proceed for 48 hours at 25 °C/room temperature, followed by a pH 4 water rinse and final acetone wash. The resultant was filtered and dried in air.

Voltage/kV	12
Tip-target distance/cm	8
Flow rate/mL/h	10

Table 3-1 Electrospinning parameters for fabricating CA fibers

Brown vapors, which could be a mixture of nitrogen oxides, were produced immediately after adding the oxidant HNO_3/H_3PO_4-$NaNO_2$ to the polymeric mat. Over time, the color of the mat changed from white to green, which is shown in Figure 3-4.

Figure 3-2 Electrospinning process

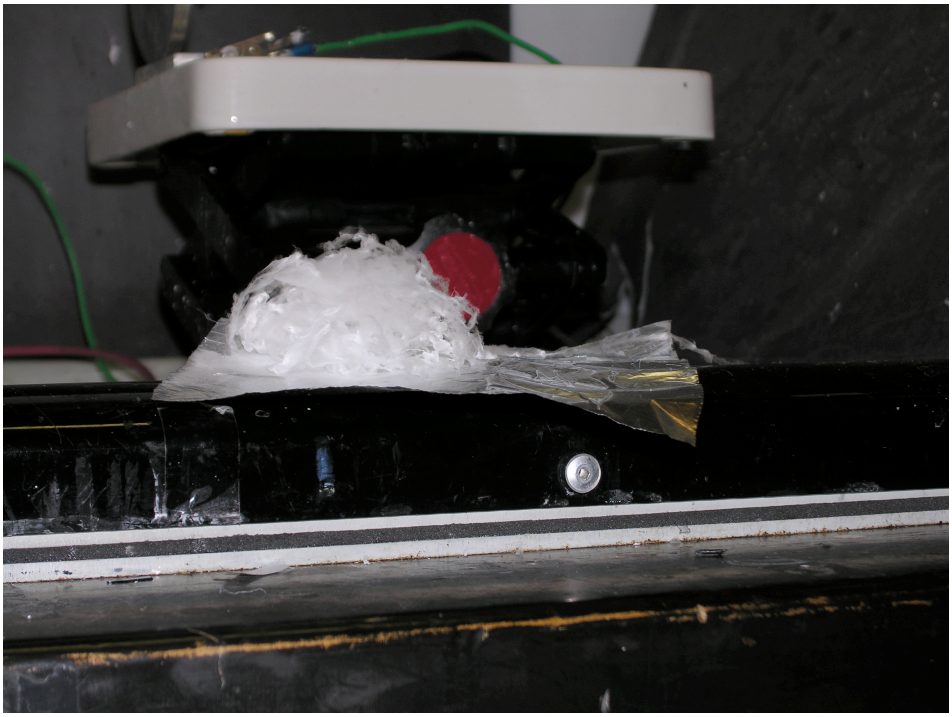

Figure 3-3 CA fibers on aluminum foil

Figure 3-4 OC oxidation process (Brown fume and green sediment)

3.1.2 Electrospinning technique

Electrospinning is an easy, inexpensive, and efficient processing method to fabricate continuous three-dimensional, non-woven, and porous fine fibers, with the diameter ranging from a few microns to a few nanometers. Little attention was given to this technique until the mid 1990s when researchers realized the tremendous potential of this technique for providing nano-scale morphology. Electrospinning can be applied in a number of areas, such as bio-scaffolding fabrication in tissue engineering, protective clothing and many others. Amongst many fiber producing methods, electrospinning

outperforms its competitors, such as drawing [80], self-assembly [81], phase separation [82] and template synthesis [83], in terms of materials versatility, meaning that electrospinning can produce fine fibers from a large selection of materials, such as polymer, ceramic, and semiconductor [84].

A typical electrospinning apparatus consists of a high voltage power supply (commonly up to 30kV) with two electrodes, a metering pump serving as the feeding control, a metallic needle connected to a syringe which contains the electrospun solution or melt, and a collector, usually a metal screen. Figure 3-5 shows a schematic illustration of a typical electrospinning setup.

Electrospinning uses electrostatic force to form a liquid jet, which is later deposited on the metallic collector to form a fibrous mat. A viscous solution or melt with high concentration is first loaded into the syringe. The metering pump feeds the solution to the tip of the needle at a controlled constant flow rate. Then if the electric field is applied to the system, the droplet of the solution at the syringe tip will become electrified, and form a conical shape, known as Taylor cone. The surface tension of the solution or melt will be overcome when the electric field strength reaches a critical value, resulting in the formation of a liquid jet ejected from the tip of the syringe. During the ejection, the liquid jet undergoes a whipping and stretching process, and the solvent evaporates before the jet solidifies on the collector in the form of thin fibrous mat. If the collector is a static metal screen, the fibers are usually randomly deposited. A dynamic rotational drum-like collector can be used to obtain aligned fibrous mat [85]. The morphology and diameter of electrospun fibers can be varied through altering the processing parameters

and also the composition of electrospun precursor solution [85]. Table 3-2 lists the major processing parameters which can modify the structure of the electrospun fibers.

In addition to a static metal screen and a rotating mandrel, the collector can also be in the form of parallel electrodes, rotating wire drum, drum with wire wound on it, rotating tube with knife-edge electrodes, disc, array of counter-electrodes, rotating drum with sharp pin inside, blade placed in line, ring placed in parallel, and yarn collection using water [84]. Each of these collectors has its own advantages and disadvantages. The selection of the fiber collector should be based upon the desired structures of fibrous mats.

Properties of electrospun solution	• Conformation of polymer chain • Viscosity or concentration of the solution • Elasticity • Electrical conductivity • Polarity and surface tension of the solvent
Electrospinning operational conditions	• Strength of electric field • The distance between the tip of the syringe and the collector • Flow rate of the metering pump
Ambient conditions	• Humidity • Room temperature

Table 3-2 Influential parameters of electrospinning process [85]

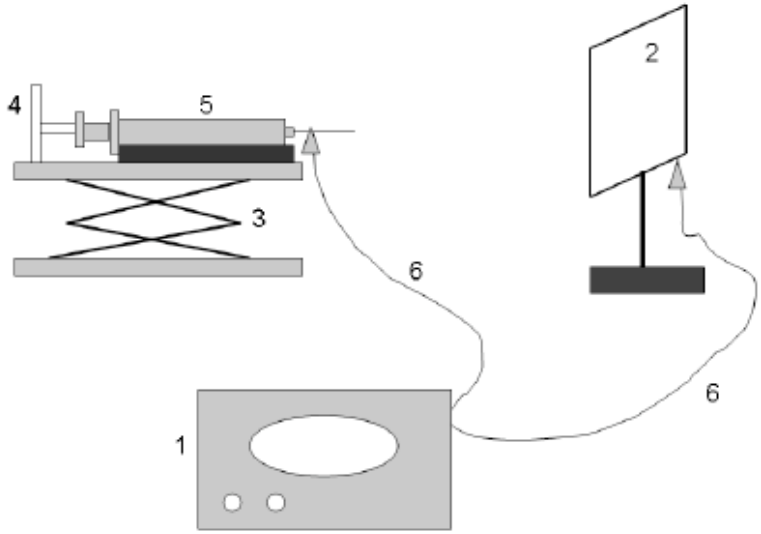

Figure 3-5 Schematic illustration of electrospinning setup. 1: high voltage power supply; 2: collector; 3: stand; 4: metering pump; 5: syringe with a metallic needle; 6: electrodes.

3.1.3 Mechanism of oxidation

In the process of oxidation of organic compounds by HNO_3 or HNO_3 with other acids and $NaNO_2$, nitrogen oxides are believed to be oxidants [86]. Nitrogen oxides can be generated in situ in several ways by HNO_3 and H_3PO_4. HNO_2 is an unstable acid, and it can be produced through reactions of: (1) $NaNO_2$ with a participating strong acid [86]; (2) water and N_2O_4 [58]; and (3) HNO_3, NO and H_3O^+ [86]. N_2O_3 is the intermediate product generated by conversion of HNO_2, which then continues to convert to NO_2 and NO. Without first converting to N_2O_3, HNO_2 can also either directly or with a participating HNO_3 be converted to NO_2. The initiation of the oxidation of OC likely

occurs through abstracting an H atom from cellulose by either NO_2 or NO due to their odd-electron nature to form the Cell-C(·)H-OH structure. Due to the high concentration in the solution, NO_2 may be more likely to initiate this reaction. Cell-$CH(OH)_2$ is produced after the reaction with NO_2·. Cell-CHO is formed after the reaction with HNO_2 and NO·. In addition to the formation pathway by reacting with NO_2·, Cell-$CH(OH)_2$ can also be formed through abstraction of a hydride ion by NO^+ and a subsequent hydrolysis process. Cell-COOH can be produced from either Cell-$CH(OH)_2$ or Cell-CHO through a hydrolysis process [56].

3.1.4 Characterization of OC and E-OC

3.1.4.1 SEM

The morphologies of fibrous cellulose and OC are shown in Figure 3-6 (a) and (b), respectively. The fibrous structure of cellulose remained after the oxidation process. The three-dimensional morphology can be observed in the SEM. No significant changes can be observed after the acidic treatment; however, a batting-like structure emerged and it existed throughout the sample.

Figure 3-7 shows the SEM images of the structures of CA powder, electrospun CA fibers, deacetylated CA fibrous mat, and E-OC, respectively. Three dimensional non-woven fibrous structures can be observed in the SEM images. No significant changes occurred to the morphology of the polymeric mat after deacetylation treatment, although a generally more convoluted structure has emerged. The 48-hour reaction with

HNO_3/H_3PO_4–$NaNO_2$ caused the structure of the polymeric mat to change dramatically. A large number of segregated fibers can be seen in the SEM image; this phenomenon is uniform throughout the whole structure of the material.

(a) Cellulose fiber

(b) OC

Figure 3-6 SEM images of (a) cellulose fiber; (b) OC.

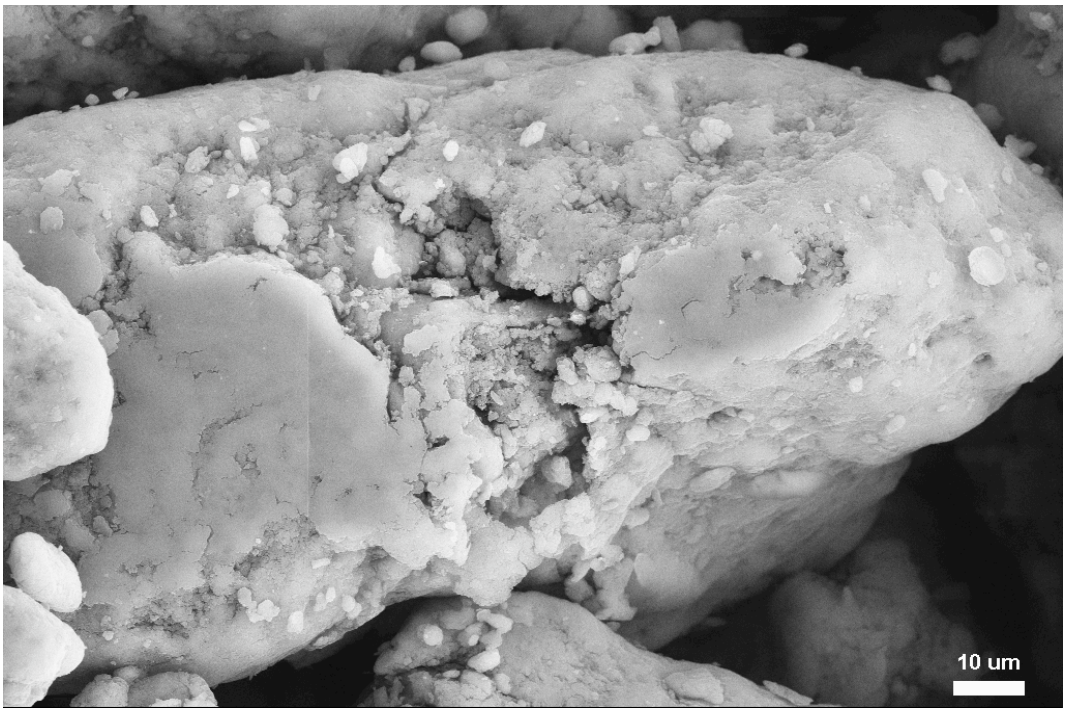

(a) CA powder

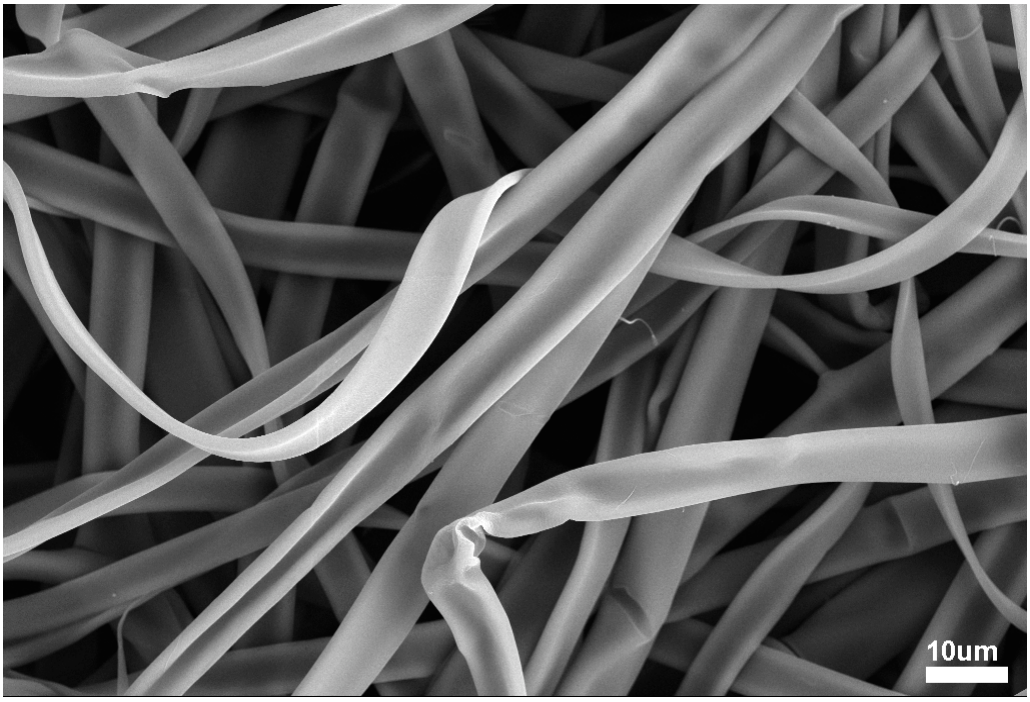

(b) Electrospun CA mat

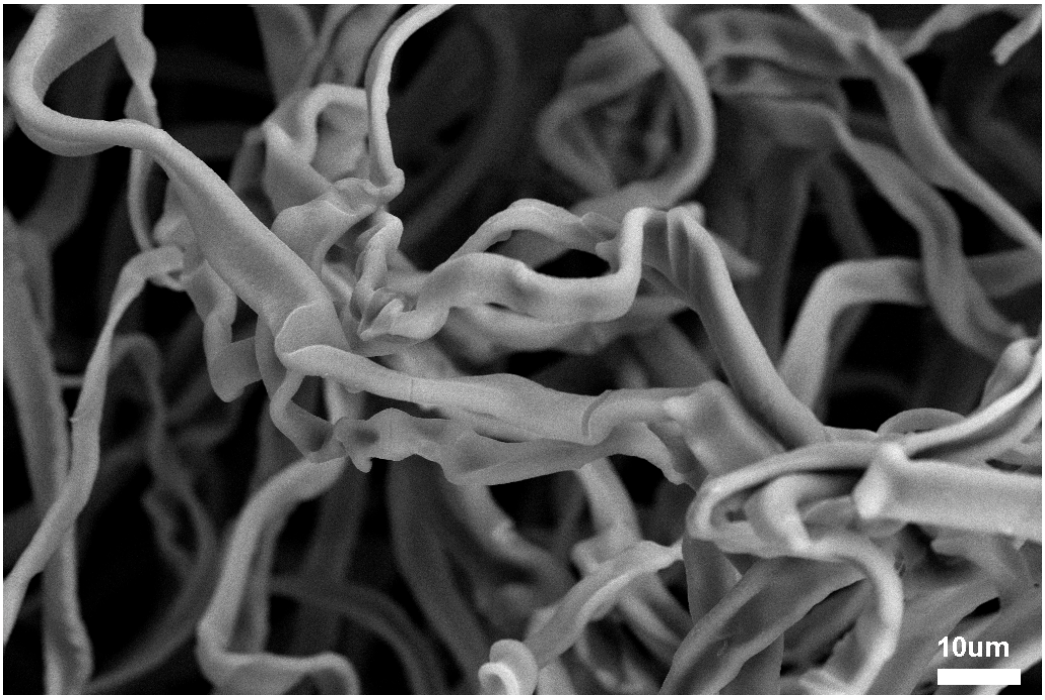

(c) Deacetylated CA mat

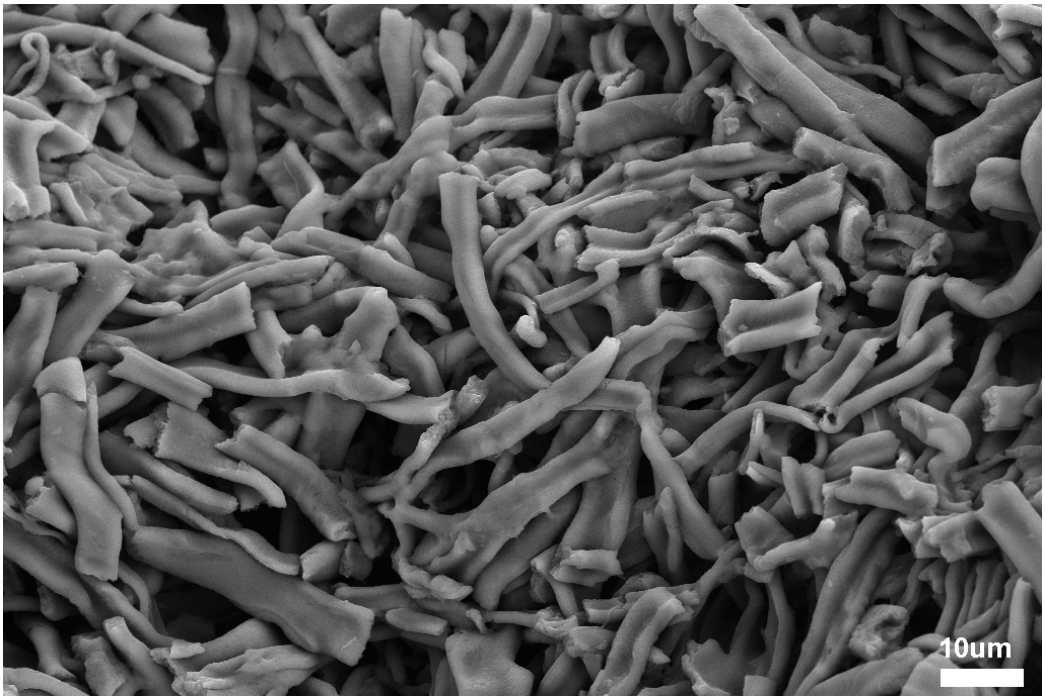

(d) E-OC

Figure 3-7 SEM images of (a) CA powder; (b) Electrospun CA mat; (c) Deacetylated CA mat; (d) E-OC

3.1.4.2 FT-IR spectroscopy

FT-IR favors detection of anti-symmetric vibrational modes. Figure 3-8 shows the FT-IR spectra of the original electrospun CA mat (a), the deacetylated CA mat (b), and E-OC (c), respectively. The signature component of CA is the acetate group (CH_3COO^-), which is comprised of a carbonyl group C=O (IR bands at 1740–1745 cm^{-1}) [87], an alkane group C–H (in acetates –O–CO–CH_3, IR symmetric deformation vibration at 1390–1340 cm^{-1}) [88], and an acetyl group C–O–C (in acetates CH_3COOR, IR bands at 1265–1205 cm^{-1}) [88]. The characteristic peaks attributed to the vibrations of the acetate group of the CA mat at 1740 cm^{-1} (C=O bond), 1366 cm^{-1} (C–C bond), and 1213 cm^{-1} (C–O–C bond) are clearly illustrated in Figure 3-8 (a). The C=O absorption

peak disappeared after deacetylation by KOH, which is demonstrated in Figure 3-8 (b). However, the absorption peak for the carbonyl vibration was detected again at 1727 cm^{-1} after acid oxidation. Generally, the C=O stretching vibration for carboxylic acids yields a band with a greater IR intensity than that for ketones or aldehydes. In both solid and liquid phases, the C=O group absorbs in the region of 1740–1700 cm^{-1}, but its stretching vibration of saturated aliphatic carboxylic acids may also be found in the region of 1785–1685 cm^{-1} [88].

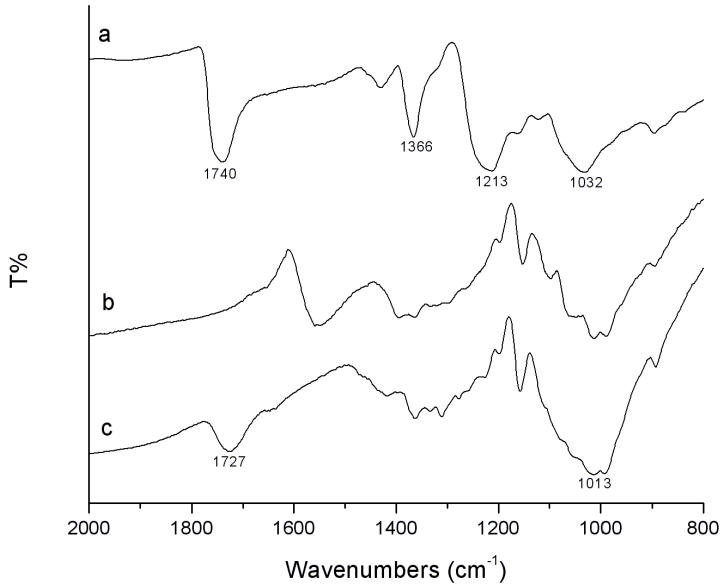

Figure 3-8 FT-IR spectra of (a) Electrospun CA mat; (b) deacetylated CA mat; (c) E-OC

3.1.4.3 Raman spectroscopy

Raman spectroscopy favors identification of symmetric vibrations of chemical bonds. Figure 3-9 shows the Raman spectra of the original electrospun CA mat (a), the deacetylated CA mat (b), and E-OC (c), respectively. The peak which appears at 1745 cm^{-1} in the spectrum of CA can be assigned to the ketone C=O stretching vibration from the branched chain of CA, which is the signature component of the structure. Two peaks appear at 1377 and 1437 cm^{-1}; the former Raman band can be assigned to the C–H deformation vibration while the latter one may be attributed to the alkane C–H deformation vibration. The band due to the C–O–C glycosidic linkage symmetric stretching vibration occurs at 1128 cm^{-1} and the Raman band for the C–O–C asymmetric stretching vibration appears at 1085 cm^{-1} [87]. The same phenomenon as was observed in FTIR was detected again by Raman; the carbonyl peak at 1745 cm^{-1} disappeared after KOH treatment and re-appeared at 1736 cm^{-1} after oxidation. Instead of the acetate group in the branch, the aliphatic alcohol group ($–CH_2–OH$) dominates the molecular branched chain after deacetylation. Bands for this functional group are due to O–H stretching and bending vibrations, and C–O stretching vibrations are generally observed. The O–H stretching band in Raman spectra is generally weak compared to the medium-to-strong band in IR spectra. The typical absorption region for the C–O group is 1200–1000 cm^{-1} due to its stretching vibration. However, hydrogen bonding results in a slight decrease in the frequency of this band. Therefore, for saturated primary alcohols, the region is 1090–1000 cm^{-1}; for secondary alcohols, the region is 1125–1085 cm^{-1}; and for tertiary alcohols, the region is 1205–1125 cm^{-1} [88]. It is worthy to note that both unsaturation

and chain branching tend to decrease the frequency of the C–O stretching vibration. Primary and secondary alcohols, both of which occur in deacetylated CA, have a strong Raman band at 900–800 cm^{-1} due to a C–C–O stretching vibration [88].

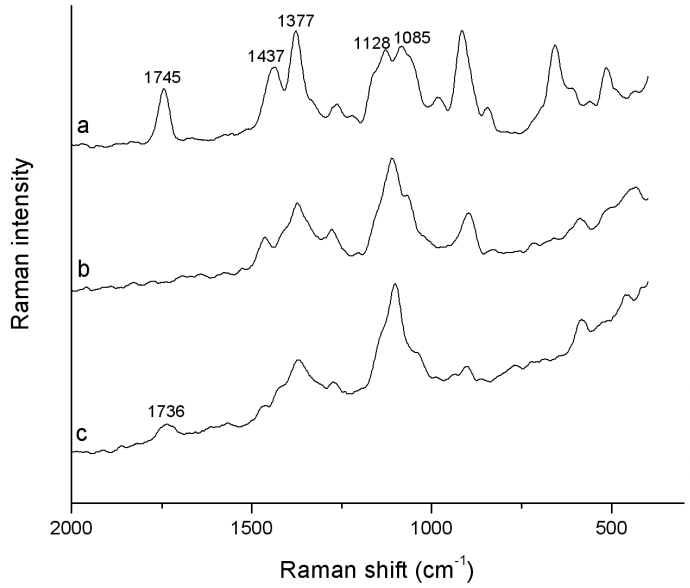

Figure 3-9 Raman spectra of (a) Electrospun CA mat; (b) deacetylated CA mat; (c) E-OC

By comparing both IR and Raman spectra of OC and E-OC (Figure 3-10 and 3-10), it is confirmed that OC possesses the same characteristic functional groups as E-OC, although the positions of peaks are slightly different, which may be partly due to their different methods of formation.

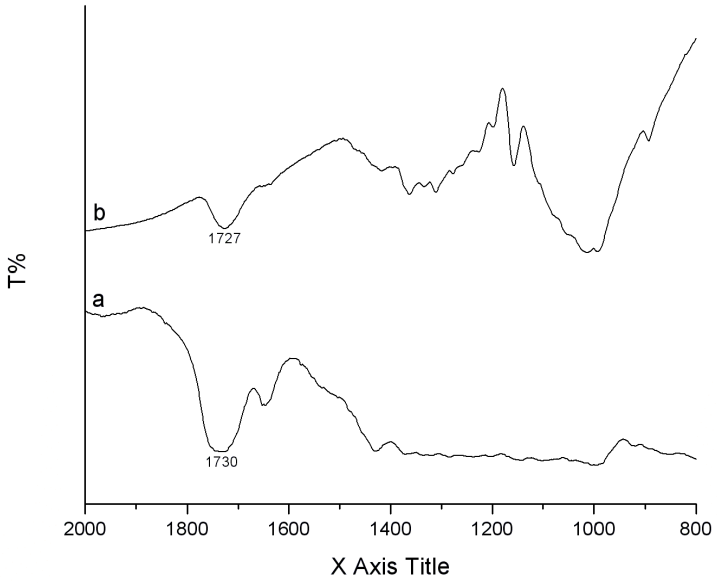

Figure 3-10 FT-IR spectra of (a) OC and (b) E-OC.

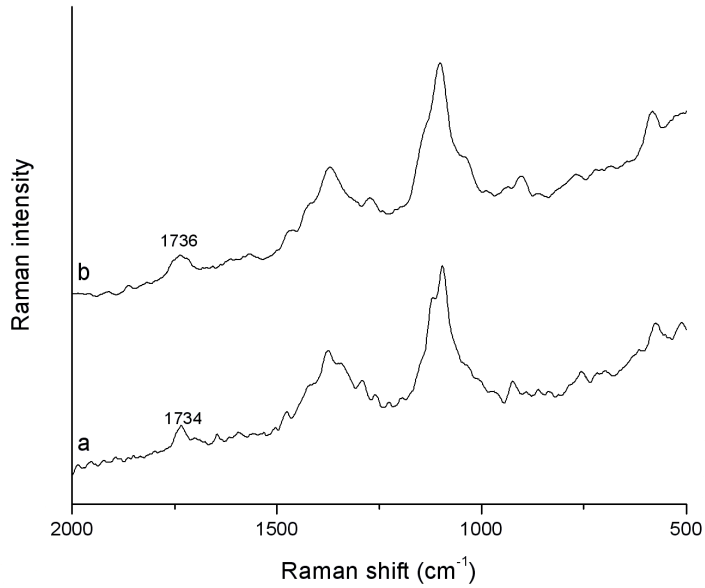

Figure 3-11 Raman spectra of (a) OC and (b) E-OC.

3.2 Chitosan

3.2.1 Materials

Low molecular weight chitosan (LCS) (molecular weight ca. 50-190kD) and high molecular weight chitosan (HCS) (molecular weight ca. 300kD) were purchased from Sigma-Aldrich Co. and used without further treatment.

3.2.2 Characterization

3.2.2.1 SEM

Figure 3-12 and 3-13 show the SEM images of LCS and HCS, respectively. Lamellar structure can be observed for LCS in the SEM, while both lamellar and fibrous structures are existent in the HCS structure.

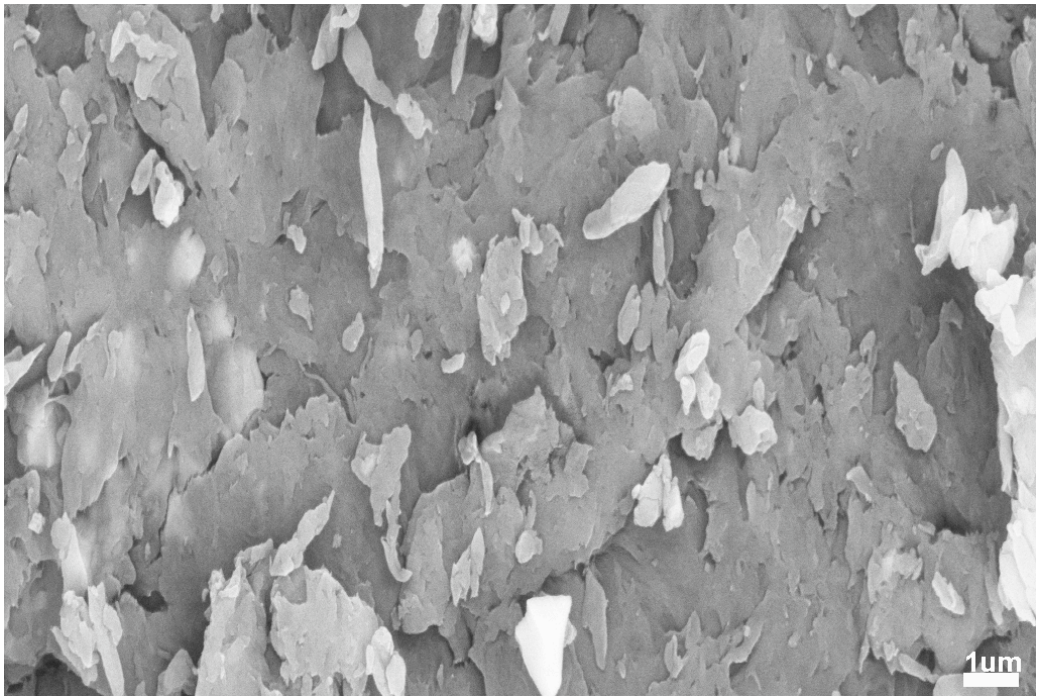

Figure 3-12 SEM image of LCS

Figure 3-13 SEM image of HCS

3.2.2.2 FT-IR spectroscopy

Figure 3-14 shows the FT-IR spectrum of LCS. LCS and HCS share the same spectra; therefore, only the LCS spectra are discussed here. A large band appearing at 3481 cm^{-1} may be attributed to O-H groups [89]. The characteristic absorption band of chitosan appears at 1597 cm^{-1} due to its $–NH_2$ content [70]. Primary aliphatic amines in general occur in the region 1140-1080 cm^{-1} due to C-N stretching vibration [88]. The peak appearing at 1127 cm^{-1} may be due to C-N stretching vibration.

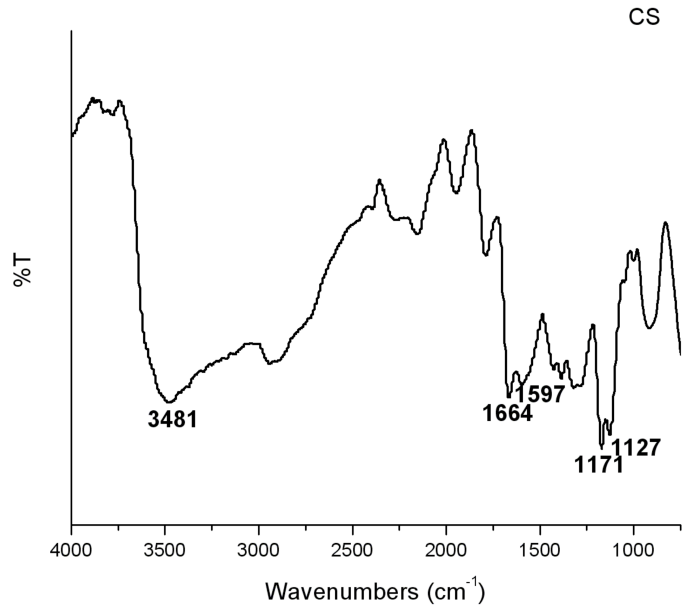

Figure 3-14 FT-IR spectrum of LCS

3.2.2.3 Raman spectroscopy

Figure 3-15 shows the Raman spectrum of LCS. Alcohol C-O stretching vibrations usually occur in the region 1200-1000 cm^{-1} [88]. The peak emerging at 1095

cm^{-1} may be due to C-O stretching vibrations. The peak appearing at 1377 cm^{-1} may be attributed to amide I group in chitosan structure, while the peak at 2892 cm^{-1} may be due to O-H stretching vibration.

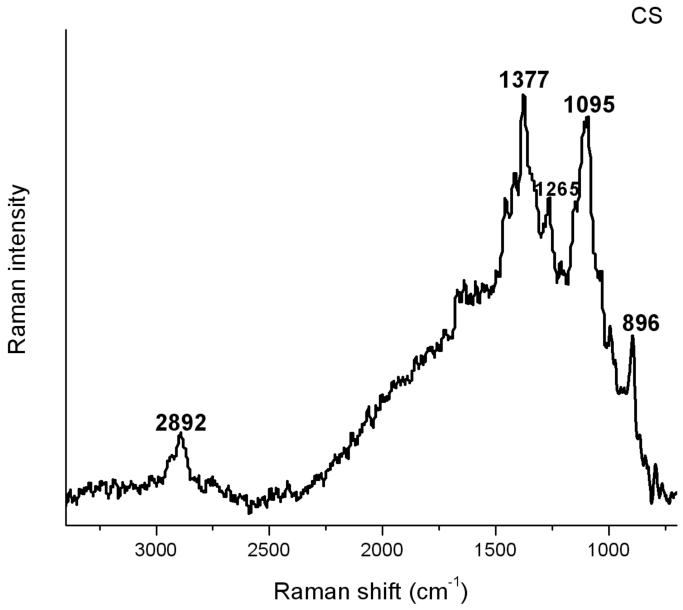

Figure 3-15 Raman spectrum of LCS

CHAPTER 4 METAL-ORGANIC MATRICES ASSOCIATION

4.1 Synthesis of metal-organic matrix complexes

4.1.1 Materials

Cerium (III) chloride heptahydrate ($CeCl_3 \cdot 7H_2O$) (99.99%) and europium (III) chloride hexahydrate ($EuCl_3 \cdot 6H_2O$) (99.99%) were purchased from Aldrich. Uranyl nitrate hexahydrate ($UO_2(NO_3)_2 \cdot 6H_2O$) (98-102%) was purchased from Spectrum Chemical MFG Corporation.

4.1.2 Metal ion solution preparation

1.0 mM metal ion solutions of each metal were prepared by mixing the compounds listed above with DI water, respectively, at room temperature. Nitric acid was used to adjust the pH of $UO_2(NO_3)_2$ solution while hydrochloric acid was used to adjust the pH of $CeCl_3$ and $EuCl_3$ solutions.

4.1.3 Synthesis of metal-polymer complexes

Time effect test

0.01 g of each polymer sorbent was immersed into 5ml of each metal ion solution and the reaction was allowed to take place for up to 7 days. In order to determine the amount of metal ion that remained in solution, solution was taken from the reactor with a syringe after the reaction began at different time intervals (1, 2, 3, 24, 48, 72, 144, 168/hour). The pH was controlled at 3.8 to mimic the actual pH of groundwater at the field test at Oak Ridge National Laboratory.

pH effect test

0.01 g of each polymer sorbent was immersed into 5ml of each metal ion solution, the pH of which ranged from 1 to 6, and the reaction was allowed to take place for 1 day. Then the solution was taken from the reactor through a syringe avoiding contact with the solid polymer matrix.

At low pH, the uranyl nitric solution shows a clear light yellow color, while cerium and europium solutions are transparent. When the pH reaches 6, precipitates begin to form in all the solutions due to metal hydrolysis occurring during the mixing procedure. Figure 4-1 shows the color change for uranyl nitric solution. Figure 4-2 shows the color change for the cerium solution.

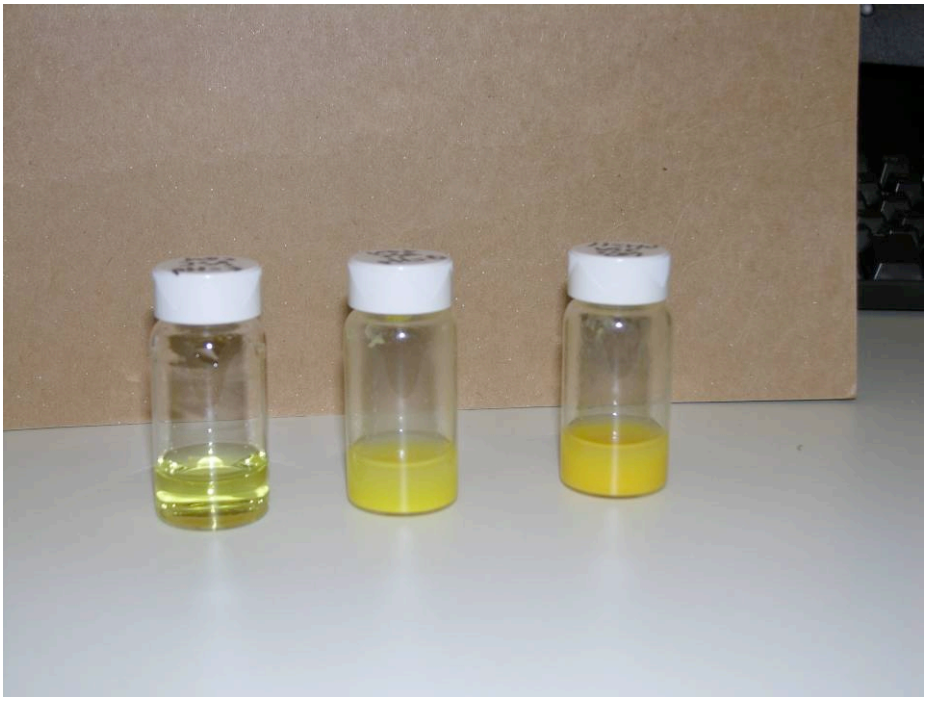

Figure 4-1 Color changes for uranyl nitric solution at pH 3 (left), pH 6 (middle) and pH 11 (right)

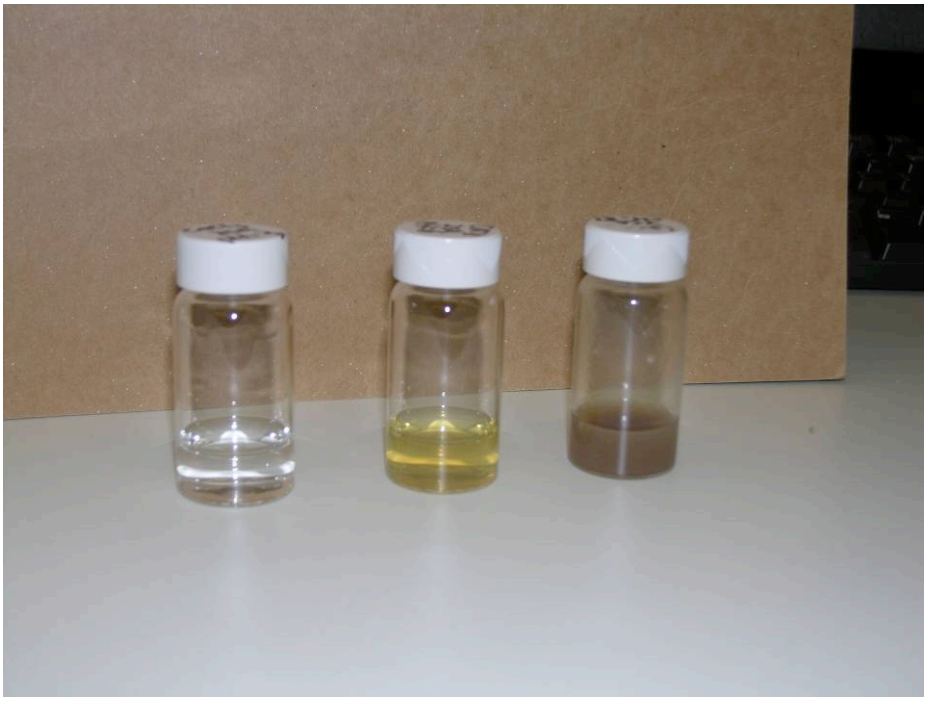

Figure 4-2 Color changes for cerium solution at pH 3 (left), pH 6 (middle) and pH 11 (right)

4.2 Characterization results and discussion

4.2.1 SEM

Figures 4-3, 4-4, 4-5 and 4-6 show the surface morphology of the selected polymer matrices before and after their reaction with metal ion solutions at pH 3. The morphologies of E-OC and OC have not been changed essentially after the reaction with the metal ion solutions; however, minor surface alterations are observable. Instead of the original fibrous and segregated structure, OC fibers show a more agglomerated structure of larger size after the exposure, which is less obvious in E-OC matrices. This supports the conclusion that electrospun materials retain their structural integrity when used for water remediation. This helps to make them attractive for field application in acidic conditions, as they would retain a permeable structure less likely to limit flowthrough of groundwater over time. No significant structural change can be observed on either HCS or LCS matrices after their reactions with U and Eu solutions; however, crystallized structures have occurred both in HCS and LCS after their exposure to Ce solutions, in which a tabular structure dominates the entire matrices. This phenomenon may be due to the nucleation and growth of Ce-containing mineral crystals on chitosan matrix.

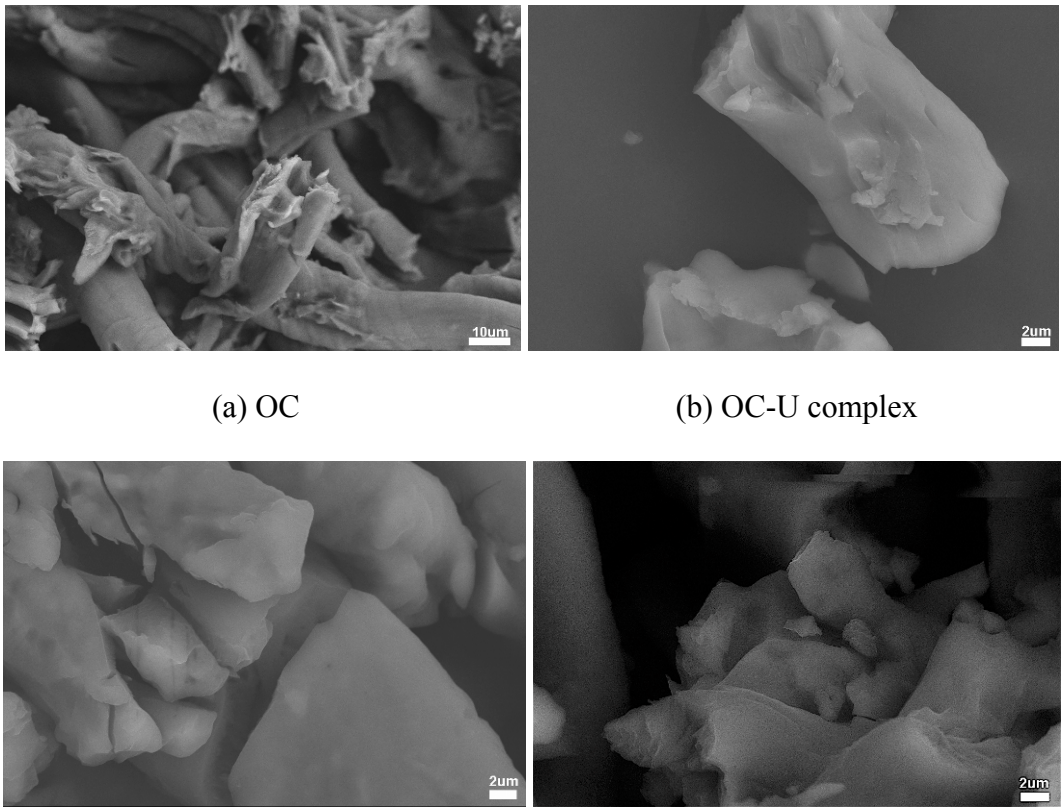

(a) OC (b) OC-U complex

(c) OC-Eu complex (d) OC-Ce complex

Figure 4-3 SEM micrographs of (a) OC; (b) OC-U complex; (c) OC-Eu complex; (d) OC-Ce complex

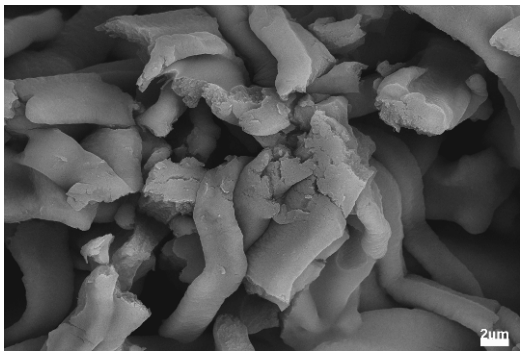

(a) E-OC

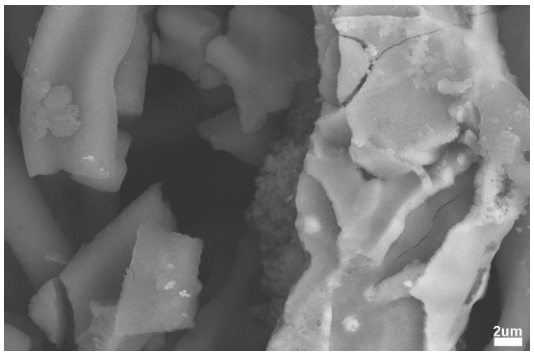

(b) E-OC-U complex

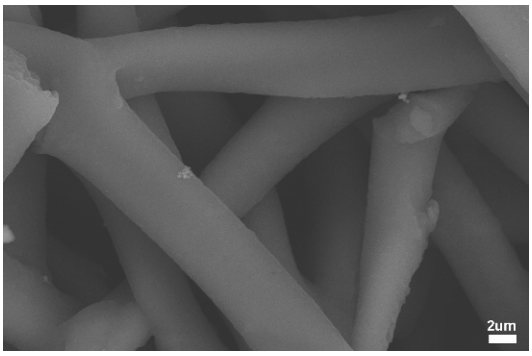

(c) E-OC-Eu complex

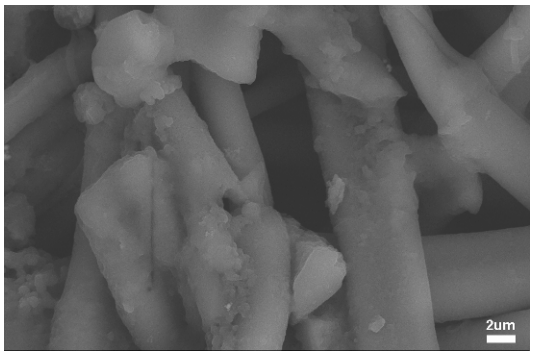

(d) E-OC-Ce complex

Figure 4-4 SEM micrographs of (a) E-OC; (b) E-OC-U complex; (c) E-OC-Eu complex; (d) E-OC-Ce complex

(a) HCS

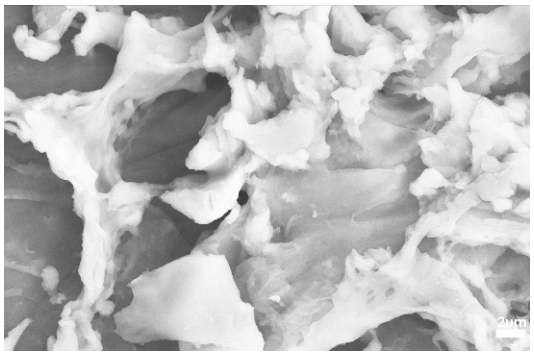

(b) HCS-U complex

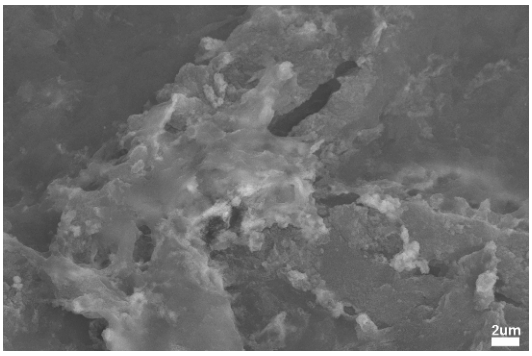

(c) HCS-Eu complex

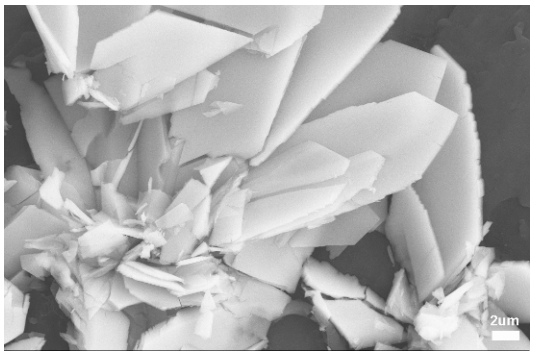

(d) HCS-Ce complex

Figure 4-5 SEM micrographs of (a) HCS; (b) HCS-U complex; (c) HCS-Eu complex; (d) HCS-Ce complex

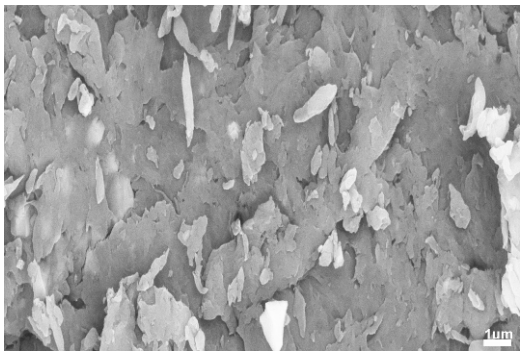

(a) LCS

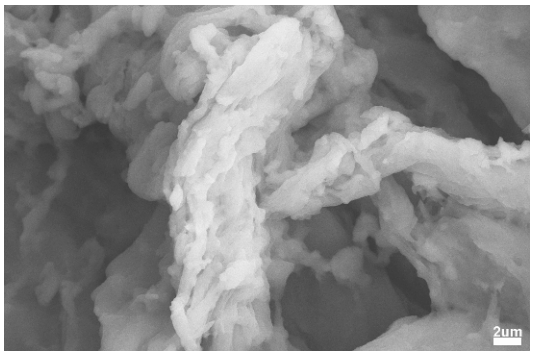

(b) LCS-U complex

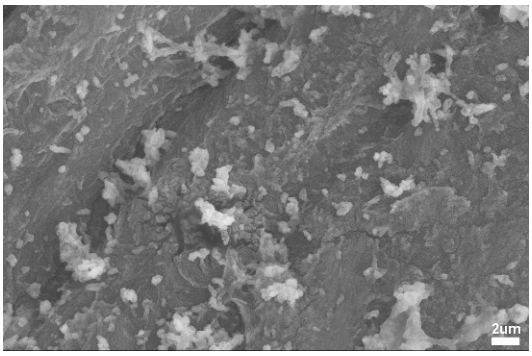

(c) LCS-Eu complex

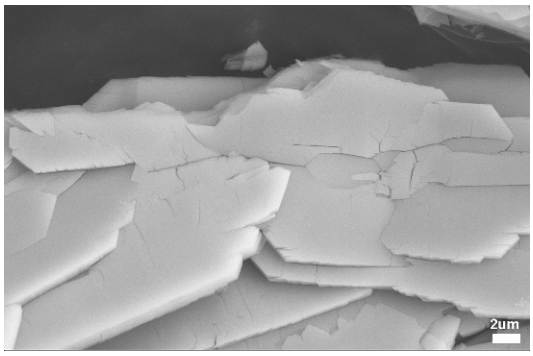

(d) LCS-Ce complex

Figure 4-6 SEM micrographs of (a) LCS; (b) LCS-U complex; (c) LCS-Eu complex; (d) LCS-Ce complex

4.2.2 FT-IR spectroscopy

At pH 3.8, uranyl nitric 1 mM solution shows a transparent light yellow color. No precipitate forms after adding E-OC. A very strong band typically occurs in the region 1695–1540 cm^{-1} for carboxylic acid salts due to the asymmetric stretching vibration of COO^{-}, and a broad band of medium intensity appears in the range 1440–1335 cm^{-1} due to the symmetric stretching vibration of the same group, and generally has two or three peaks [88]. Figure 4-7 shows the infrared spectrum of E-OC–U complexes at pH 3.8 before (b) and after (c) DI water rinse, together with the original E-OC spectrum (a). A new absorption band, which occurs at 924 cm^{-1}, can be assigned to the asymmetric stretching vibration of UO_2^{2+}. The intensity of this band decreases after the water rinse, which can be taken as evidence that some amount of UO_2^{2+} was in fact physically or weakly bond to E-OC. The intensity of the absorption band at 1727 cm^{-1} (C=O stretching vibrations of the carboxylic group) decreased since a portion of COOH groups were converted to COO– during the complexation process [90]. The broad peak at 1599 cm^{-1} may be assigned to the formation of COO—UO_2^{2+} groups.

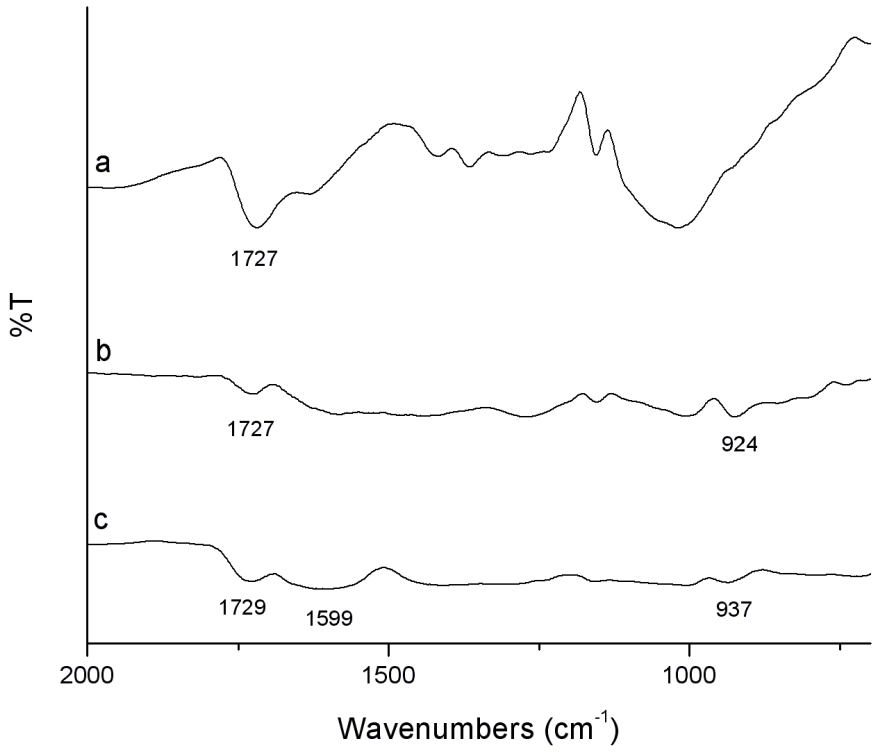

Figure 4-7 FT-IR spectra of (a) E-OC; (b) E-OC-U complex without water rinse; (c) E-OC-U complex after water rinse

Similar phenomena took place during the formation of E-OC–Ce and E-OC–Eu complexes (Figure 4-8). In both cases, formation of peaks associated with a COO— metal ion complex were noted (1588 cm^{-1} and 1597 cm^{-1} for E OC–Ce and E-OC–Eu, respectively), retained following a water rinse. The spectra for OC–Ce and OC–Eu showed similar evidence of COO—metal complexation, though the features were less distinct. This may be due to instrument and sample configuration factors, resulting in overall more IR sorption by the sample.

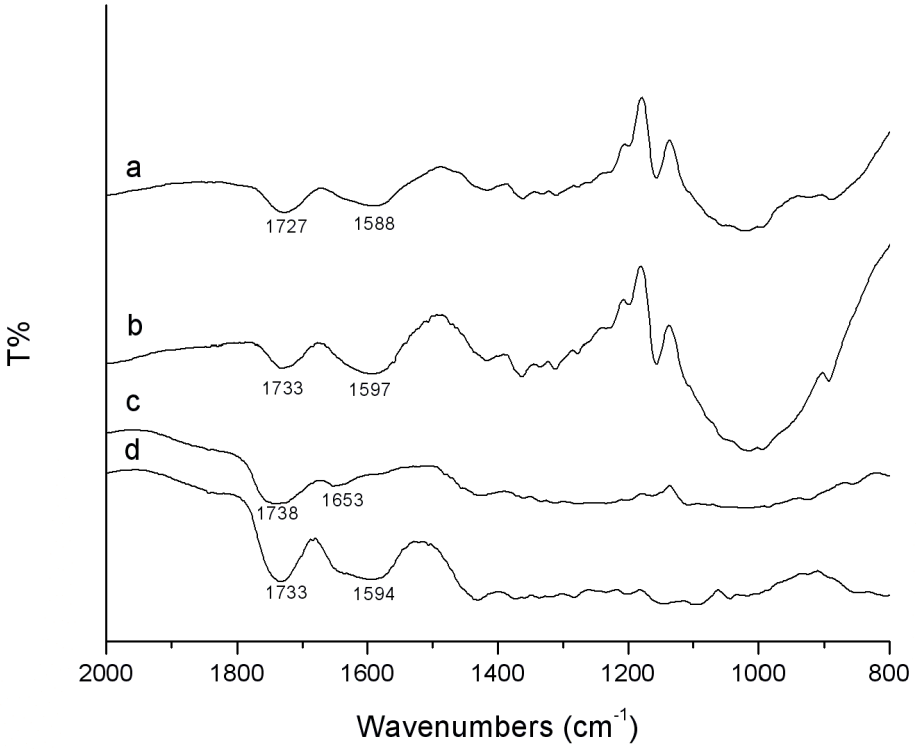

Figure 4-8 FT-IR spectra of (a) E-OC–Ce complex; (b) E-OC–Eu complex; (c) OC–Ce complex; (d) OC–Eu complex

Figure 4-9 shows the FT-IR spectra of HCS and its complexes with the selected metal ions. The characteristic absorption band of saturated primary amines can be usually located in the range of 1650-1580 cm^{-1} [70, 88], which in figure 4a appears at 1588 cm^{-1}, the descriptive band of $–NH_2$ in chitosan. Due to the high degree of deacetylation (more than 85%) of the chitosan used in this study, the amide band can be located at 1662 cm^{-1} in the spectrum [89]. The changes in the $–NH_2$ band occurring after the exposure to metal ion solutions serves as evidence of its role as the sorbent site for the metal ions during the reaction. HCS-U shows the most overall broadening and loss of definition in the region in question, which may be related to H-bonding between N and

UO_2^{2+}. HCS-Ce shows the second greatest change, which may indicate some degree of amine-metal ion interaction in the complex. This observation is consistent with the sorptive capacity of LCS/HCS for Ce as indicated by Figure 4-14 (b).

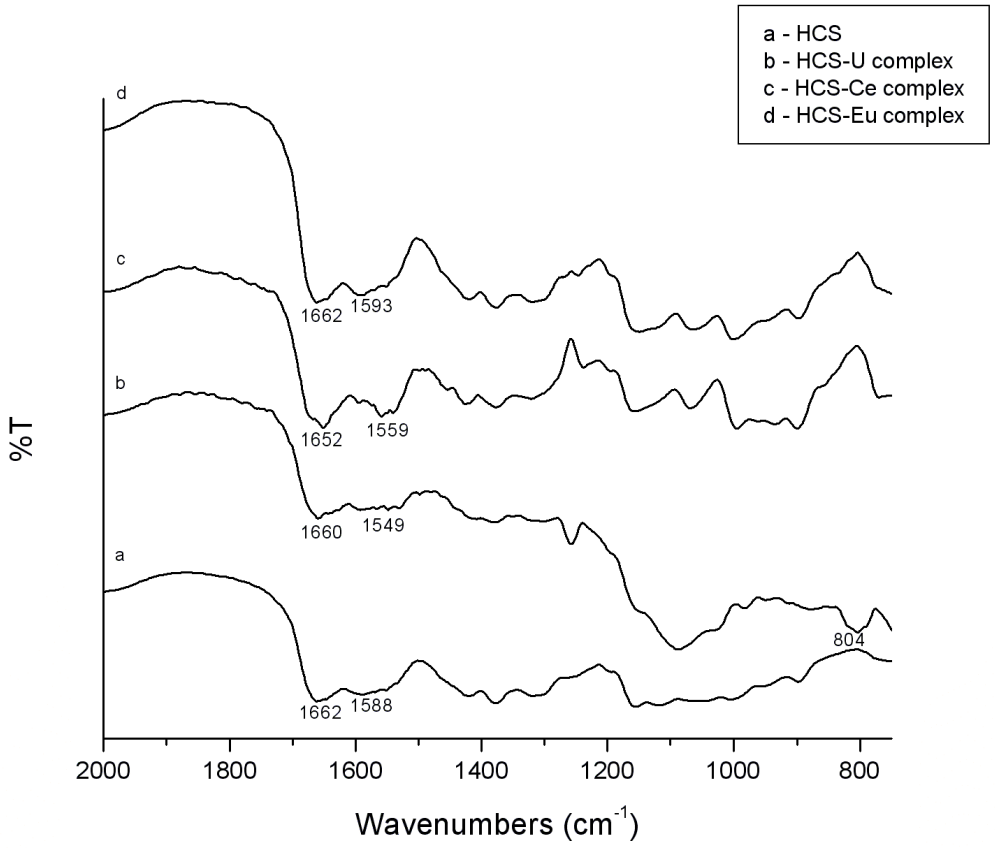

Figure 4-9 FT-IR spectra of HCS and its complexes with metal ions

4.2.3 Raman spectroscopy

Figure 4-10 shows the Raman spectra of the E-OC–U complex and E-OC. The band at 862 cm^{-1} is attributed to the symmetrical stretching vibration of UO_2^{2+} [91]. The lack of intensity at 853 cm^{-1} (15) suggests that little or no uranyl hydrolysis species $(UO_2)_2(OH)_2^{2+}$ was formed during the complexation process as would be expected at pH

3.8. The vanishing of the peak from the C=O group at 1736 cm–1 reinforces the conclusion that the complexation process causes conversion of carboxylic groups to COO—metal complex; because most of COOH groups were converted to COO–, the few remaining COOH groups could not be detected by Raman.

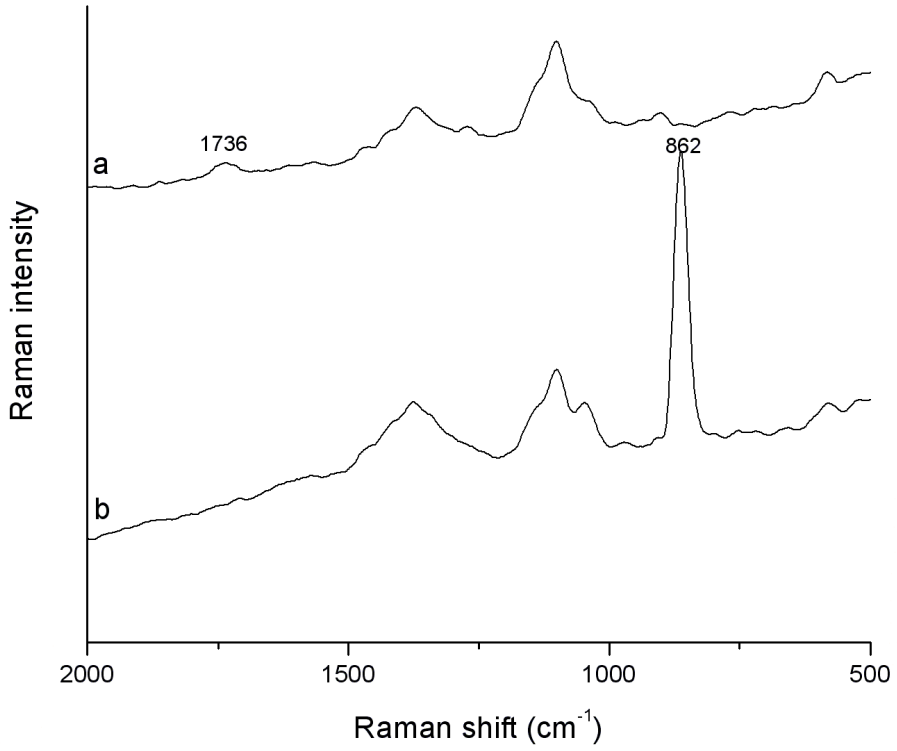

Figure 4-10 Raman spectra of (a) E-OC and (b) the E-OC–U complex at pH 3

4.3 Direct Current Argon Plasma Atomic Emission Spectrometer (DCP-AES)

Elemental analyses were carried out with an ARL Spectraspan VB Direct Current Argon Plasma Atomic Emission Spectrometer (DCP-AES). This system uses a Czerny-Turner spectrometer with an Echelle grating and 30° prism for order separation. At 400 nm reciprocal linear dispersion is 0.122 nm/mm and for a 25 microns entrance slit, spectral bandpass is 0.0030 nm.

Analyses were performed in single element mode, using standard settings and a solution flow rate of 0.5 ml/min. Emission lines used for analyses were U (409.014 nm), Eu (466.188 nm) and Ce (418.660 nm). Standards used for calibration for Ce, Eu and U analyses were prepared from commercially available single element 1000 ppm emission spectroscopy stock solution standards prepared in 1-2% nitric acid. Net counts were calibrated using a "two-point" calibration system involving a blank and a high standard that was prepared to be slightly more concentrated than the highest concentration sample, thus bracketing the concentration range of the samples. Three to four additional standards, spanning the full concentration range of the samples, were also prepared and run as "unknowns" to confirm linear calibration curves and to monitor reproducibility. Samples were run in duplicate.

4.3.1 Sorption of metal ion with time

The following figures show the DCP-AES data for the concentration of metal ions remaining in the solution after a certain period of reaction time (Time Factor determination).

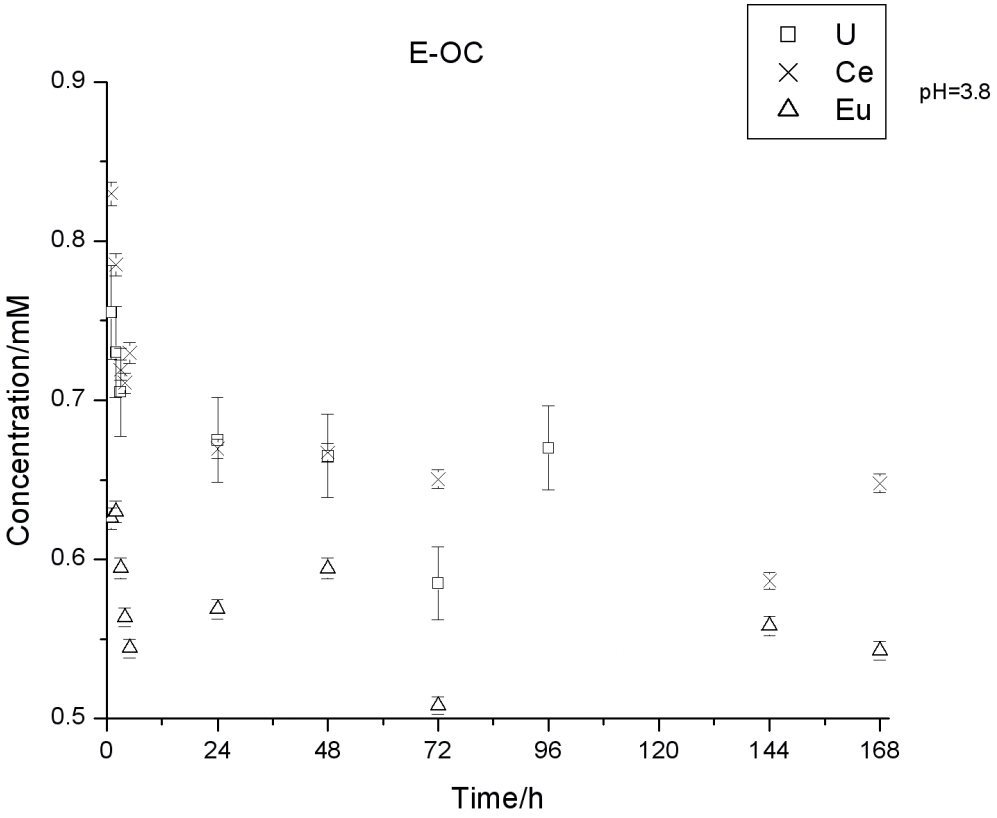

(a) E-OC

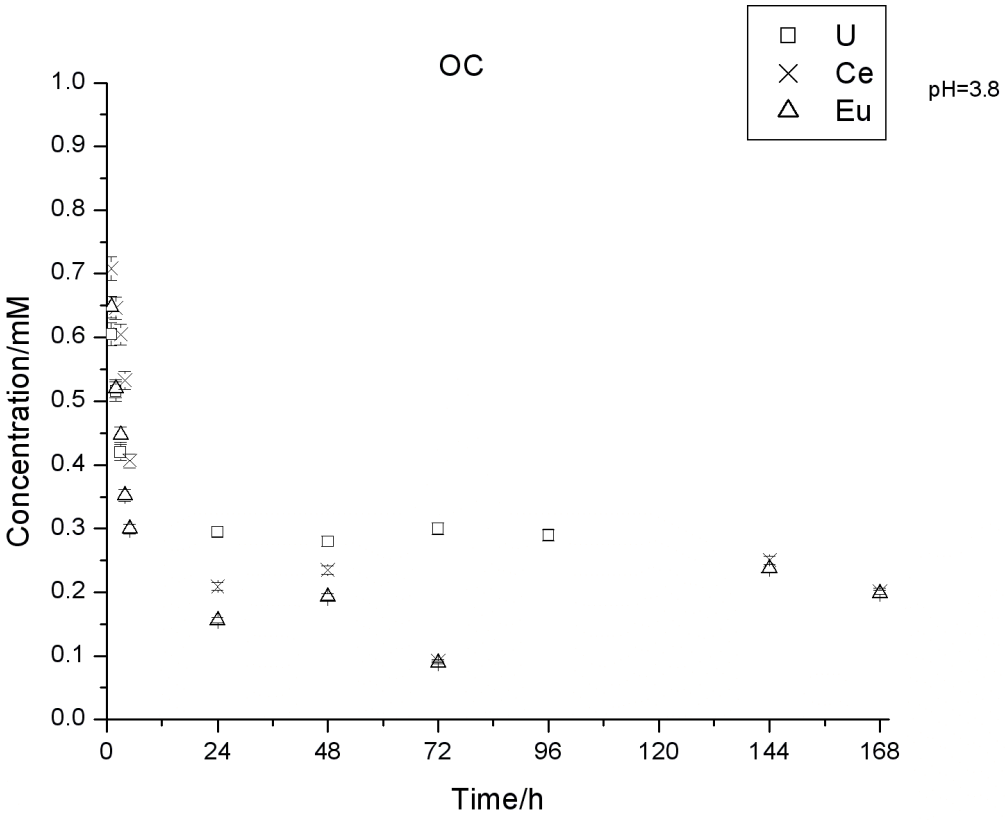

(b) OC

Figure 4-11 Contact time factor experiment-cellulosic matrices

With the pH of the reaction environment set at 3.8 in order to represent a highly mobile condition for metal ion transport and to mimic the acidic condition of the radioactively contaminated flow plume at Department of Energy's Oak Ridge Field Research Center (ORFRC), the four selected polysaccharide matrices were tested for their adsorption capabilities on three different types of metals, U (radionuclide), Ce and Eu (analogs for transuranic metal ions). Proper filtration materials and PRB filler alternatives should possess the capacity for removing metals to acceptable levels under a

certain period of time and to retain these metals. The experiments were set to allow the reaction between the matrices and metal ions to take place for up to 7 days.

Figure 4-11 a and b show the concentration of metal ions remaining in solution after the exposure to E-OC and OC decreases with increasing time. It is worthy to note that the initial three hours during the reaction is crucial for adsorption. The majority of metal ions were adsorbed onto the matrices in the first few hours, after which time the concentration in the solution tends to level off, though slight fluctuations can be observed. This indicates that the reaction between modified cellulosic matrices and selected metal ions is rapid. The capability of adsorption of E-OC for the three selected metals is nearly the same with the final reduced concentration of the solution approximately 0.6 mM (Figure 4-11a), while OC is demonstrated to possess more effective capability for adsorption of these metals with the final reduced concentration of the solution around 0.2 mM (Figure 4-11b).

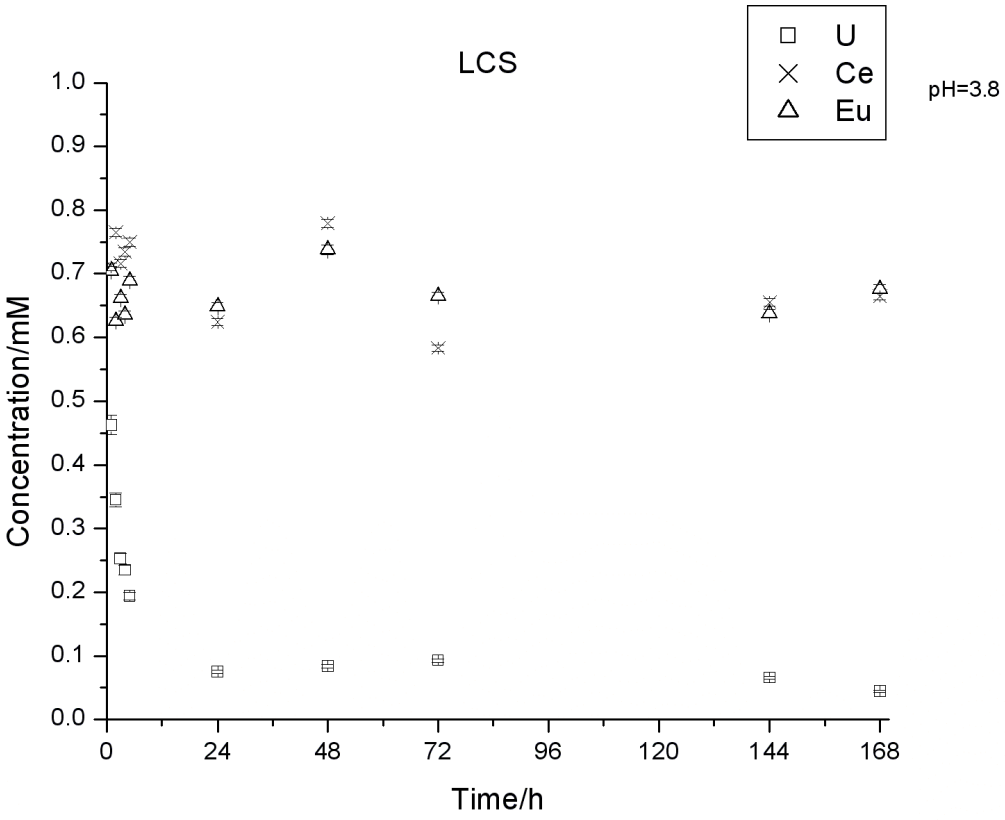
LCS
U
Ce
Eu
pH=3.8
Concentration/mM
Time/h
0.0
0.1
0.2
0.3
0.4
0.5
0.6
0.7
0.8
0.9
1.0
0
24
48
72
96
120
144
168

(a) LCS

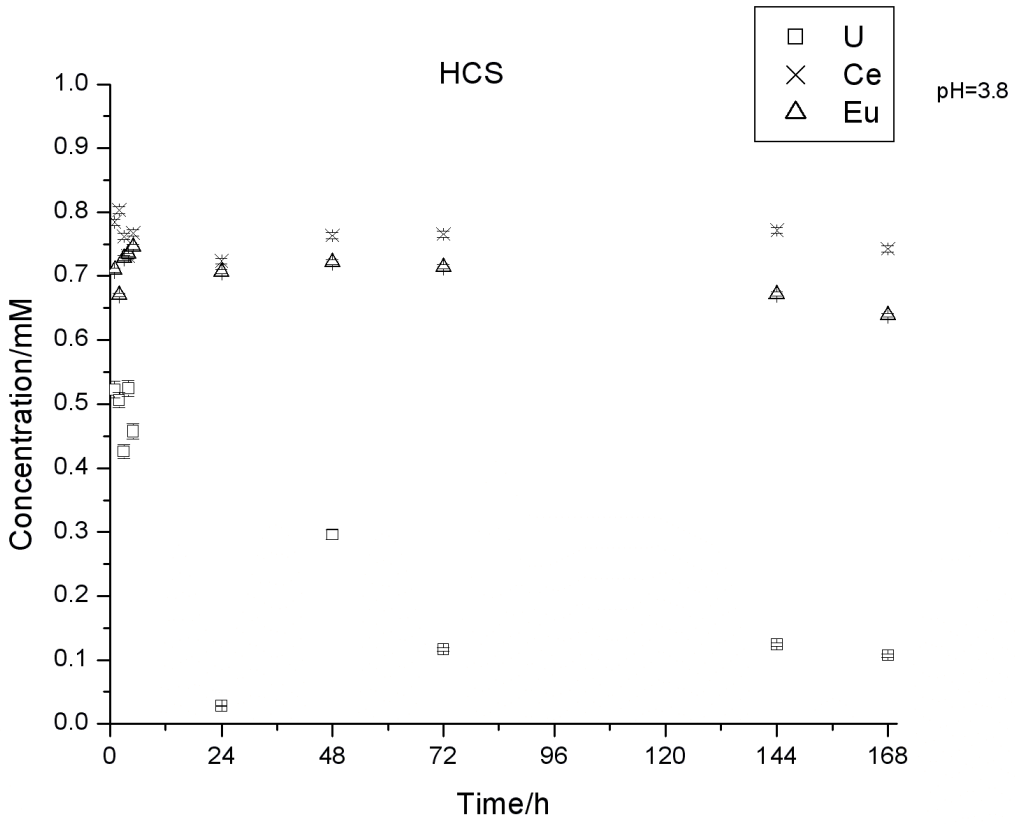

(b) HCS

Figure 4-12 Contact time factor experiment-chitosan matrices

Both LCS and HCS can be seen in Figure 4-12a and b to be satisfactory chelators for uranyl ions, and less satisfactory for Ce and Eu. As with OC, the initial few hours were crucial resulting in U uptake by around 20% (LCS) and 42% (HCS). With increasing reaction time, the concentration of uranyl ions in solution continued to decrease. The most U uptake by HCS took place at 24 h, with roughly 97.3% of the uranyl ion being adsorbed by the matrix. However, some of the adsorbed uryanl ions began to leach back into the solution after this particular time, and the solution

concentration reached another low point at 10.7% on day 7. Any leaching was much less pronounced in the case of the LCS, with the lowest concentration of solution, 4.43%, being reached on day 7.

It is postulated to be the free doublets of nitrogen atoms in amino groups contained in the chitosan structure that are responsible for polymer-metal complexation [70]. Piron et al. have proposed a "pendent model" mechanism of chitosan-uranyl ion complex formation, in which the complexation between chitosan and uranyl ion is neutral (not electrostatic) and the UO_2^{2+} is coordinated to the amino group in chitosan, two hydroxyls and another site being either a water molecule or a hydroxyl group on the chitosan chain [70].

The comparison amongst the four polymeric matrices shows that chitosan represents a more effective matrix in adsorbing U, probably due to the pendent model structure it possesses. The lack of this structure in the case of adsorption of both Ce and Eu may explain the reason why the adsorption of the two metals was not as effective as U. On the other hand, OC was demonstrated to be more effective in adsorbing Ce and Eu, most likely because of the greater carbonyl content of the structure as compared to E-OC.

4.3.2 Affect of pH variation on metal ion sorption

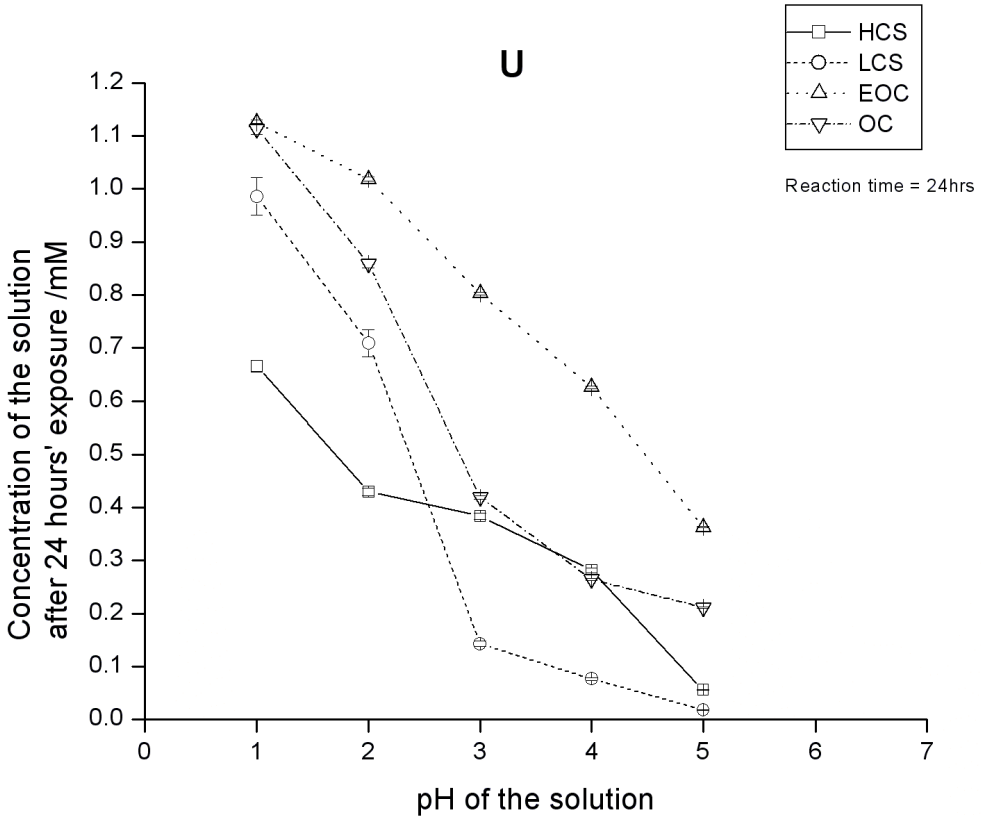

(a) U

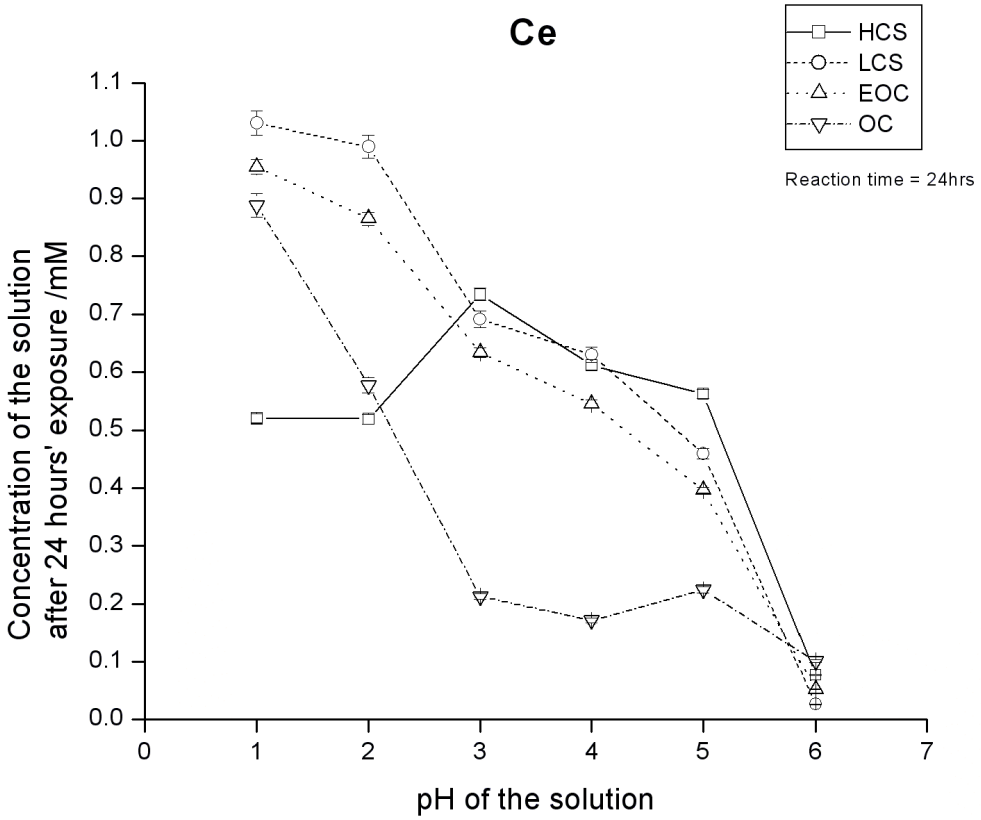
Ce
HCS
LCS
EOC
OC
Reaction time = 24hrs
Concentration of the solution after 24 hours' exposure /mM
pH of the solution
0.0
0.1
0.2
0.3
0.4
0.5
0.6
0.7
0.8
0.9
1.0
1.1
0
1
2
3
4
5
6
7

(b) Ce

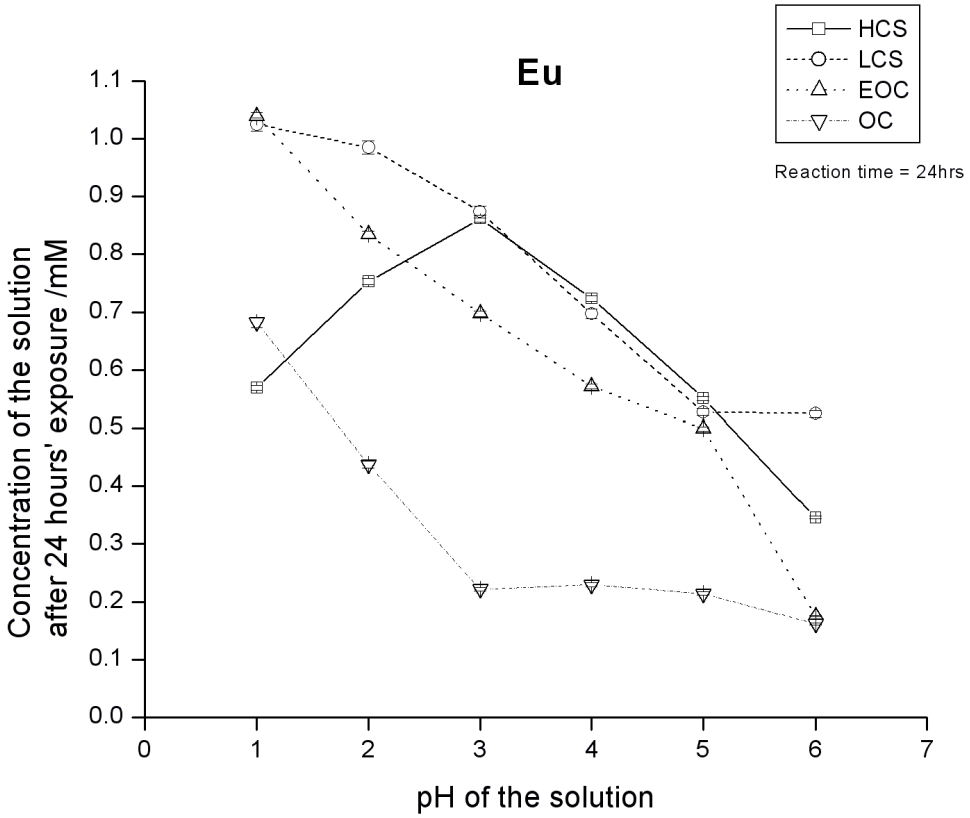

(c) Eu

Figure 4-13 DCP result of variation on metal ion sorption

The pH of the reaction environments was controlled to vary from 1 to 6, except for uranyl solution, for which precipitation generally occurs after a few days at pH 6. Exposure of metal ions and the selected matrices was allowed to take place for 24 hours. From Figure 4-13, it is clear that higher pH environments boost the adsorption of metal ions onto the polysaccharides in all experiments. HCS and LCS, at pH 5, show greater capacity for sorption of uranyl than their counterparts, E-OC and OC; however, cellulosic materials are more effective in taking up Eu at pH 6. No significant adsorption difference

was observed in uptake of Ce at pH 6. For both Eu and Ce, OC is the best sorbent from pH 3-5, though for Ce, LCS is the most effective matrix at pH 6. At very low pH, 1-2 for Ce and 1 for Eu, HCS is the best chelator for metal ions. This may be due to the charge on chitosan functional groups at low pH resulting in electrostatic interaction between amine and metal cations. The trend that the amount of adsorbed uranyl increases with increasing pH may corroborate the theory of the "pendent model" of chitosan-uranyl complex formation, because the two hydroxyl groups that are coordinated to UO_2^{2+} are more stable at higher pH, resulting in a more stable structure overall for uranyl chelation to the polysaccharide chain.

4.4 Summary of adsorption capabilities of the selected polysaccharides on U, Eu, and Ce

4.4.1 pH effect

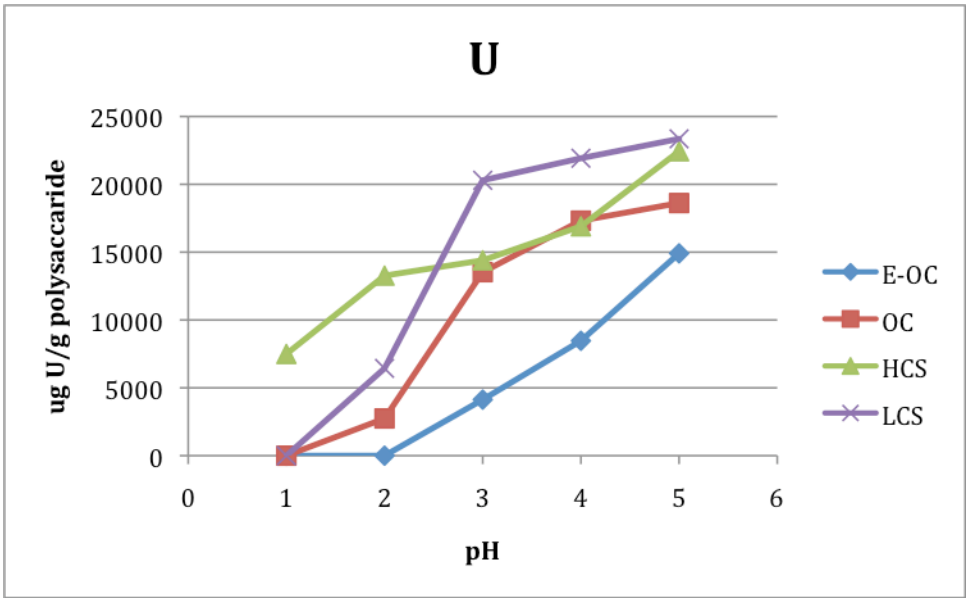

Figure 4-14 pH effect on adsorption capability of the selected polysaccarides on U

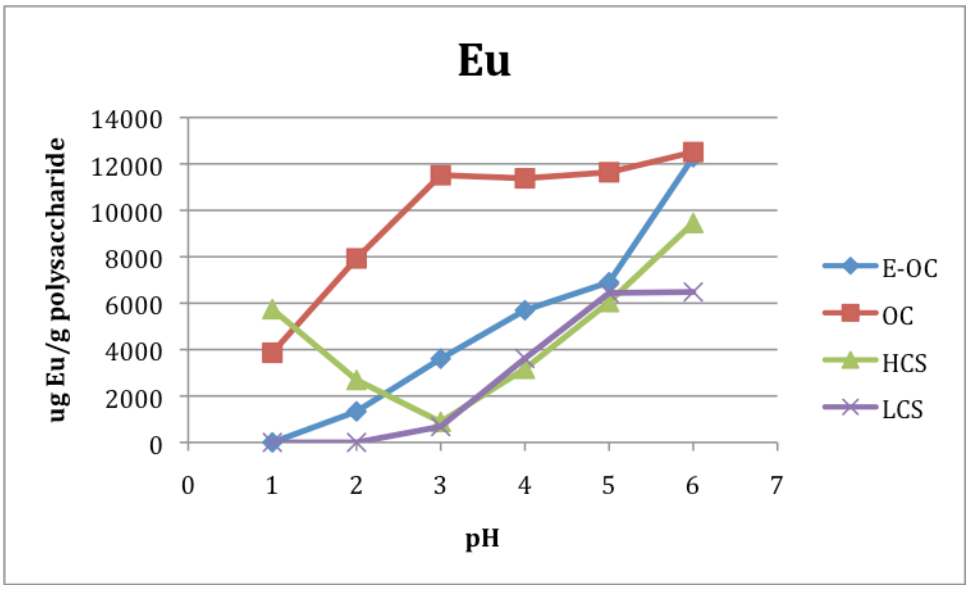

Figure 4-15 pH effect on adsorption capability of the selected polysaccarides on Eu

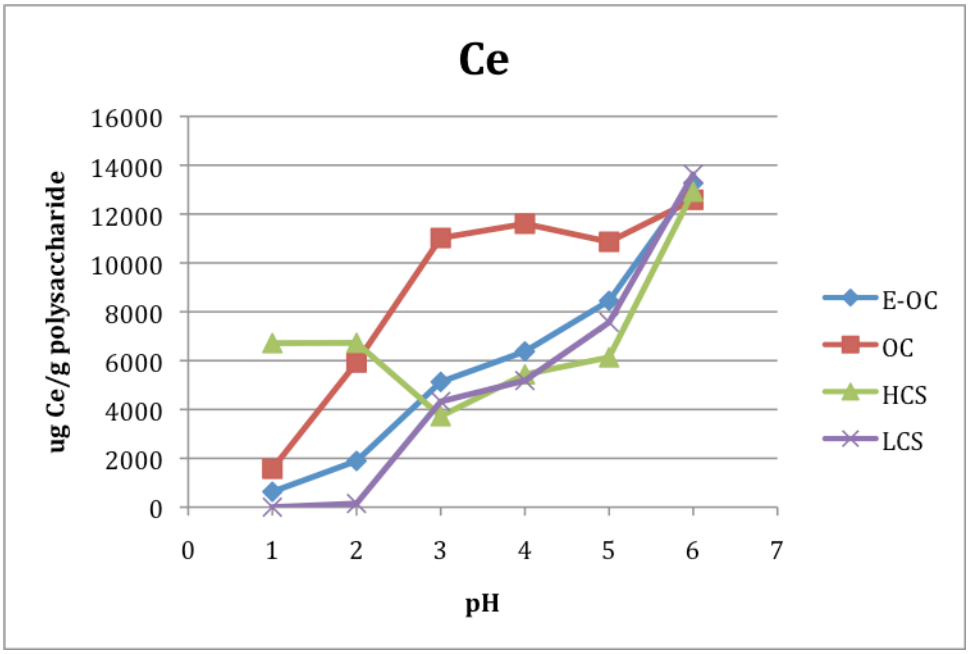

Figure 4-16 pH effect on adsorption capability of the selected polysaccharides on Ce

Figures 4-14, 4-15, and 4-16 show the pH effect after one hours' reaction on adsorption capability of the selected polysaccharides (E-OC, OC, HCS, and LCS) on tested metals, U, Eu, and Ce. For example, at pH 3, 0.01 g of E-OC was able to remove 3.61×10^{-4} g of U from the solution after one hour.

4.4.2 Time effect

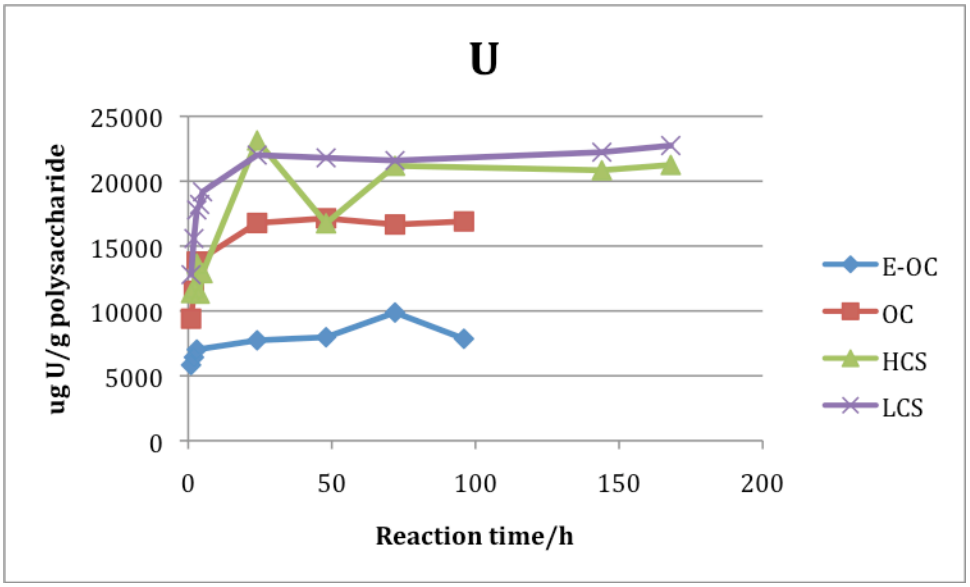

Figure 4-17 Time effect on adsorption capability of the selected polysaccarides on U

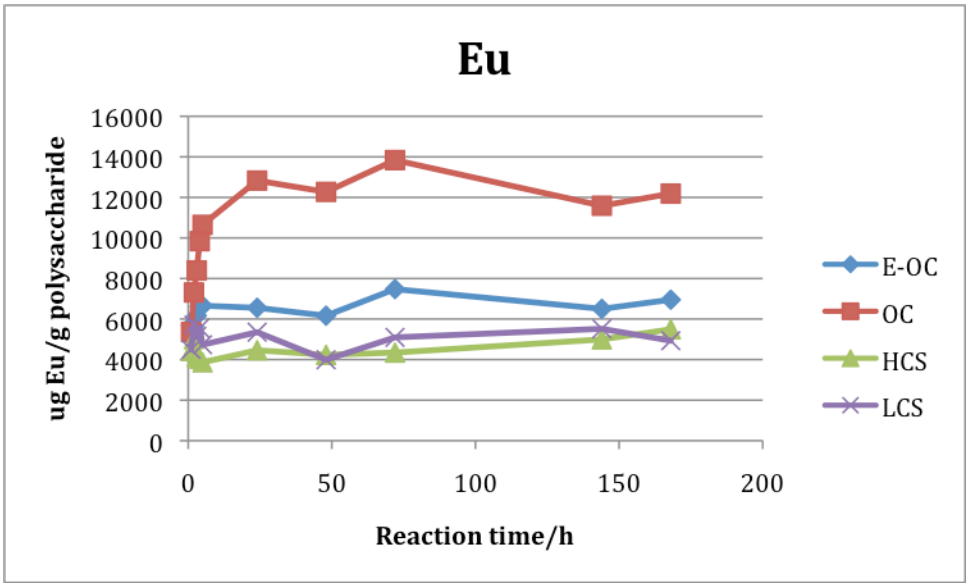

Figure 4-18 Time effect on adsorption capability of the selected polysaccarides on Eu

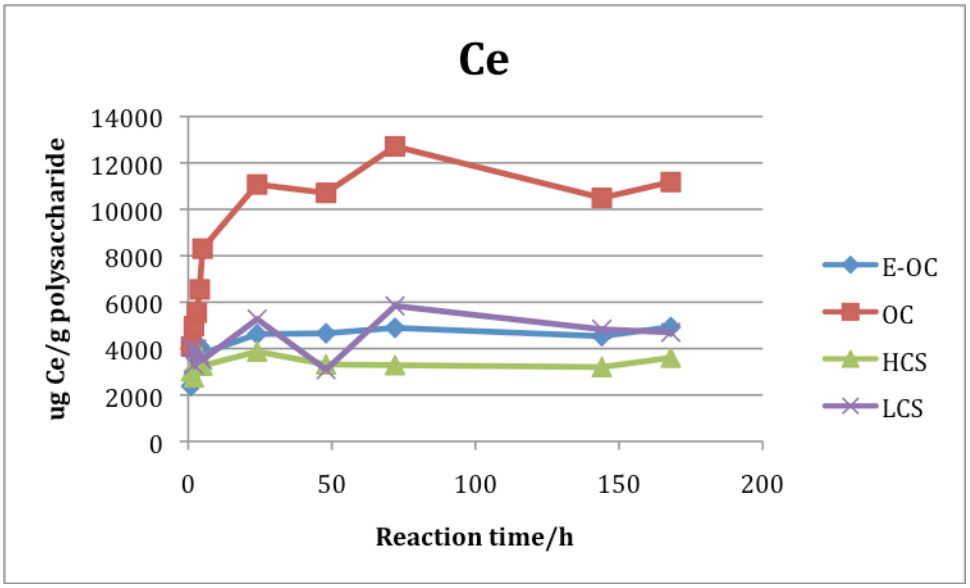

Figure 4-19 Time effect on adsorption capability of the selected polysaccarides on Ce

Figures 4-17, 4-18, and 4-19 show the time effect at pH 3 on adsorption capability of the selected polysaccharides (E-OC, OC, HCS, and LCS) on tested metals, U, Eu, and Ce. For example, at pH 3 and after 5 hours' reaction, 0.01 g of OC was able to remove 8.30×10^{-4} g with standard deviation 8.12×10^{-6} of Ce from the solution.

CHAPTER 5 MOLECULAR MODELING

5.1 Introduction of Molecular Modeling

As stated earlier, uranium is a frequently reported radionuclide found in contaminated groundwater and soil in both military and civil nuclear processing facilities. Remediation research involves chemical and bio- remediation processes. Combined with experimental data, molecular level studies can give researchers a clear view of the "understanding and information about the microscopic mechanisms of the complexation and speciation, the adsorption to surfaces of minerals, and the mechanisms for changing between species; the data obtained at the microscopic level can be used to develop macroscopic adsorption models for predicting the migration or transport of uranium [92]." When the experiments are extremely expensive or dangerous, the theoretical methods can therefore be the replacement of the real experiments.

Molecular modeling in fact is the combination of theoretical methods and computational techniques to simulate the activities of molecules. Many scientific fields such as computational chemistry, computational biology and materials science use molecular modeling technique in order to carry out the research on molecular systems.

Different from quantum chemistry where electrons are considered explicitly, molecular modeling however, describes molecular systems on atomistic level and therefore, atoms are the smallest units. The atomic interactions are described by both spring-like interactions and van der Waals forces. Not only can molecules be modeled in a vacuum, but they can also be modeled in a solvent chemical environment [93, 94].

Gaussian molecular modeling program was used throughout this research to provide theoretical standards to complement experimental data yielded from FT-IR and Raman spectroscopy. *Gaussian* is a powerful program, which is able to provide researchers with predicted properties of both molecules and reactions between molecules, such as IR and Raman spectra, NMR shifts, vibrational frequencies, molecular energies and structures, bond and reaction energies, etc [95]. Theoretical calculations can be performed under either gaseous or solution conditions, and in either stable ground state or excited state [95].

Based fully or partially upon the fundamental laws of physics, chemical structures of molecules and reactions between them can be simulated numerically by computational chemistry [95]. Molecular mechanics and electronic structure theory are two major areas in computational chemistry, both of which perform same calculations, including computation of energy of a particular molecular structure , geometry optimization calculation, and computation of vibrational frequencies of molecules [95].

Molecular mechanics uses classical physics to make predictions of properties and structures of molecules, based upon characterization by a particular force field. A force field comprises three components, including a set of equations, a series of atom types, and one or more parameter sets. Electrons are neglected during the simulation, while the

calculation is based only on nuclei interactions. Molecular mechanics computation is very inexpensive, and can be used for huge systems. Limitation of molecular mechanics can be found in its ability to use only certain types of molecules, and also its inability for performing calculations on a system in which electronic effects prevail due to its neglect of electrons in calculations [95].

Different from molecular mechanics methods, electronic structure methods use quantum mechanics as the basis instead of classical physics. By solving the Schrödinger equation, $H\Psi=E\Psi$, properties and energy of a molecular may be obtained. However, it is impractical to obtain exact solutions; therefore, different mathematical approximations need to be applied into calculations. Semi-empirical methods and ab initio methods are two major electronic structure methods. Semi-empirical methods apply parameters obtained from experiments to simplify the computation. Different from semi-empirical methods, ab initio methods use pure quantum mechanics laws, and some physical constants, including the speed of light, the masses and charges of electrons and nuclei, and Planck's constant [95].

The selection of the methods is based upon the needs. Semi-empirical methods are fairly inexpensive and are able to provide reasonably good results. While ab initio methods are capable of providing high quality result, but require better CPU performances [95].

In addition to semi-empirical and ab initio electronic structure methods, a third type method, density functional methods (DFT), has recently become more widely used. DFT methods, requiring approximately the same amount of Hartree-Fock theory computation resources (the least expensive ab initio method), are similar to ab initio

methods in many aspects. Effects of electrons are included in the DFT methods, which can provide the same accuracy which more expensive ab initio methods can provide with less computational resources [93].

A combination of theoretical procedure and basis set must be specified in model chemistries. A theoretical procedure corresponds to a specific approximation method based on levels of theory. A more accurate method requires a more expensive computation. A basis set is chosen to restrict each electron to a particular region of orbital space. A larger basis set restricts electrons less and reflects a system closer to reality [95]. Table 5-1 lists commonly used theories. Table 5-2 lists commonly used basis sets.

Keyword	**Method**	**Availability**
HF	Hartree-Fock Self-Consistent Field	Through 2nd derivatives
B3LYP	Becke-style 3-Parameter Density Functional Theory (using the Lee-Yang-Parr correlation functional)	Through 2nd derivatives
MP2	2nd Order Møller-Plesset Perturbation Theory	Through 2nd derivatives
MP4	4th Order Møller-Plesset Perturbation Theory (including Singles, Doubles, Triples and Quadruples by default)	Energies only
QCISD(T)	Quadratic CI(Single, Doubles & Triples)	Energies only

Table 5-1 Commonly used *Gaussian* approximations [95]

Basis set [Applicable Atoms]	Description	# Basis Functions		Default Function Types
		1st row atoms	Hydrogen atoms	
3-21 G [H-Xe]	Split valence: 2sets of functions in the valence region provide a more accurate representation of orbitals. Use for very large molecules for which 6-31 G(d) is too expensive	9	2	6D
6-31 G(d) 6-31G* [H-Cl]	Adds polarization functions to heavy atoms: use for most jobs on up to medium/large sized systems. (This basis set uses the 6-component type d functions.)	15	2	6D 7F
6-31+G(d) [H-Cl]	Adds diffuse functions: important for systems with lone pairs, anions, excited states.	19	2	6D 7F

Table 5-2 Commonly used basis sets [95]

5.2 Computational methods and Results

5.2.1 Computational methods

Hybrid density functional theory (DFT) calculations were performed on all model systems using the program *Gaussian* 03 [98]. The basis set 6-31G9d,p) [99-102] was used for atoms H, C, and O. The Stuttgart pseudopotential ECP60MWB and the

corresponding ECP60ANO basis set [103-104] were used for atom U. The Becke 3-parameter exchange [105-106] and Lee, Yang and Parr [107] correlation functionals were used for energy minimizations, Gibbs free energy calculations, and frequency analysis. All atoms were allowed to relax during energy minimizations, and no symmetry constraints were applied. The starting configuration of each model was obtained by drawing the structure using the program Cerius2 from Accelrys Inc., San Diego, CA. Frequency calculations and thermodynamics were performed at 298.15 K.

5.2.2 Results

Figure 5-1 shows the calculated molecular structures of cellulose (a), chitosan (b), OC (c), and OC- UO_2^{2+} complex (d), respectively, after energy and geometry optimizations. Only a few units were included in the calculations for polymeric materials. Figure 5-2 and Figure 5-3 show the calculated IR and Raman spectra of the aforementioned compounds, respectively. *Gaussian* is also capable of presenting motions of bonds. One example is shown in Figure 5-4, in which O-H stretching vibration can be observed.

The calculated IR spectrum of OC was compared with the one yielded from the experiment. Table 5-3 summarizes the main bands with the assignments by observing the animations provided by *GaussView*. Figure 5-5 shows the agreement between the calculated IR frequencies and those observed from the experiment for OC. It is clear that agreement to some degree is well presented. The difference between the predicted and experimental data may be because (1) lack of the CH_2OH group in the predicted structure

of OC; (2) the water and CO_2 in the chemical environment is not taken into consideration in the calculation.

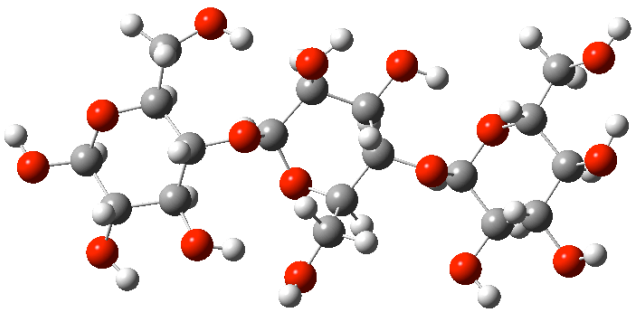

(a) Cellulose

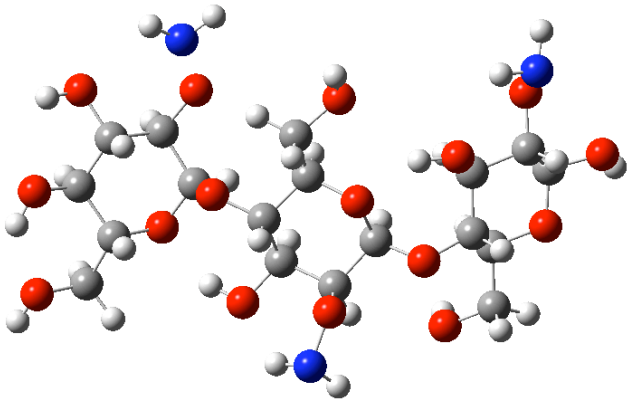

(b) Chitosan

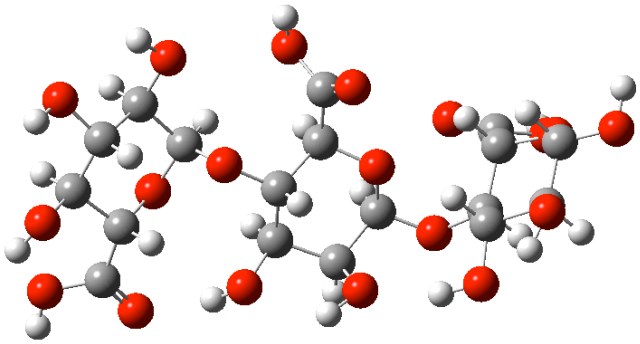

(c) OC

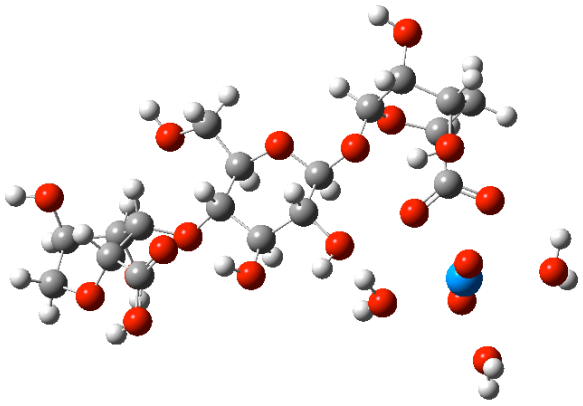

(d) OC-UO_2^{2+} complex

Figure 5-1 Calculated optimized molecular structures of (a) cellulose; (b) chitosan; (c) OC; and (d) OC-UO_2^{2+} complex

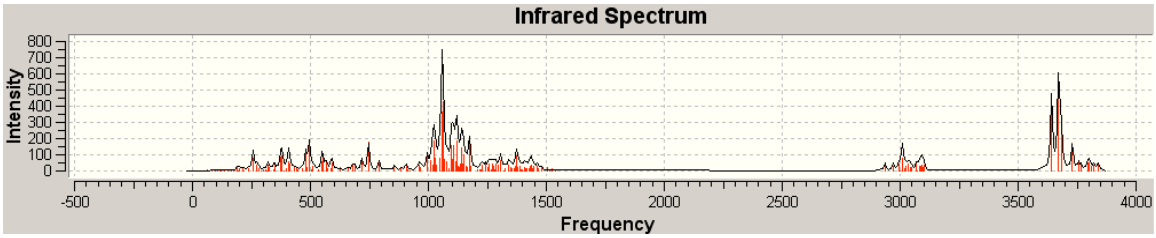

(a) cellulose

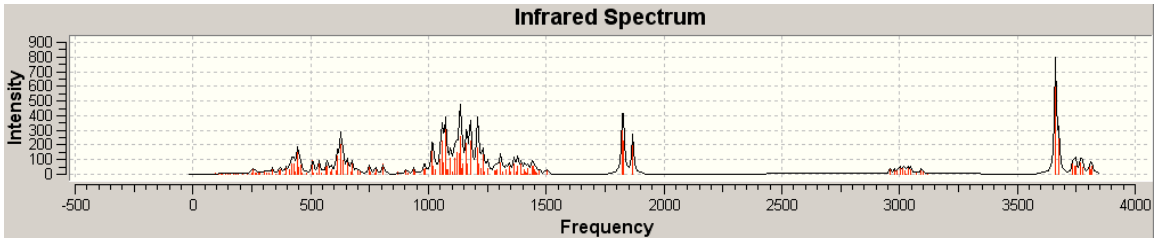

(b) OC

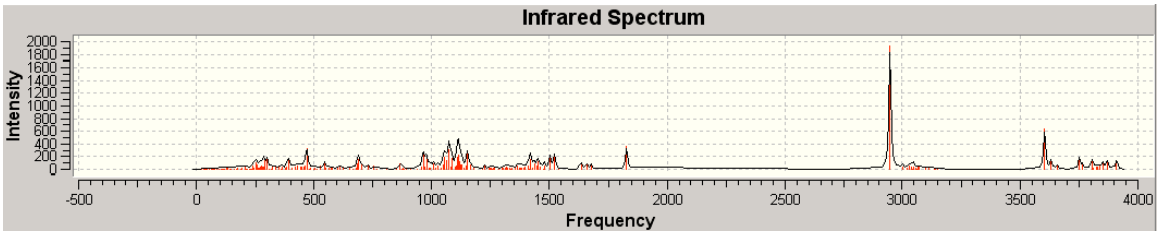

(c) OC-UO_2^{2+} complex

Figure 5-2 Calculated IR spectra of (a) cellulose; (b) OC; (c) OC-UO_2^{2+} complex

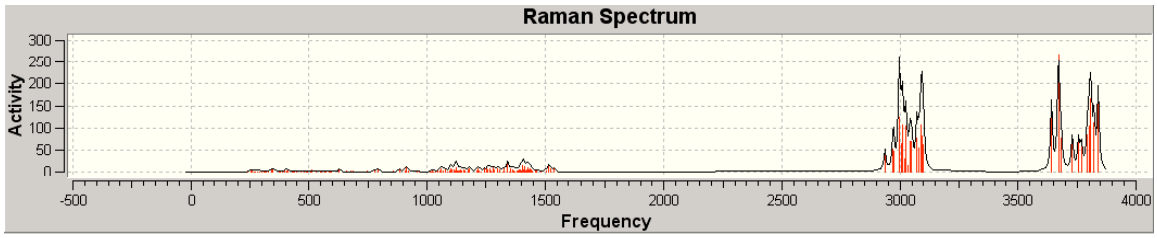

(a) Cellulose

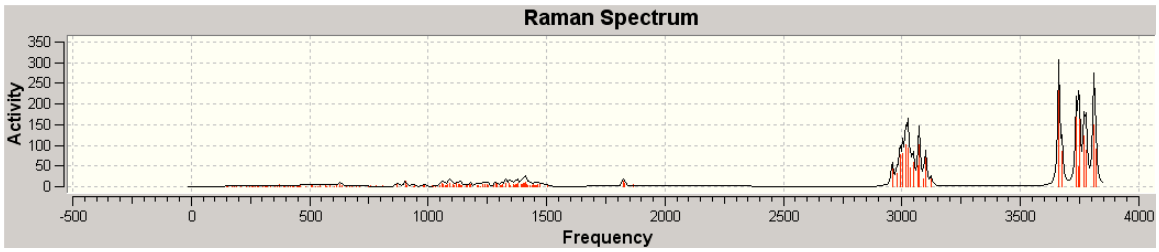

(b) OC

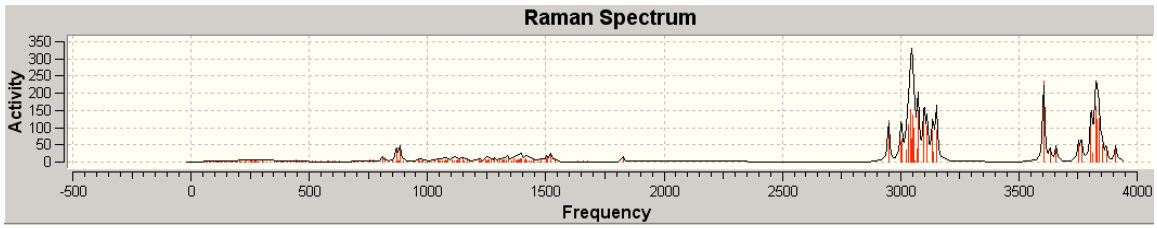

(c) OC-UO_2^{2+} complex

Figure 5-3 Calculated Raman spectra of (a) cellulose; (b) OC; (c) OC-UO_2^{2+} complex

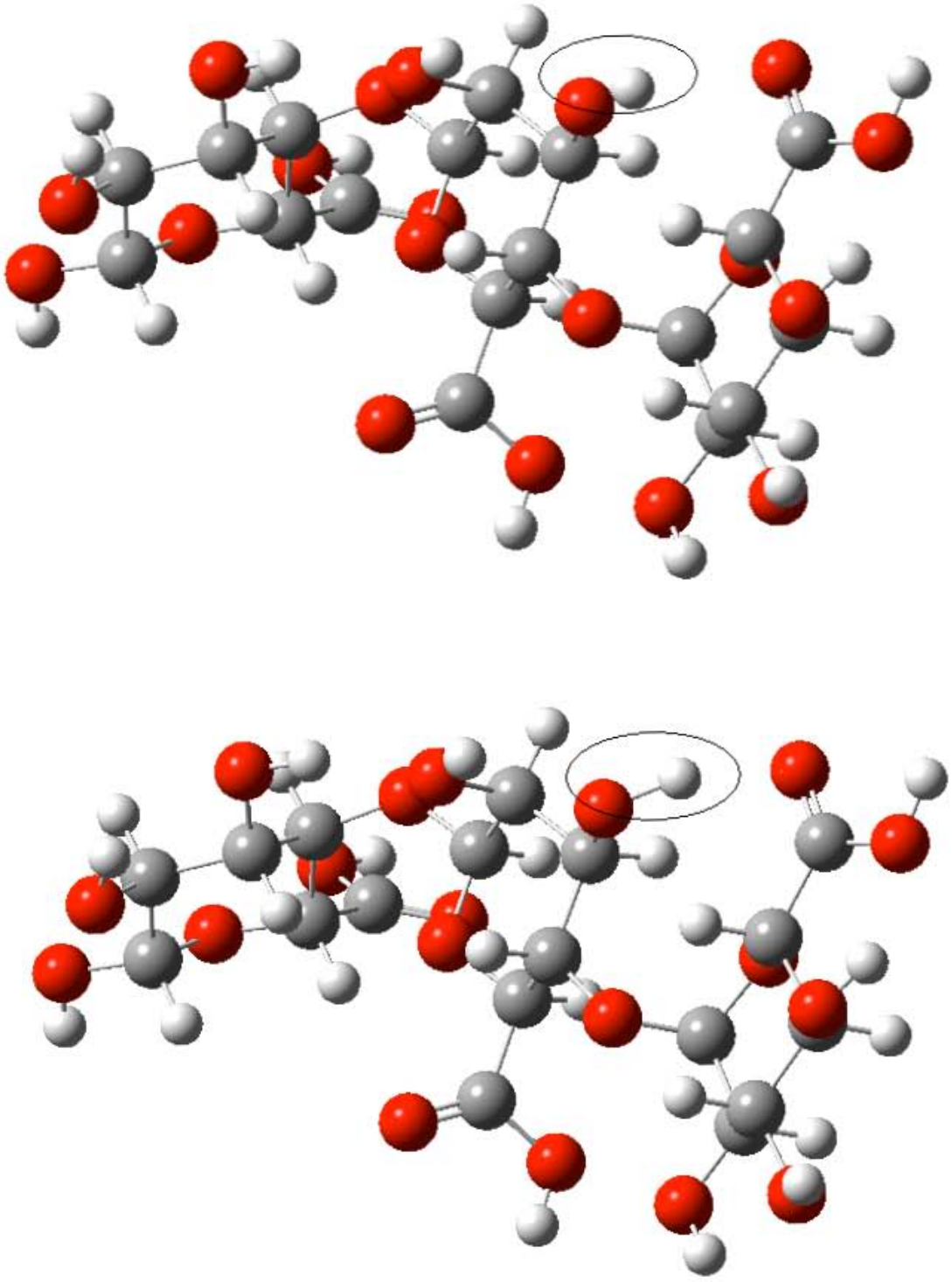

Figure 5-4 Snapshots of O-H stretching vibration

Wavenumber (cm^{-1})	**Assignment (predicted)**
Predicted/Experimental (if any)	
3661/3414	O-H str.
3025/2902	C-H str.
1828/1721	C=O str.
1371/1364	C-H def.; C-C str.; O-H def.
1305/1305	C-O str.; C-H def.; O-H def.
1133/1154	C-O str.; C-C def.
1072/1017	C-C def.; C-C str.; O-C str.; O-H def.; C-H def.
628	C-C def.; C=O def.; C-O def.; C-H def.; O-H def.
444	C-H def.; C-C def.; O-H def.

Table 5-3 IR wavenumbers (cm^{-1}) with assignments of OC

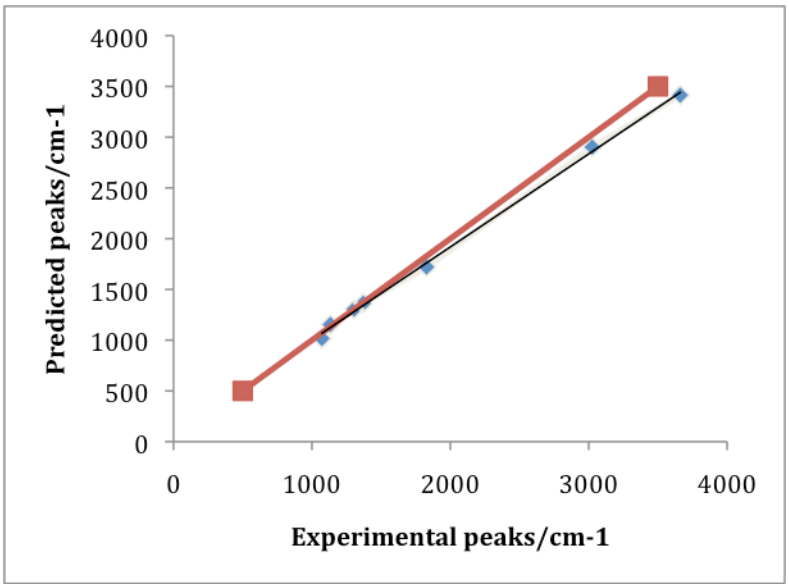

Figure 5-5 Calculated IR frequencies vs. observed IR frequencies for OC (red line is parity line)

CHAPTER 6 FIELD TESTS AT OAK RIDGE NATIONAL LABORATORY

6.1 Samples

Cellulose, CA, electrospun CA (E-CA), E-OC, OC, chitosan (CS), and neat polymers were tested on their adsorption capabilities on a contaminated groundwater plume containing metal ions, U and Th, at Department of Energy's Field Research Site at Oak Ridge National Laboratory. Each tested polymeric material was approximately 0.30 g.

6.2 Methods

Permeable environmental leaching capsules (PELCAPs) were molded from polyacrylamide gels to encapsulate aforementioned samples and were immersed in the contaminated wells, FW106 and SS5, to allow interaction between matrices and

contaminant metals, such as U and Th, to take place. Figure 6-1 shows the sample encapsulated PELCAPS [REF: http://www.esd.ornl.gov/people/brooks/pelcap-web.pdf].

Figure 6-1 Sample encapsulated PELCAPs

6.3 Results

Preliminary data show that OC and E-OC adsorbed a considerably larger amount of Th than equal weights of their counterparts (cellulose, CA, electrospun CA, CS, and neat polymers, which are the encapsulation materials by themselves) in a given time. CS

adsorbed a considerably larger amount of Th than its counterparts. Although the amount of U that E-OC adsorbed was less than CS, it was larger than other tested materials. The first 200 hours was very crucial for U adsorption and 500 hours for Th adsorption, after which time the amount of the adsorbed metal tended to remain the same. This phenomenon corroborates the observation on the laboratory-scale experiments.

After approximately 1300 hours of deployment, samples were transferred to a non-contaminated well to test for leaching of complexed metal ions. It is of interest to note that while sorption of U was more rapid, retention of Th was greater over time. Also, an equal mass of E-OC sorbed over three times more U ions than non-electrospun OC, which may be due to its larger surface area. The leaching phenomenon was not obvious for U on CS, which means that U adsorbed on CS was strongly bonded onto the matrix. E-OC and OC represent two strong bonding matrices for Th. Over time, the amount of Th adsorbed on E-OC and OC remained the same.

Figure 6-2 shows the adsorption capabilities of the tested polysaccharides on selected metals, U, Th, Sr, Rb, Ba, Fe, and Mn.

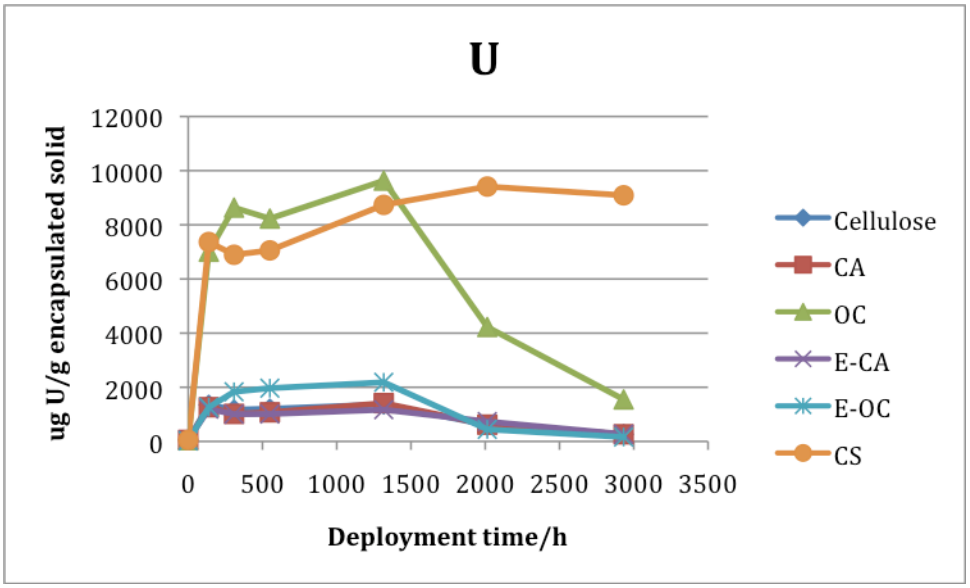

(a) Adsorption capabilities of polysaccharides on U

(b) Adsorption capabilities of polysaccharides on Th

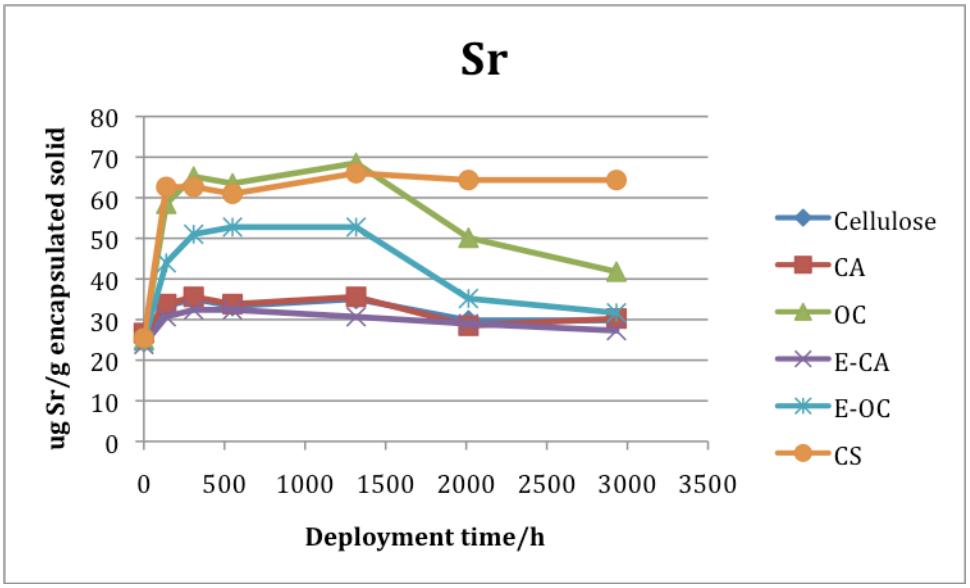

(c) Adsorption capabilities of polysaccharides on Sr

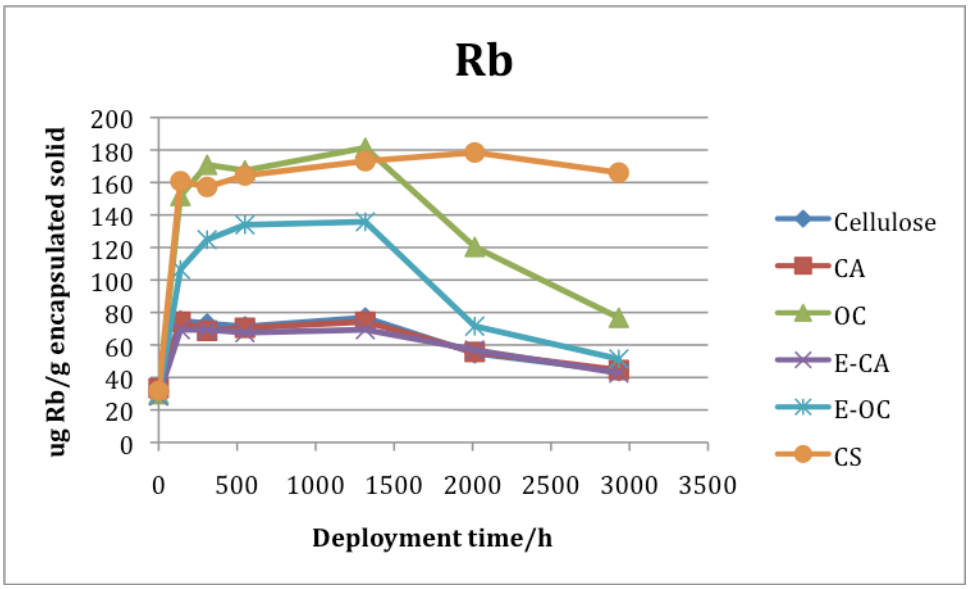

(d) Adsorption capabilities of polysaccharides on Rb

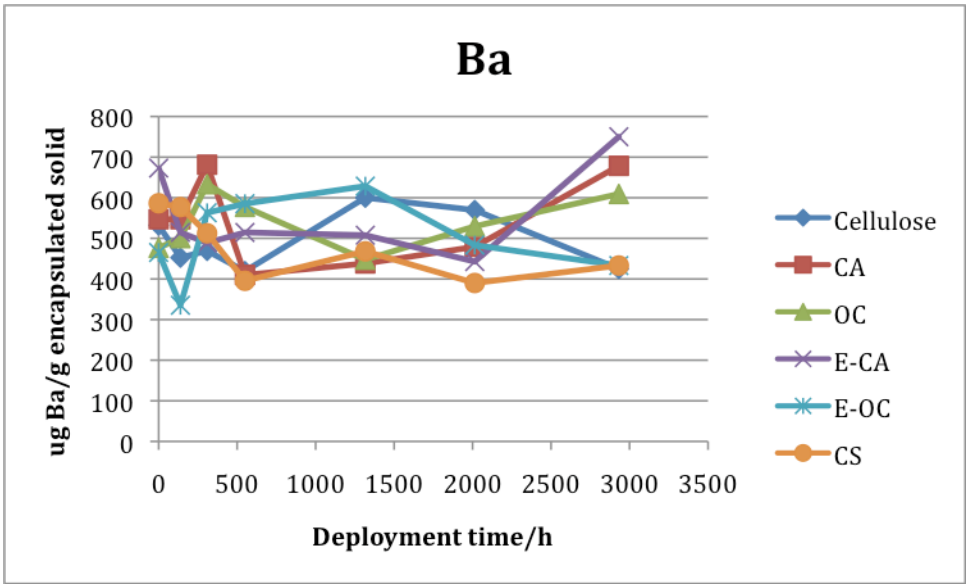

(e) Adsorption capabilities of polysaccharides on Ba

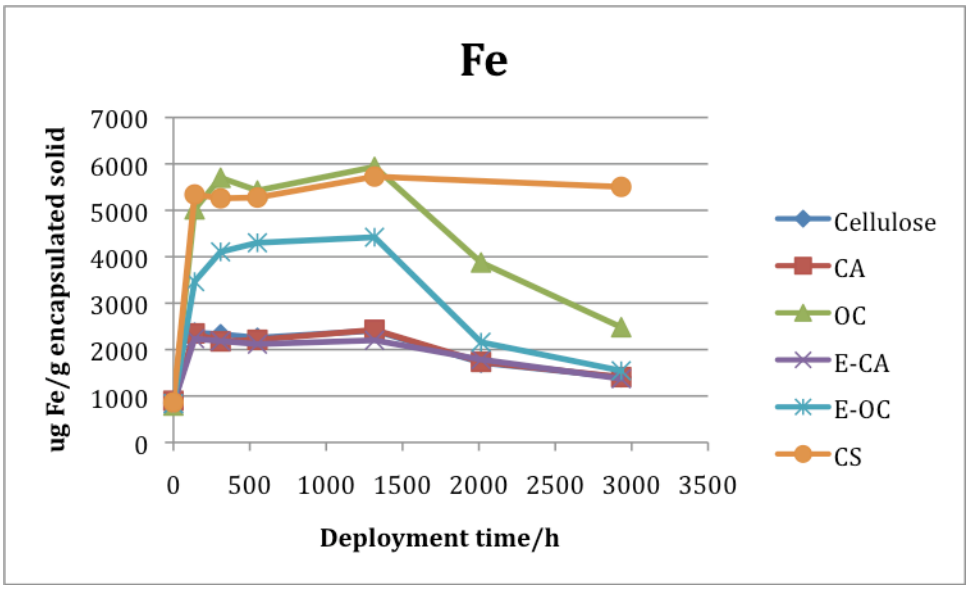

(f) Adsorption capabilities of polysaccharides on Fe

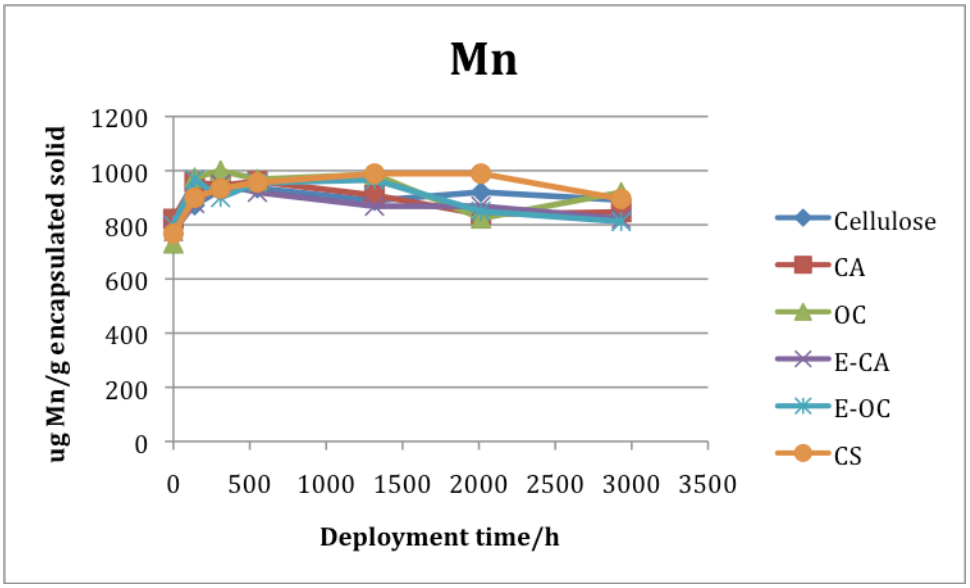

(g) Adsorption capabilities of polysaccharides on Mn

Figure 6-2 Adsorption capabilities of polysaccharides on selected metals

In comparison with the laboratory data shown in Chapter 4, it is noteworthy that there is discrepancy between the data from the two different sources. For instance, at pH 3 and after 96 hours' reaction time in laboratory experiments, the adsorption capabilities of E-OC and OC on U were 7854 μg U/g E-OC and 16898 μg U/g OC, respectively, which were much more than the values obtained from field tests, 1261.35 μg U/g E-OC and 7005.74 μg U/g OC, respectively at similar conditions. The adsorption capabilities of LCS and HCS on U obtained from laboratory experiments, 22233.96 μg U/g LCS and 20840.47 μg U/g HCS, were also significantly more than the test field value, which was 7365.34 μg U/g CS. The reason for this difference might be due to the presence of multiple metal ions in solution under field test conditions. Therefore, there might be a

competition in which some of the metal ions were more favorable in terms of being bond onto polysaccharide matrices than others, resulting in less amount of a certain types of metal ions adsorbed by the matrices.

Selected SEM micrographs and EDAX spectra for some particles found in the matrices retrieved from the S-3 test wells are shown below. This provides some information on retention of structure following 3000-hour immersion in wells, and the nature of some of the larger particles retained in the matrices following leaching (through redeployment in the clean well).

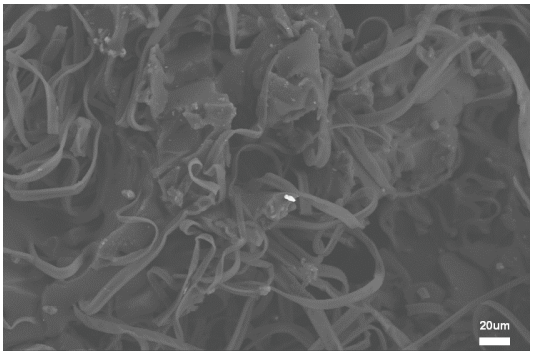

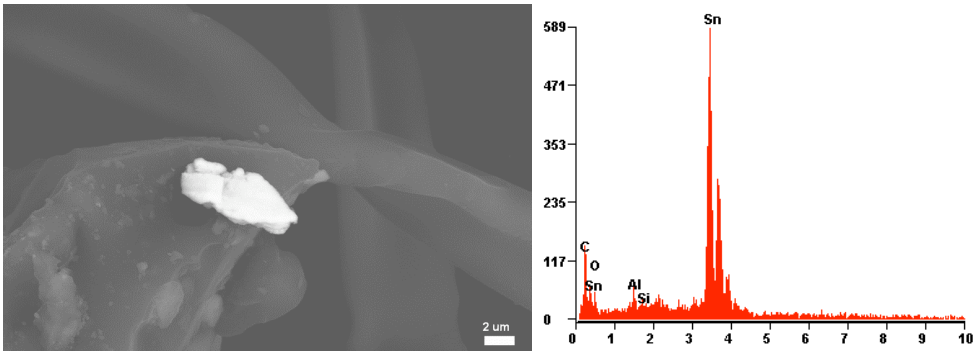

Figure 6-3 SEM/EDAX images of cellulose acetate following removal from groundwater

Figure 6-3 shows the retention of the electrospun fiber structure and primarily shows the sorbtions of Sn particle.

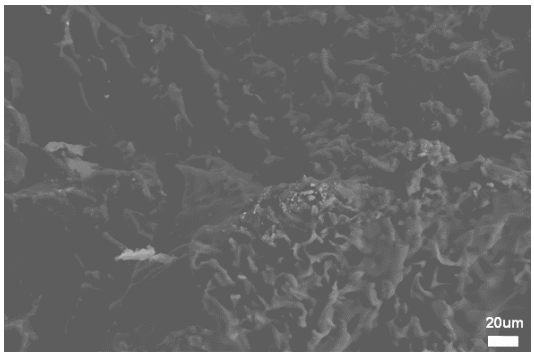

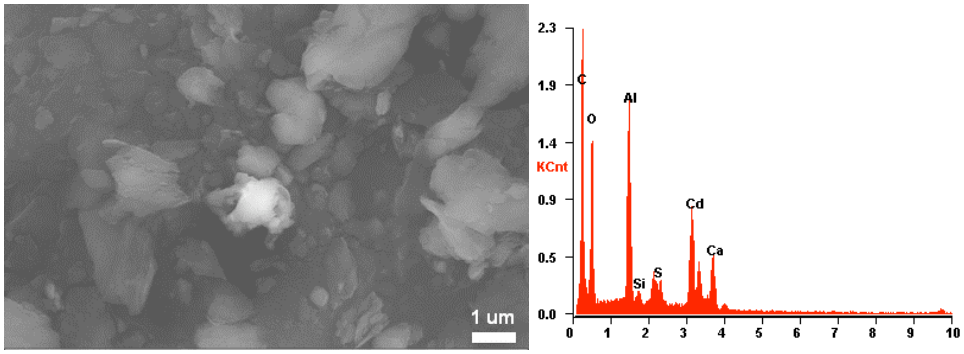

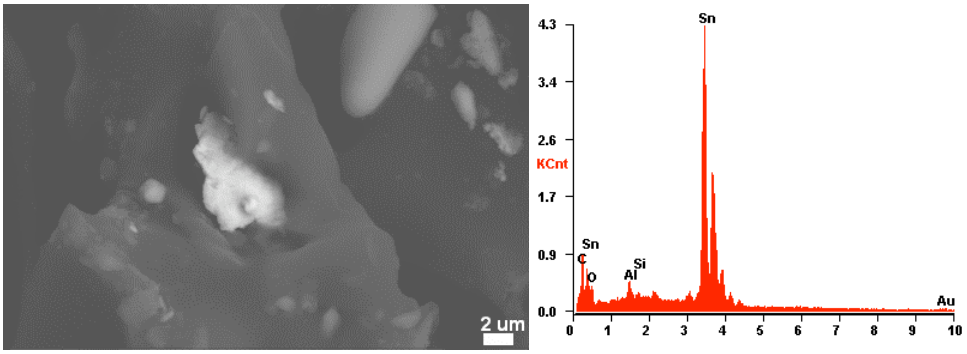

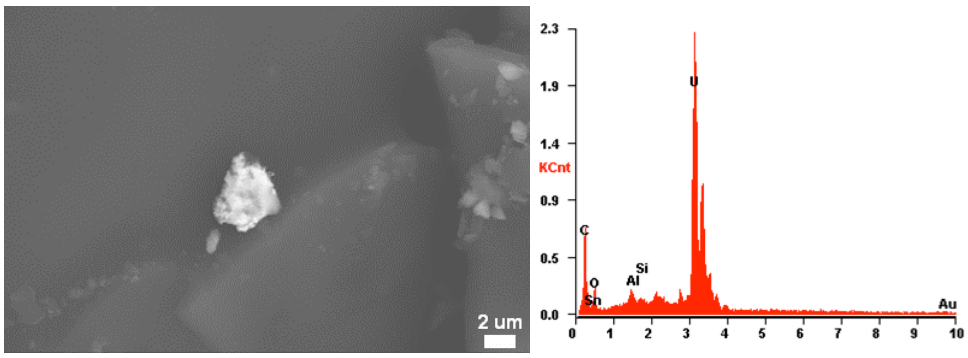

Figure 6-4 SEM/EDAX images of electrospun oxidized cellulose following exposure to groundwater at ORNL

Figure 6-4 shows partial retention of E-OC structure, and sorbtion for Al/Cd/S, Ca (co-associated) Sn and U.

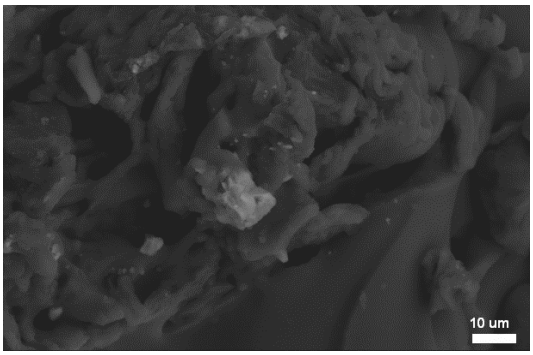

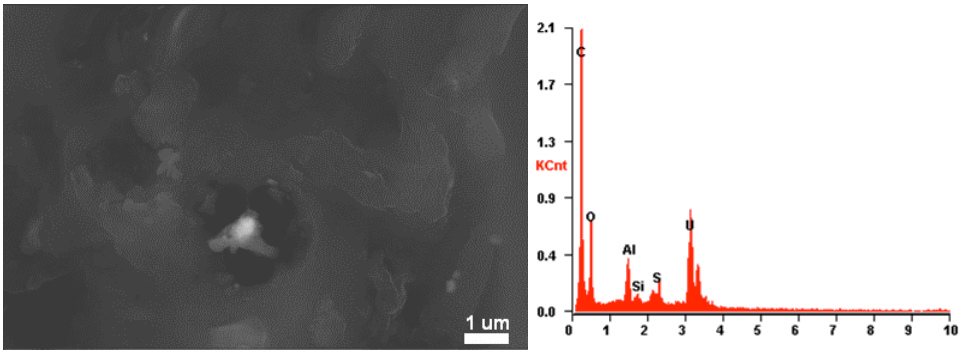

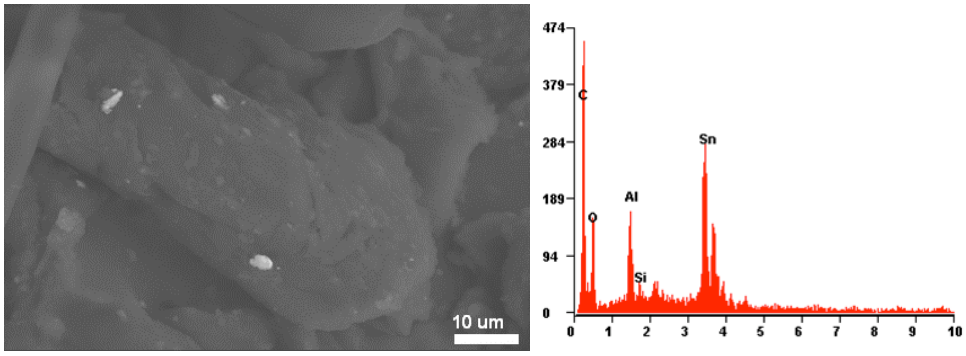

Figure 6-5 SEM/EDAX images of chitosan following exposure to groundwater at ORNL

Figure 6-5 shows the evidence of retention of chitosan structure even at acidic conditions, and identifications of sorbed U/Al/S (co-associated) and sorbed Sn/Al (co-associated), Fe.

CHAPTER 7 CONCLUSIONS

OC and E-OC were successfully fabricated through the reported methods. IR and Raman spectroscopic data demonstrate the formation of characteristic carboxylic groups, which possess the chemical ability to chelate certain types of metal ions in the structure of the final products. SEM images reveal that electrospun OC retains its structure following exposure to acidic solutions containing heavy metal contaminants, ensuring permeability for groundwater remediation applications (e.g. use as PRB fillers). SEM/EDAX data from samples retrieved from deployment at the Oak Ridge Field Research site also show retention of structure, even after over 3000 hours of deployment. DCP-AES data determines the amount of metal that polymeric matrices adsorbed in laboratory samples, while XRF was used to identify the amount of sorbed ions at the FRC. Both laboratory and field experiment data suggest the potential possibility of the use of polysaccharides, OC, E-OC, LCS and HCS as permeable reaction barrier fillers or ex situ sorbents for metal contaminated groundwater treatment. Uranyl ions are most effectively sorbed and retained by chitosan, especially at acidic pH ranges where U tends to be not mobile in soil and groundwater. Analytical results support a "pendant" model (involving both amine and hydroxyl ligands) for uranyl sorbtion. Trivalent transuranic

analogs, Eu(III) and Ce(III), are more strongly sorbed by oxidized cellulose in middle acidic pH's (3-5). Chitosan is more or equally effective at very low (~1) and higher (~6) pH ranges. Association at low pH may occur through electrostatic interaction at amine sites.

The comparison between the IR and Raman spectra yielded from molecular modeling and those obtained from experiments shows a good agreement, which suggests a method to predict the structural and chemical properties of molecules when it is impractical to carry out experiments due to technical difficulty or limited resources.

CHAPTER 8 SUGGESTIONS FOR FUTURE WORK

The improvement of functionalized polysaccharide matrices for adsorbing metal ions from polluted groundwater can be achieved by enlarging the effective surface areas of the matrices. In this work, electrospun and non-electrospun OC showed great potential for adsorbing a certain types of metals; however, due to their structures, not all the carboxyl groups were able to participate in binding metal ions. Therefore, research on how to make the matrices more effective would be of substantial importance to make the OC matrices competitive amongst other binding materials.

Electrospinning was proven to be able to produce more porous structures with larger surface ratio. Future work may also include using this technique to fabricate more porous chitosan-based binding materials.

Future research could also be carried on testing the competitiveness of different binding materials when multiple metal ions are present in solution.

Lastly, leaching studies on laboratory prepared metal-polysaccharide matrices could also be extensively performed

References:

1. Goldschmidt B. *Uranium's scientific history 1789-1939. Fourteenth international symposium by the Uranium Institute in London.* 1989.
2. Emsley J. *Nature's Building Blocks: An A-Z Guide to the Elements* 2003: Oxford University Press, USA
3. Ewing RC. *The metamict state: 1993 - the centennial.* Nuclear Instruments and Methods in Physics Research Section B, 1994, **91**(1-4): p. 22-29.
4. Burns PC, and Finch R. *Uranium: Mineralogy, Geochemistry and the Environment*, ed. P.H. Ribbe. 1999: The Mineralogical Society of America.
5. Adloff JP, and MacCordick HJ. *The dawn of radiochemistry.* Radiochimica Acta, 1995, **70/71**: p. 13-22.
6. Badash L. *Radioactivity in America: Growth and Decay of a Science*. 1979, Baltimore, Md.: Johns Hopkins University Press. 328.
7. Bourdon B, Henderson GM, Lundstrom CC, and Turner SP. *Uranium-series geochemistry*. Reviews in Mineralogy and Geochemistry. Vol. 52. 2003.
8. Cordfunke EHP. *The chemistry of uranium* 1969: Elsevier Publishing Company.
9. Katz JJ, and Rabinowitch E. *The chemistry of uranium* Part I The element, its binary and related compounds. 1951: McGraw-Hill Book Company, Inc.
10. Palei PN. *Analytical chemistry of uranium*. 1970: Ann Arbor-Humphrey Science publishers.
11. Latimer W. *Oxidation states of elements and their potentials in aqueous solutions*. 1952, N.Y.: Prentice-Hall.
12. Starr C. *The future of nuclear power.* Nuclear News, 1997: p. 58-60.
13. Pavelescu M, Pavelescu A, and Sandulescu A. *Nuclear power and the environment.* Rom. Journ. Phys., 2005, **50**: p. 473-491.
14. Eng C. *Spectroscopic studies of uranium species for environmental decontamination applications*, in *Materials Science and Engineering*. 2005, Stony Brook University: Stony Brook. p. 202.
15. [cited; Available from: http://periodic.lanl.gov/elements/92.html.
16. Lloyd JR, and Renshaw JC. *Bioremediation of radioactive waste: radionuclide-microbe interactions in laboratory and field-scale studies.* Curr Opin Biotechnol, 2005, **16**(3): p. 254-60.

17. Francis AJ. *Microbial Dissolution and Stabilization of Toxic Metals and Radionuclides in Mixed Wastes.* Experientia, 1990, **46**(8): p. 840-851.

18. Francis AJ, Dodge CJ, Gillow JB, and Cline JE. *Microbial Transformations of Uranium in Wastes.* Radiochimica Acta, 1991, **52-3**: p. 311-316.

19. Munoz JA, Gonzalez F, Blazquez ML, and Ballester A. *A Study of the Bioleaching of a Spanish Uranium Ore .1. A Review of the Bacterial Leaching in the Treatment of Uranium Ores.* Hydrometallurgy, 1995, **38**(1): p. 39-57.

20. Tuovinen OH. *Acid-leaching of uranium ore materials with microbial catalysis.* Biotechnol Bioengin Symp, 1986, **13**: p. 65-72.

21. Hiemenz PC. *Principles of Colloid and Surface Chemistry*. 2nd ed. 1986, New York: Marcel Dekker, Inc.

22. Travis CC, and Doty CB. *Can contaminated aquifers at superfund sites be remediated?* Environmental Science and Technology, 1990, **24**: p. 1464-1466.

23. Francis AJ, and Dodge CJ. *Remediation of soils and wastes contaminated with uranium and toxic metals.* Environmental Science and Technology, 1998, **32**: p. 3993-3998.

24. Cornish JE, Goldberg WC, Levine RS, and Benemann JR. *Phytoremediation of soils contaminated with toxic elements and radionuclides.* Bioremediation of Inorganics, 1995, **3**: p. 55-62.

25. Cantrell KJ, Kaplan DI, and Wietsma TW. *Zero-valent iron for the in situ remediation of selected metals in groundwater.* Journal of Hazardous Materials, 1995, **42**(2): p. 201-212.

26. Abdelouas A, Lutze W, Nuttall HE, and Gong W. *Remediation of U (VI)-contaminated water using zero-valent iron.* Comptes Rendus de l'Academie des Sciences, Serie IIa: Sciences de la Terre et des Planetes, 1999, **328**(5): p. 315-319.

27. Morrison SJ, and Spangler RR. *Extraction of uranium and molybdenum from aqueous solutions: A survey of industrial materials for use in chemical barriers for uranium mill tailings remediation* Environmental Science and Technology, 1992, **26**: p. 1922-1931.

28. Kauffman JW, Laughlin WC, and Baldwin RA. *Microbiological treatment of uranium mine waters.* Environmental Science and Technology, 1986, **20**: p. 243-248.

29. Lovley DR, Phillips EJP, Gorby Y, and Landa E. *Microbial reduction of uranium.* Nature, 1991, **350**: p. 413-416.

30. Lovley DR, Roden EE, Phillips EJP, and Woodward JC. *Enzymatic iron and uranium reduction by sulfate-reducing bacteria.* Marine Geol, 1993, **113**: p. 41-53.

31. Francis AJ, Dodge CJ, Lu F, Halada GP, and Clayton CR. *XPS and XANES studies of uranium reduction by Clostridium sp.* . Environmental Science and Technology, 1994, **28**: p. 636-639.

32. Barton LL, Choudhury K, Thomson BM, Steenhoudt K, and Groffman AR. *Bacterial reduction of soluble uranium: The first step of in situ immobilization of uranium.* Radioac Waste Manag Environ Restor, 1996, **20**: p. 141-151.

33. Ganesh R, Robinson KG, Reed GD, and Sayler GS. *Reduction of hexavalent uranium from organic complexes by sulfate- and iron-reducing bacteria.* Applied and Environmental Microbiology, 1997, **63**: p. 4385-4391.

34. Suzuki Y, Kelly SD, Kemner KM, and Banfield JF. *Microbial populations stimulated for hexavalent uranium reduction in uranium mine sediment.* Applied and Environmental Microbiology, 2003, **69**: p. 1337-1346.

35. Navarro A, Chimenos JM, Muntaner D, and Fernandez AI. *Permeable reactive barriers for the removal of heavy metals: lab-scale experiments with low-grade magnesium oxide.* Ground Water Monitoring & Remediation, 2006, **26**(4): p. 142-152.

36. *Permeable reactive barrier technologies for contaminant remediation*. 1998, EPA, Office of Solid Waste and Emergency Response: Washington, D.C.

37. Day SR, O'Hannesin SF, and Marsden L. *Geotechnical techniques for the construction of reactive barriers.* J Hazard Mater, 1999, **67**(3): p. 285-97.

38. Blowes DW, Ptacek CJ, Benner SG, McRae CWT, Bennet TA, and Puls RW. *Treatment of inorganic contaminants using permeable reactive barriers.* Journal of Contaminant Hydrology 2000, **45**: p. 123-137.

39. Navarro A, Rosell A, Villanueva J, and Grimalt JO. *Monitoring of hazardous waste dumps by the study of metals and solvent-soluble organic chemicals.* Chemosphere, 1991, **22**(9): p. 913-928.

40. Ma QY, Traina SJ, and Logan TJ. *In situ lead immobilization by apatite.* Environmental Science and Technology, 1993. **27**: p. 1803-1810.

41. Randall JM, Bermann RL, Garett V, and Waiss AC Jr. *Use of bark to remove heavy metal ions from waste solutions.* Forest Products Journal, 1974, **24**(9): p. 80-84.

42. Vazquez G, Antorrena G, Gonzalez J, and Doval MD. *Adsorption of heavy metal ions by chemically modified Pinus Pinaster bark.* Bioresource Technology, 1994. **48**: p. 251-255.

43. Randall JM, Hautala E, and Waiss AC Jr. *Removal and recycling of heavy metal ions from mining and industrial waste streams with agricultural byproducts*. in *Proceedings of the Fourth Mineral Waste Utilization Symposium*. 1974. Chicago, IL.

44. Srivastava SK, Singh , and Sharma A. *Studies on the uptake of lead and zinc by lignin obtained from black liquor - a paper industry waste material.* Environmental Technology, 1994, **15**: p. 353-361.

45. Matis KA, and Zouboulis AI. *Flotation of cadmium-loaded biomass.* Biotechnol Bioeng, 1994, **44**(3): p. 354-60.

46. Niu H, Xu XS, Wang JH, and Volesky B. *Removal of lead from aqueous solutions by Penicillium biomass.* Biotechnol Bioeng, 1993, **42**(6): p. 785-7.

47. Volesky B, and Prasetyo I. *Cadmium removal in a biosorption column.* Biotechnol Bioeng, 1994, **43**(11): p. 1010-5.

48. Flynn CM Jr., Carnahan TG, and Lindstrom RE. *Adsorption of heavy metal ioins by xanthated sawdust*. 1980, United States Bureau of Mines.

49. [cited; Oak Ridge Rield Research Center]. Available from: http://public.ornl.gov/orifc/orfrc3_site.cfm#Anchor1.

50. Klemm D, Heublein B, Fink HP, and Bohn A. *Cellulose: fascinating biopolymer and sustainable raw material.* Angew Chem Int Ed Engl, 2005, **44**(22): p. 3358-93.

51. Kennedy JF, Phillips GO, Wedlock DJ, and Williams PA. *Cellulose and its derivatives*. 1 ed. 1985: Ellis Horwood Limited.

52. Wang N [cited; Available from: www.engr.umd.edu/~nsw/ench485/lab4.htm.

53. Son WK, Youk JH, and Park WH. *Preparation of ultrafine oxidized cellulose mats via electrospinning.* Biomacromolecules, 2004, **5**(1): p. 197-201.

54. Johnson, & Johnson Patient Care, Inc., *Surgical Absorbable Hemostate*. 1989: USA.

55. Abaev IK, Kaputskii VE, Adarchenko AA, and Sobeshchukh OP. *Mechanism of the antibacterial action of monocarboxycellulose and other ion-exchange derivatives of cellulose.* Antibiotics and medical biotechnology, 1988, **31**(8): p. 624-628.

56. Tokunaga Y, Kojima T, and Naruse T. *Antitumor effect of oxycellulose as a hemostatic during operation.* Cancer biotherapy & radiopharmaceuticals, 1998, **13**(6): p. 437-445.

57. Kumar V, and Yang T. *HNO_3/H_3PO_4–$NaNO_2$ mediated oxidation of cellulose — preparation and characterization of bioabsorbable oxidized celluloses in high yields and with different levels of oxidation.* Carbohydrate Polymers, 2002, **48**: p. 403-412.

58. Walimbe AM, Pandya BN, and Lalla JK. *Preparation of oxidized cellulose BP.* Research and Industry, 1978, **23**(3): p. 162-165.

59. Gert EV, Shishonok MV, Zubets OV, Torgashov VI, and Kaputskii FN. *Preparation of powdered oxidized cellulose in nitric acid.* Polymer Science, 1995, **37**(7): p. 670-675.

60. Wanleg H. *Process for the preparation of oxidation products of cellulose*. 1956: USA.

61. Painter TJ. *Preparation and periodate oxidation of C-6-oxycellulose: conformational interpretation of hemiacetal stability.* Carbohydrate Research, 1977, **55**(95-103).

62. Besemer AC, De Nooy AEJ, and Van Bekkum H. *Methods for the selective oxidation of cellulose: preparation of 2,3-dicarboxycellulose and 6-carboxycellulose*. in *ACS Symposium Series*. 1998: American Chemical Society.

63. Bertocchi C, Konowicz P, Signore S, Zanetti F, Flaibani A, Paoletti S, and Crescenzi V. *Synthesis and characterization of polyglucuronan.* Carbohydrate Polymers, 1995, **27**(4): p. 295-297.

64. Bailey SE, Olin TJ, Bricka RM, and Adrian DD. *A review of potentially low-cost sorbents for heavy metals.* Wat. Res., 1999, **33**: p. 2469-2479.

65. Chen CL, Wang YM, Liu CF, and Wang JY. *The effect of water-soluble chitosan on macrophage activation and the attenuation of mite allergen-induced airway inflammation.* Biomaterials, 2008, **29**(14): p. 2173-2182.

66. Onsoeyen E, and Skaugrud O. *Metal recovery using chitosan.* Journal of Chemical Technology and Biotechnology, 1990, **49**(4): p. 395-404.

67. Wantanaphong J, Mooney SJ, and Bailey EH. *Natural and waste materials as metal sorbents in permeable reactive barriers (PRBs).* Environmental chemistry letters, 2005, **3**: p. 19-23.

68. Benguella B, and Benaissa H. *Cadmium removal from aqueous solutions by chitin: kinetic and equilibrium studies.* Water Research, 2002, **36**(10): p. 2463-2474.

69. Brugnerotto J, Lizardi J, Goycoolea FM, Arguelles-Monal W, Desbrieres J, and Rinaudo M. *An infrared investigation in relation with chitin and chitosan characterization.* Polymer, 2001, **42**(8): p. 3569-3580.

70. Yang TC, and Zall RR. *Absorption of metals by natural polymers generated from seafood processing wastes.* Industrial & Engineering Chemistry Product Research and Development, 1984, **23**(1): p. 168-72.

71. Piron E, and Domard A. *Interaction between chitosan and uranyl ions. Part 2. Mechanism of interaction.* International Journal of Biological Macromolecules, 1998, **22**: p. 33-40.

72. Felt O, Buri P, and Gurny R. *Chitosan: a unique polysaccharide for drug delivery.* Drug Development and Industrial Pharmacy, 1998, **24**(11): p. 979-993.

73. Biagini G, Bertani A, Muzzarelli R, Damadei A, DiBenedetto G, Belligolli A, Riccotti G, Zucchini C, and Rizzoli C. *Wound management with N-carboxybutyl chitosan.* Biomaterials, 1991, **12**(3): p. 281-6.

74. Kurita K, Sannan T, and Iwakura Y. *Studies on chitin. VI. Binding of metal cations.* Journal of Applied Polymer Science, 1979, **23**(2): p. 511-515.

75. Masri MS, Reuter FW, and Friedman M. *Binding of metal cations by natural substances.* Journal of Applied Polymer Science, 1974, **18**(3): p. 675-681.

76. Jha IN, Iyengar L, and Rao AVSP. *Removal of cadmium using chitosan.* Journal of Environmental Engineering (Reston, VA, United States), 1988, **114**(4): p. 962-974.

77. McKay G, Blair HS, and Findon A. *Equilibrium studies for the sorption of metal ions onto Chitosan.* Indian Journal of Chemistry, Section A: Inorganic, Physical, Theoretical & Analytical, 1989, **28A**(5): p. 356-360.

78. Udaybhaskar P, Iyengar L, and Rao AVSP. *Hexavalent chromium interaction with chitosan.* Journal of Applied Polymer Science, 1990, **39**(3): p. 739-747.

79. Peniche-Covas C, Alvarez LW, and Arguelles-Monal W. *The adsorption of mercuric ions by chitosan.* Journal of Applied Polymer Science, 1992, **46**(7): p. 1147-1150.

80. Rorrer GL, Hsien TY, and Way JD. *Synthesis of porous-magnetic chitosan beads for removal of cadmium ions from wastewater.* Industrial & Engineering Chemistry Research, 1993, **32**(9): p. 2170-2178.

81. Jayaraman K, Kotaki M, Zhang YZ, Mo XM, and Ramakrishna S. *Recent advances in polymer nanofibers.* Journal of Nanoscience and Nanotechnology, 2004, **4**: p. 52-65.

82. Hartgerink JD, Beniash E, and Stupp SI. *Peptide-amphiphile nanofibers: a versatile scaffold for the preparation of self-assembling materials.* The Proceedings of the National Academy of Sciences USA, 2002, **99**: p. 5133-5138.

83. Witte D, Dijkstra PJ, Berg JWA, and Feijen J. *Phase separation process in polymer solutions in relation to membrane formation.* Journal of Membrane Science, 1996, **117**: p. 1-31.

84. Chakarvarti SK, and Vetter J. *Template synthesis-membrane based technology for generation of nano-/micro materials: a review.* Radiation Measurements 1998, **29**: p. 149-159.

85. Teo WE, and Ramakrishna S. *A review on electrospinning design and nanofibre assemblies.* Nanotechnology, 2006, **17**: p. 89-106.

86. Li D, and Xia Y. *Electrospinning of nanofibers: reinventing the wheel?* Advanced Materials, 2004, **16**: p. 1151-1170.

87. Ogata Y. *Organic chemistry: oxidation in organic chemistry part C, oxidation with nitric acid or nitrogen oxides*. 1978.

88. Adebajo MO, Frost RL, Kloprogge JT, and Kokot S. *Raman spectroscopic investigation of acetylation of raw cotton.* Spectrochim Acta A Mol Biomol Spectrosc, 2006, **64**(2): p. 448-53.

89. Socrates G. *Infrared and Raman characteristic group frequencies*. 3 ed. 2001: John Wiley & Sons, LTD.

90. Jansson-Charrier M, Saucedo I, Guibal E, and Le Cloirec P. Approach *of uranium sorption mechanisms on chitosan and glutamate glucan by IR and carbon-13 NMR analysis.* Reactive & Functional Polymers, 1995, **27**: p. 209-221.

91. Schmeide K, Sachs S, Bubner M, Reich T, Heise KH, and Bernhard G. *Interaction of uranium (VI) with various modified and unmodified natural and synthetic humic substances studied by EXAFS and FTIR spectroscopy.* Inorganica Chimica Acta, 2003, **351**: p. 133-140.

92. Fujii T, Fujiwara K, Yamana H, and Moriyama H. *Raman spectroscopic determination of formation constant of uranyl hydrolysis species* $(UO_2)_2(OH)_2^{2+}$. Journal of alloys and compounds, 2001, **323-324**: p. 859-863.

93. Nichols JA, Harrison RJ, deJong WA, and Dixon DA. *Density functional studies of uranyl complexes using relativistic effective core potentials.* William R. Wiley Environmental Molecular Sciences Laboratory.

94. Frenkel D, and Smit B. *Understanding Molecular Simulation: From Algorithms to Applications*. 1996: Academic Press.

95. Leach AR. *Molecular Modelling: Principles and Applications*. 1996, Harlow, England: Longman.

96. Foresman JB, and Frisch A. *Exploring Chemistry with Electronic Structure Methods.* Second ed. 1996: Gaussian, Inc.

97. Beck BR, Becker JA, Beiersdorfer P, Brown GV, Moody KJ, Wilhelmy JB, Porter FS, Kilbourne CA, and Kelley RL. *Energy splitting of the ground-state doublet in the nucleus* ^{229}Th. Physical review letters, 2007, **98** (14).

98. Frisch MJT, Schlegel GW, Scuseria HB, Robb GE, Cheeseman MA, Montgomery JR Jr., Vreven JA, Kudin T, Burant KN, Millam JC, Iyengar JM, Tomasi SS, Barone J, Mennucci V, Cossi B, Scalmani M, Rega G, Petersson N, Nakatsuji GA, Hada H, Ehara M, Toyota M, Fukuda K, Hasegawa R, Ishida J, Nakajima M, Honda T, Kitao Y, Nakai O, Klene H, Li M, Knox X, Hratchian JE, Cross HP, Bakken JB, Adamo V, Jaramillo C, Gomperts J, Stratmann R, Yazyev RE, Austin O, Cammi AJ, Pomelli R, Ochterski C, Ayala JW, Morokuma PY, Voth K,

Salvador GA, Dannenberg P, Zakrzewski JJ, Dapprich VG, Daniels S, Strain D, Farkas MC, Malick O, Rabuck DK, Raghavachari AD, Foresman K, Ortiz JB, Cui JV, Baboul Q, Clifford AG, Cioslowski S, Stefanov J, Liu BB, Liashenko G, Piskorz A, Komaromi P, Martin I, Fox RL, Keith DJ, Al-Laham T, Peng MA, Nanayakkara CY, Challacombe A, Gill M, Johnson PMW, Chen B, Wong W, Gonzalez MW, C. and Pople JA, *Gaussian* 03. Revision C.02. Wallingford CT; 2004.

99. Ditchfield R, Hehre WJ, and Pople JA. *Self-consistent molecular orbital methods. 9. Extended Gaussian-type basis for molecular orbital studies of organic molecules*. J Chem Phys, 1971, **54**: p.724-728.

100. Hehre WJ, Ditchfield R, and Pople JA. *Self-consistent molecular orbital methods. 12. Further extensions of gaussian-type basis sets for use in molecular-orbital studies of organic-molecules*. J Chem Phys, 1972, **56**: p.2257-2261.

101. Rassolov VA, Ratner MA, Pople JA, Redfern PC, and Curtiss LA. *6-31G* basis set for third-row atoms.* J Comp Chem, 2001, **22**: p.976-984.

102. Rassolov VA, Pople JA, Ratner MA, and Windus TL. *6-31G* basis set for atoms K through Zn*. J Comp Chem, 1998, **109**: p.1223-1229.

103. Küchle W, Dolg M, Stoll H, and Pesuss H. *Energy-adjusted pseudopotentials for the actinides - parameter sets and test calculations for thorium and thorium monoxide*. J Chem Phys, 1994, **100**: p.7535-7542.

104. Cao X, Dolg M, and Stoll H. *Valence basis sets for relativistic energy-consistent small-core actinide pseudopotentials*. J Chem Phys, 2003, **118**: p.487-496.

105. Becke AD. *Density-functional thermochemistry .5. Systematic optimization of exchange-correlation functionals*. J Chem Phys, 1997, **107**: p.8554-8560.

106. Stephens PJ, Devlin FJ, Chabalowski CF, and Frisch MJ. *Ab-initio calculation of bibrational absorption and circular-dichroism spectra using density-functional force-fields*. J Phys Chem, 1994, **98**: p.11623-11627.

107. Lee CT, Yang WT, and Parr RG. *Development of the Colle-Salvetti correlation-energy formula into a functional of the electron-density.* Phys Rev B, 1998, **37**: p.785-789.